

NMR RELAXATION TIMES AND RELATED PORE  
GEOMETRY IN THE MORROW GROUP  
(PENNSYLVANIAN), HEMPHILL  
COUNTY, TEXAS AND TEXAS  
COUNTY, OKLAHOMA

By

RACHAEL AJVANO

Bachelor of Science

Texas Tech University

Lubbock, Texas

1999

Submitted to the Faculty of the Graduate College of the  
Oklahoma State University in partial fulfillment of  
the requirements for the Degree of  
MASTER OF SCIENCE December, 2001

NMR RELAXATION TIMES AND RELATED PORE  
GEOMETRY IN THE MORROW GROUP  
(PENNSYLVANIAN), HEMPHILL  
COUNTY, TEXAS AND TEXAS  
COUNTY, OKLAHOMA

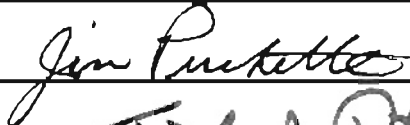
Thesis Approved:

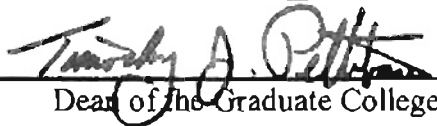
  
\_\_\_\_\_

Thesis Adviser

  
\_\_\_\_\_

  
\_\_\_\_\_

  
\_\_\_\_\_

  
\_\_\_\_\_

Dean of the Graduate College

## ACKNOWLEDGMENTS

I would like to thank Dr. Stanley Paxton, my thesis advisor, for all of his time and help in writing my thesis. I am sincerely grateful for all the constructive criticism he gave me. I would also like to thank my committee members Dr. Zuhair Al-Shaieb and Dr. James Puckette for their help with my thesis. My sincere appreciation goes to Dr. James Howard of Phillips Petroleum Company for all of the time and effort he put into assisting me. He donated time and access to equipment that were critical to the completion of this thesis.

I would also like to thank the Phillips Petroleum Company's Borger Office for their contribution of the logs and their thoughts on the project.

Finally, I would like to thank my parents for their support and encouragement throughout my life. My parents have always supported everything I have done and without them I would not be where I am today.

## TABLE OF CONTENTS

Chapter		
I.	INTRODUCTION	
	a. Study Area.....	1
	b. Purpose of Study.....	6
	c. NMR Background.....	6
II.	CORE DESCRIPTIONS	
	a. Log Description.....	22
	b. Kaser Well.....	24
	c. McQuiddy Well.....	26
	d. Bowers Well.....	27
III.	METHODOLOGY	
	a. Sample Selection.....	33
	b. Core Analysis.....	33
	c. NMR Measurement and Data Processing.....	35
	d. Thin Section Procedure.....	39
	e. Mercury Pore Measurements.....	42
IV.	RESULTS	
	a. NMR Curves.....	46
	b. Petrography and Core Analysis Data.....	55
	c. Porosity Relationships.....	64
	d. $T_2$ Cutoff.....	67
	e. Timur-Coates Permeability Equation.....	70
	f. SDR Permeability Equation.....	75
V.	CONCLUSIONS	
	a. Recommendations.....	82
APPENDICIES		
	a. Appendix 1 – Thin section analysis.....	86
	b. Appendix 2 - NMR curve descriptions.....	113

---

REFERENCE .....	166
-----------------	-----

## LIST OF FIGURES

Figure	
1. Study Area .....	2
2. Stratigraphic Column of Anadarko Basin .....	3
3. Paleotransport Direction during Morrowan Time .....	5
4. Schematic of $B_1$ and $B_0$ Magnetic fields .....	8
5. Illustration of Rate of Decay and Corresponding T2 Relaxation Times .....	10
6. Illustration of Changes in Magnetization over Time .....	11
7. Multi-frequency NMR Tool Measurements .....	17
8. Alternating Frequencies .....	19
9. Sensitivity of NMR Tool .....	20
10. Paleogeography and Structural Features During the Morrow .....	23
11. Kaser Log 6200' – 6300' .....	25
12. McQuiddy Log 11700' – 11800' .....	29
13. McQuiddy Log 13200' – 13400' .....	30
14. Bowers Log 12800'-12900' .....	31
15. Bowers Log 13600'-13700' .....	32
16. Diagram Illustrating FID .....	37
17. Graduated Microscope Ocular .....	40
18. Diagram of "Box" Used In Thin Section Analysis .....	41

19. Grain Size Measurement Procedure.....	43
20. Example Of MICP Curve.....	45
21. Diagram Illustrating Relationship Between Pore-Groups And NMR Relaxation Times.....	47
22. Crossplot of Weighted $T_2$ vs Average $T_2$ .....	49
23. Thin Section Photo of K 6264.1.....	51
24. NMR Curve for Sample K 6264.1.....	52
25. Thin Section Photo of M 13288.....	53
26. NMR Curve for Sample M 13288.....	54
27. Crossplot of Core Porosity vs Log of Core Permeability.....	56
28. Thin Section Photo of K 6264.1.....	59
29. Crossplot of Core Porosity vs NMR Porosity.....	65
30. Crossplot of Core Porosity vs MICP Porosity.....	66
31. Histogram of Distribution of Swi Cutoff Times.....	68
32. K 6240.6 Swi Curve.....	69
33. K 6249A Swi Curve.....	71
34. Core Permeability- Std Swi Permeability Crossplot.....	72
35. Core Permeability- Swi Permeability-Std C-T Permeability Crossplot.....	73
36. Core Permeability-Calculated Swi Permeability Crossplot.....	74

37. Core Permeability-Std C-T Permeability Crossplot .....	76
38. Core Permeability –Equation 26-Equation 27 Permeability Crossplot.....	77
39. Core Permeability-Calculated C-T Permeability .....	78
40. Core Permeability-Std SDR Permeability .....	80
41. Core Permeability-Calculated SDR Permeability.....	81



## Chapter 1- Introduction

The Morrow Sandstone in the Texas and Oklahoma Panhandles has been a major producer of oil and gas throughout the later half of the 20<sup>th</sup> century. The Morrow Sandstone outcrops in northeast Oklahoma and western Arkansas. The Arkoma Basin in southeast Oklahoma contains stratigraphically equivalent rocks.

Production in the Morrow Sandstone is economical because of relatively large fields that produce oil and gas at moderate depths. Along the shelf of the Anadarko Basin in Oklahoma the drilling depth is approximately 12000-13000 feet. In the Oklahoma Panhandle the depths are shallower and the Morrow Sandstone produces at 8000 feet or less (Andrews, 1999). The Morrow Sandstone mainly produces gas, but oil and condensates are also produced. In 1999 the Morrow Sandstone produced 183 billion cubic feet of gas (BCF) and 3.1 million barrels of oil (MMBO) per year. Over the last twenty years the Morrow Sandstone has produced 7 trillion cubic feet of gas (TCF) (Andrews, 1999).

The Morrow Sandstone is a Pennsylvanian-age sandstone of varying thickness and is recognized over a wide geographic area in the Anadarko Basin. The study area is highlighted in yellow (Figure 1). Figure 2 is a stratigraphic column illustrating the position of the Morrow Sandstone. The Morrow unconformably overlies the Springer Formation. The 13 Finger Limestone unconformably overlies the Morrow Sandstone in the study area.

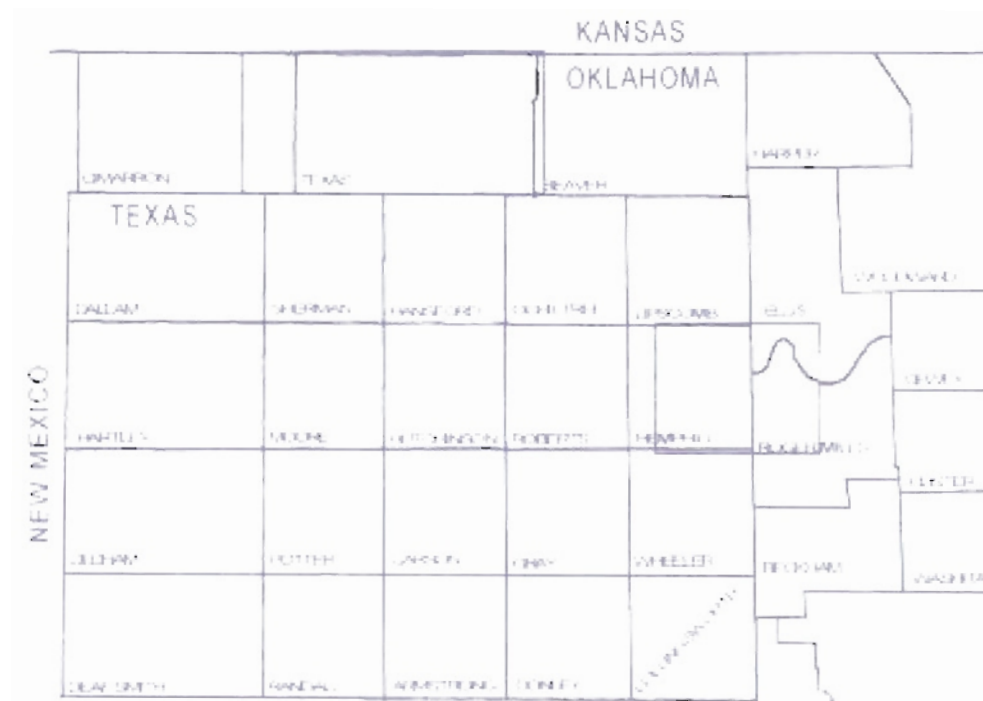


Figure 1. Map of Texas and Oklahoma Panhandles. Study area highlighted. (Modified after Puckette, 1996)

PERIOD	SERIES
	QUATERNARY
	CRETACEOUS
	JURASSIC
	TRASSIC
PERMAIN	GRIOAN GUADALUPIAN LEONARDIAN WOLF CAMPIAN
PENNSYLVANIAN	VIRGILIAN MISSOURIAN DESMOINESIAN ATOKAN MORROWAN
MISSISSIPPIAN	CHESTERIAN MIRAMECTIAN OSAGEAN KINDERHOOKIAN
DEVONIAN	UPPER MIDDLE LOWER
SILURIAN	
ORDOVICIAN	UPPER MIDDLE LOWER
CAMBRIAN	UPPER MIDDLE LOWER
	PRECAMBRIAN

Figure 2. Stratigraphic column of the Anadarko Basin. The Morrow formation is highlighted.

The Morrow Sandstone is commonly divided into two sections, an upper and lower section. In the Panhandles of Texas and Oklahoma, the Upper and Lower Morrow sections are separated by a thick shale (Andrews, 1999). Along the shelf, the Upper and Lower Morrow is separated by a thick shale and a limy unit called the Squaw Belly.

The Lower Morrow in the study area consists mainly of marine sandstones which were deposited as shoreface to transgressive valley fill sands (Puckette, 1996). The deposition of the Upper Morrow in the Texas and Oklahoma Panhandles was controlled by deltaic processes (Puckette, 1996). The dominant sediment transport direction during Late Morrowan time was toward the southwest as illustrated by the arrows on the regional map (Figure 3). The distribution of Morrow reservoirs on the northwest shelf of the Anadarko Basin was controlled by sea level fluctuations. During lowstand of sea level, the shelf was exposed and channels were incised into the shelf. As sea level rose, these channels were filled with fluvial, estuarine, and flood plain sediments (Puckette, 1996). These incised valley deposits are fining upward sequences. During highstand, the valley deposits were covered with sealing marine mud.

The production from the Morrow Sandstone is attributed to different lithofacies in different depositional environments, both marine and nonmarine. Despite the differences in depositional environments, the Morrow Sandstone in the Oklahoma and Texas Panhandles and along the shelf of the Anadarko Basin contains an abundance of microporosity that results in low-resistivity wireline responses. The low resistivity readings result in a higher water saturation calculation from logs than expected for a hydrocarbon-saturated interval. The high water saturation indicates that a well will produce more water (high water cut) than is actually present.

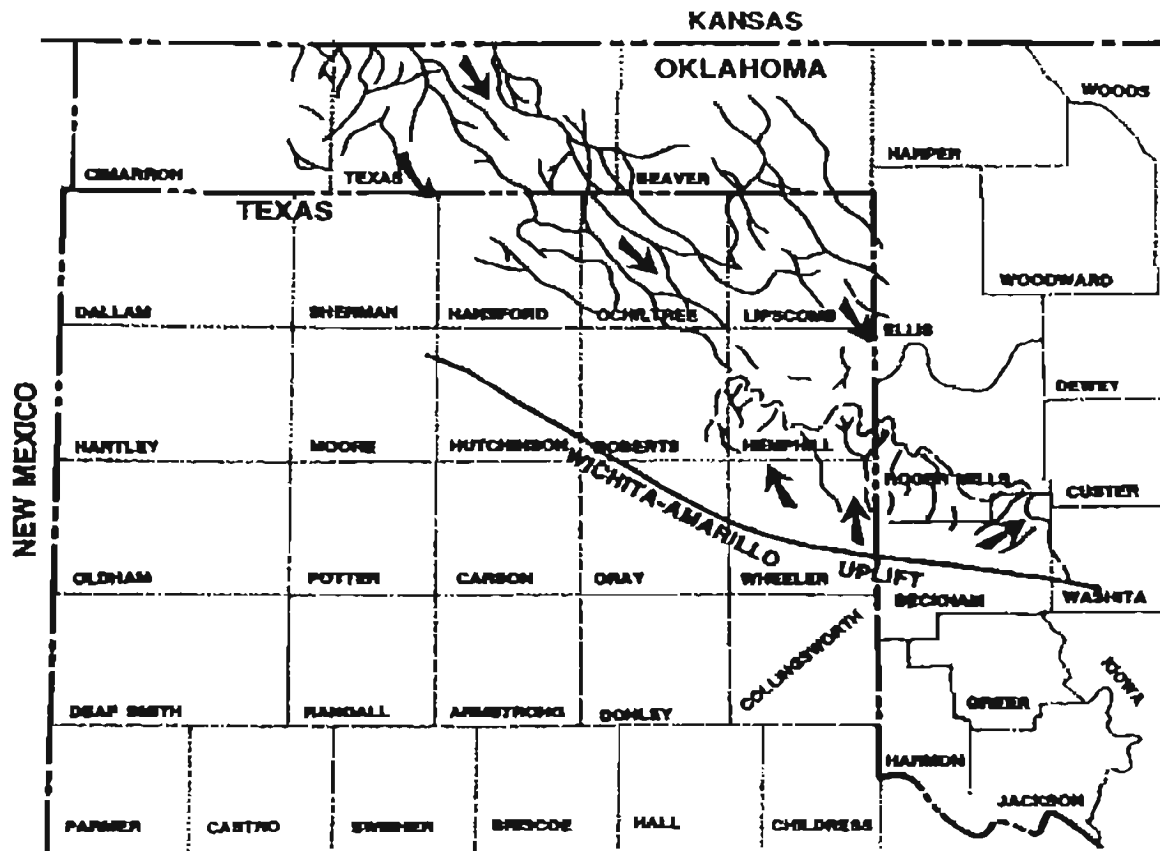


Figure 3. Paleotransport direction during late Morroian time (Puckette, 1996).

Developing new fields requires better tools to more accurately determine reservoir characteristics. The use of the nuclear magnetic resonance (NMR) technique in reservoir modeling can produce better estimates of irreducible water saturation and permeability values. NMR is a technique for estimating porosity, permeability, type of fluid, and the amount of bound and free fluid in the sandstone. The NMR logging tool, which uses some of the same principles as the laboratory NMR instrument, can assist geoscientists in more effectively developing new fields in the Morrow Sandstone when used in conjunction with conventional wireline logs.

The purpose of this study is to use pore geometry information obtained from NMR measurements to understand how microporosity influences Morrow Sandstone reservoir properties response in Hemphill County, Texas and Texas County, Oklahoma. The samples used in this study cover a range of porosity and permeability values and pore sizes found in Morrow sandstones. Core analysis and petrographic data were collected with the intention of providing additional information that helps with the interpretation of the NMR logs. This study also determines which of the NMR conventional permeability equations is most effective in estimating permeability in Morrow Sandstones. The purpose of calculating permeability from NMR is to find a best estimate of formation permeability that can be assigned to specific layers or lithofacies. Improved estimates of permeability are useful for generating more accurate reservoir flow models.

NMR measures the behavior of hydrogen protons in the presence of a magnetic field. The actual experiment is accomplished by altering the spin behavior of the hydrogen protons in the liquid phase in a fully water-saturated core. In this thesis the hydrogen nuclei will be referred to as protons. The protons are initially aligned in a static

magnetic field, often called the  $B_0$  field. The protons precess around the  $B_0$  axis at a frequency dependent upon the nuclei being measured. The frequency of the spinning protons is called the Larmor Frequency ( $f$ ), which is determined by

$$f = (\gamma B_0) / 2\pi \quad (\text{Eqn. 1})$$

where  $\gamma$  is the gyrometric ratio, and  $B_0$  is the strength of the magnetic field (Coates et al., 1999). Each nuclear species has its own gyrometric ratio. Therefore, it is possible to “tune” an NMR experiment in a given magnetic field to detect specific nuclei, e.g.  $H^1$ ,  $C^{13}$ , etc. Moreover, in a given magnetic field, each element has a different Larmor Frequency. The spinning protons also precess about the  $B_0$  field in a low-energy state. The bulk magnetism is the difference between the number of protons spinning parallel to the  $B_0$  field and those spinning anti-parallel to the  $B_0$  field.

The protons are then “tipped”  $90^\circ$  from their original alignment by applying a second magnetic field perpendicular to the  $B_0$  field. This second magnetic field is called the  $B_1$  field (Figure 4). The Larmor Frequency of the  $B_1$  field must equal the frequency of the  $B_0$  field. The application of the  $B_1$  field will excite the protons from a low-energy state to a high-energy state. The angle at which the protons are tipped is calculated by

$$\theta = \gamma B_1 \tau \quad (\text{Eqn. 2})$$

where  $\theta$  is the angle that the protons are tipped,  $\gamma$  is the gyrometric ratio,  $B_1$  is the amplitude of the oscillation field and  $\tau$  is the time  $B_1$  is applied. By increasing the time or strength at which  $B_1$  is applied, the proton-tipping angle will be increased. For this experiment it is important to tip the protons exactly 90 degrees. When the  $B_1$  field is turned off, the protons will begin to dephase and return to their equilibrium state. The receiver coil that measures magnetization in the transverse plane will begin to detect a decay signal.

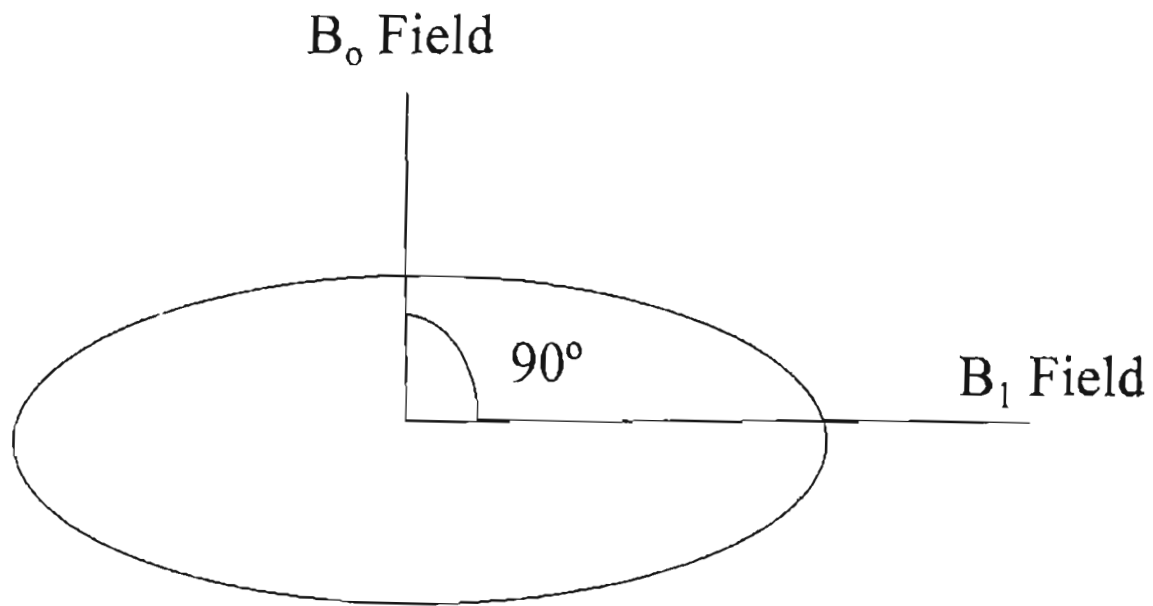


Figure 4. Schematic of the relationship between B<sub>0</sub> and B<sub>1</sub> magnetic fields and the xy measurement plane (indicated by the circle).



Proton decay is exponential and is calculated by

$$M(t) = M_0 e^{-t/T_2} \quad (\text{Eqn. 3})$$

where  $M(t)$  is the measured magnetization at any time,  $M_0$  is the initial magnetization, and  $T_2$  is the first order rate constant that describes the exponential decay of magnetization with time ( $t$ ). The decay occurs in a perfectly homogeneous field.

Departure from this simple exponential decay law can be attributed to inhomogeneities in the static magnetic field or the presence of multiple  $T_2$  relaxation components, e.g. different pore sizes.

Relaxation is characterized by the time constant associated with the return of protons to equilibrium as defined in Equation 3. The initial amplitude of the decay curve is proportional to the number of polarized hydrogen protons in the sample. The shape of the exponential decay curve represents the relaxation time. If the decay curve is short, fast relaxation times will result. A long decay curve will result in slow relaxation times (Figure 5).

There are two major NMR pulse experiments commonly used to characterize fluids in porous media. The first is  $T_1$  relaxation, which is the longitudinal relaxation time. It is important to measure  $T_1$  relaxation because diffusional processes do not affect it.  $T_1$  relaxation also corresponds to the time required for the polarization of protons that is required before executing a CPMG pulse sequence (Carr-Purcell Meiboom Gill), commonly used to determine the  $T_2$  properties.  $T_1$  is the “build up” or polarization of magnetization when the  $B_0$  magnetic field is applied (Figure 6). The arrows at the top indicate the degree of proton alignment as the protons are exposed to the  $B_0$  field.

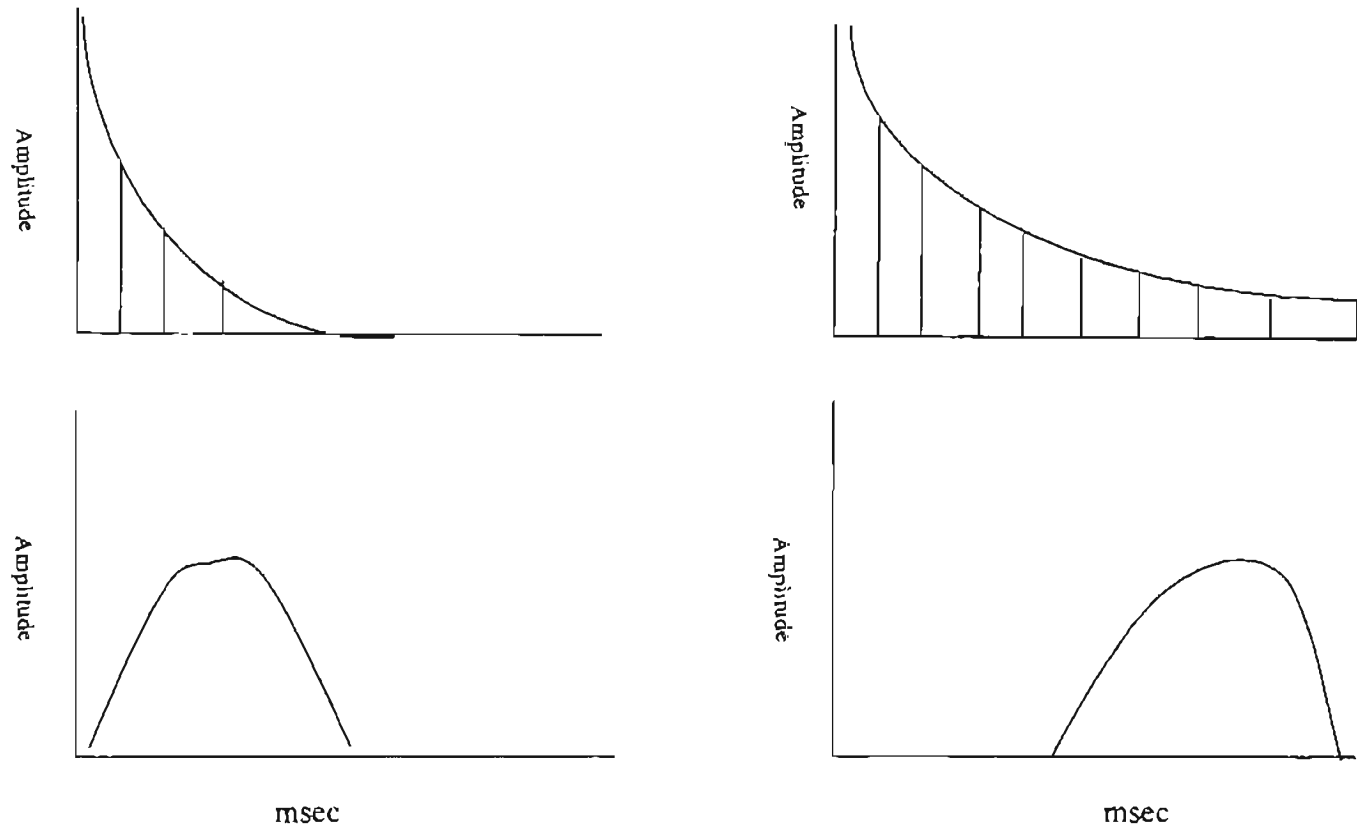


Figure 5. Diagram illustrating how the rate of decay determines the T2 relaxation time. The top figures are the rate of decay curves and the bottom figures represent the corresponding relaxation distributions. Modified after Stambaugh, 2000.

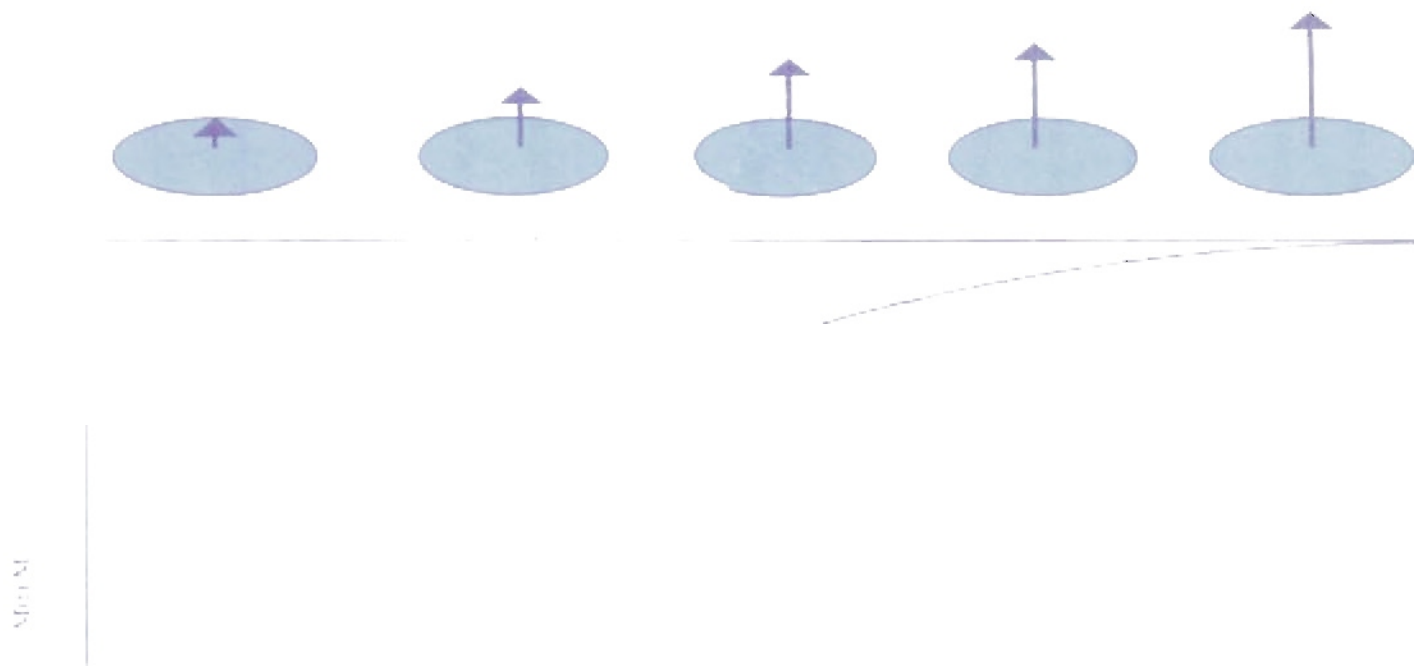


Figure 6 Schematic diagram illustrating changes in magnetization with time (Coates et al., 1999)

Relaxation in the transverse plane is called  $T_2$  relaxation. When the  $B_1$  magnetic field is turned off the protons will begin to lose coherence and a decay signal is detected. The  $T_2$  experiment is the measure of decay in the  $B_1$  direction.

The CPMG pulse sequence will negate the dephasing that is caused by the gradients from the  $B_0$  field. Once dephasing from diffusion occurs, the protons can not be repolarized completely and the spin echo train decays. To monitor the decay in the transverse plane, the NMR tool measures the amplitude of the spin echoes in a CPMG pulse sequence. After the spin echo train is measured, the protons are repolarized and another CPMG pulse sequence begins.

There are three components to  $T_2$  relaxation that are combined in measured  $T_2$  value.

$$1/T_2 = 1/T_{2\text{bulk}} + 1/T_{2\text{surface}} + 1/T_{2\text{diffusion}} \quad (\text{Eqn. 4})$$

The first term in the expression refers to bulk relaxation rate. Bulk relaxation is an intrinsic property of a fluid that is controlled by its physical properties, such as viscosity and chemical composition. In practice, the fluid to be measured is placed in a test tube to minimize surface effects. The test tube represents a pore of infinite size. By minimizing the effects of surface relaxation, the fluid is considered contained in a pore with infinite size.

Surface relaxation occurs at the pore-fluid interface and is the property we are most interested in determining because of the relationship

$$1/T_{2\text{surface}} = \rho S/V \quad (\text{Eqn. 5})$$

where  $\rho$  is the surface relaxivity in units of length/time, and  $S/V$  is the surface area to volume ratio in units of  $\text{length}^{-1}$ .  $S/V$  is a measure of  $1/\text{pore size}$ . Surface relaxivity is a measure of a mineral surface's (pore wall) ability to promote relaxation and varies with

mineralogy.  $T_1$  will speed up the converting mechanism. Conversions to  $T_2$

The last occurs when grain dephasing occurs resulting in the  $T_1$  natural gradient device, i.e. magnetic tool. In a laboratory therefore the extent because of the fast gradient effects  $\lambda$  spacing does not rephase between

In order to  $T_{2\text{surface}}, T_{2\text{bulk}}$  and small number be minimized because dephasing causes. Therefore, under  $1/T_{2\text{surface}} \cdot T_1$  relationship. Diffusion-induced

the distribution of  $T$   
curve.

In a fully saturated  
single exponential decay  
a variety of pore sizes  
mean pore size.  $A_i$   
in a sample:

$$M_s(t) = \sum A_i$$

where  $M_s(t)$  is the total  
pore sizes.  $A_i$  is the  
decay time constant  
 $A_i$  versus  $T_i$  the distribution  
distributions. Two exponential  
pore decays as a single  
independently of one  
large  $A_1$  at a short  $T_2$   
suggests large pores

Procedurally,  
pore sizes are commonly characterized  
curves are used to correlate  
pore sizes. Although MIC  
should be a relationship

mineralogy. The presence of paramagnetic minerals, such as iron bearing minerals, will speed up the relaxation times. Surface relaxivity is a correction factor that aids in converting measurements of time to length. The importance of time to length conversions to permeability will be discussed later in the chapter.

The last component of  $T_2$  relaxation is diffusion-induced relaxation. Diffusion occurs when gradient magnetic fields are present to promote the diffusion process. Extra dephasing occurs as molecules move into an area of different magnetic strength, resulting in the protons precessing at different rates. There are two gradient sources; a natural gradient within the pore and an external gradient imposed by the measurement device, i.e. magnet inhomogeneities, within either a laboratory spectrometer or logging tool. In a laboratory spectrometer the magnetic fields are static homogeneous fields, therefore the external gradient is essentially zero. The internal gradient is evident because of the faster  $T_2$  relaxation times when the echo spacing is increased. Internal gradient effects will increase as the pore size decreases. If there is no diffusion, the echo spacing does not matter. As diffusion becomes important, the ability of the protons to rephase between pulses is lessened.

In order to determine the pore size from measured  $T_2$ , the contributions from  $T_{2\text{surface}}$ ,  $T_{2\text{bulk}}$  and  $T_{2\text{diffusion}}$  must be taken into account. The value for  $1/T_{2\text{bulk}}$  is a very small number because the  $T_2$  for water is very slow (3 sec). The  $1/T_{2\text{diffusion}}$  value is also minimized because the gradients in a static magnetic field are small. The extra dephasing causes a decrease in the  $T_2$  relaxation in that the  $1/T_{2\text{diffusion}}$  value increases. Therefore, under most laboratory conditions the measured  $1/T_2$  is approximately equal to  $1/T_{2\text{surface}}$ .  $T_1$  relaxation is composed of bulk relaxation and surface relaxation. Diffusion-induced relaxation does not affect  $T_1$  relaxation and therefore the changes in

the distribution of  $T_1$  and  $T_2$  might be attributed to diffusion-induced relaxation in the  $T_2$  curve.

In a fully saturated sample, the NMR measurement represents the combination of single exponential decays associated with each distinct pore size. Because rocks contain a variety of pore sizes a single exponential fit to the decay curve will only determine a mean pore size. A multi-exponential decay is needed to describe the range of pore sizes in a sample:

$$M_s(t) = \sum A_i \exp^{-t/T_i} \quad (\text{Eqn. 6})$$

where  $M_s(t)$  is the total magnetization at time (t) the sum of the decaying signals for all pore sizes,  $A_i$  is the number of protons in pores of  $i^{\text{th}}$  size and  $T_i$  is the corresponding decay time constant either  $T_1$  or  $T_2$  associated with pore  $i$  (Kenyon, 1997). By plotting  $A_i$  versus  $T_i$  the distribution of relaxation time is useful in determining pore size distributions. Two assumptions are used with the above formula. The first is that each pore decays as a single exponential. The second assumption is that pores decay independently of one another (Kenyon, 1997). From the relaxation-time distributions a large  $A_i$  at a short  $T_2$  time indicates small pores whereas a small  $A_i$  at a long  $T_2$  time suggests large pores are present.

Procedurally, thin section and mercury injection (MICP) measurements of pore size are commonly compared to NMR distribution curves. MICP size distributions curves are used to confirm the relationship between NMR relaxation times and pore sizes. Although MICP data measures pore throats and NMR measures pore bodies there should be a relationship between the two (Kenyon, 1997).



While NMR responds to pore size and permeability is controlled largely by throat size, it is possible to generate an expression to calculate permeability from NMR results (Kenyon, 1997). Permeability values are measured in milliDarcies, where

$$1 \text{ md} = 1 \text{ micron}^2 \quad (\text{Eqn. 7})$$

From a modification of equation 5 (Kenyon, 1997)

$$L_{\text{NMR}} = V/S = \rho T_2 \quad (\text{Eqn. 8})$$

where  $L_{\text{NMR}}$  is the pore size from NMR measurements. In order to have all the units the same the equation is squared.

$$K_e = c L_{\text{NMR}}^2 = c (\rho T_2)^2 \quad (\text{Eqn. 9})$$

where  $K_e$  is the permeability and  $c$  is a constant. These equations relate NMR pore size from  $T_2$  relaxation to permeability. Changes in  $\rho$  affect permeability, along with pore-throat to pore body-size ratio. There should be a direct relationship between permeability and  $T_2^x$ . The exponent for  $T_2$  should be close to 2 since permeability has units of length squared.

There are two commonly used equations that estimate permeability from NMR measurements, both use porosity and pore size to calculate permeability. The first permeability equation, called the SDR equation, uses the  $T_2$  value to estimate pore size (Kenyon, 1997):

$$K = c * \phi^4 * T_2^2 \quad (\text{Eqn. 10})$$

where  $K$  is permeability,  $c$  is a constant (usually 4 for sandstones), and  $\phi$  is porosity from NMR, conventional logs, or core analysis. The  $\phi$  value is in fractional form.

The second equation, the Timur-Coates equation, uses the free-fluid to bound-fluid ratio to estimate pore size:

$$K = (\phi/c)^4 * (\text{FFL/BVI})^2 \quad (\text{Eqn. 11})$$

frequencies is the  
measurements at  
measurements of  
the rocks being r

The logg  
signal to noise ra  
and measuremen  
CPMG echo train

The anten  
long which deten  
sequence. A long  
will decrease. Th  
stationary. As th  
a rate that is prop

$$VR = L +$$

where VR is the  
speed, TC is the c  
The cycle time is

$$TC = TW$$

where TE is the ex

The depth  
Larmor frequency  
the formation (Fig  
investigation, and



(

$B_0$  field is decrea:

also controls the c

and causes the de

If a washc

cause the NMR p

the mud is hydrog

of the high surfac

NMR sign

correct for the sig

measurement the z

noise is randomly

noise level is redu

The purpos

Morrow Sandstone

reservoir interval.

correlated to Morro

This analysis will b

calculated from NM

core analysis techn

different estimates

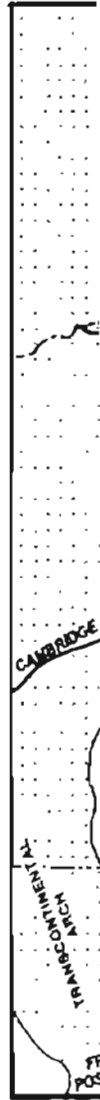
more accurately in

Cores evaluated

B1 and McQuiddy A1  
wells from Hemphill  
basin and are deeper than  
County, Oklahoma (F

The Bowers B  
interest in the McQuiddy  
zone of interest in the  
6269'. The samples from

The well logs show  
spontaneous potential  
The gamma ray log measures  
formation. Shales contain  
therefore, the shales will  
than the sandstones. It  
alone. Shaley sands contain  
Therefore, the resistivity  
measures the resistivity  
than water and therefore



where  $K$  is the permeability,  $\phi$  value is in percent, FFI is the free-fluid volume and BVI is the bound-fluid volume.

The two permeability equations calculate permeability by using porosity and either  $T_2$  measurement or FFI/BVI ratio to describe pore size. The accuracy of permeability calculated from these equations is contingent on whether  $T_2$  and the FFI/BVI ratio actually correspond to pore size.

The application of NMR interpretation models based on ideal laboratory measurements is made more complicated by the difficulties inherent in downhole logging measurements. NMR logging uses the same principals as laboratory measurements. The following is an example of NMR logging techniques.

The Larmor frequency of the protons varies as the tool moves through the formation. The antenna of the tool serves as the oscillating field producer, the transmitter and as the spin echo receiver. The oscillating field (the  $B_1$  field) is applied perpendicular to the  $B_0$  field thus tipping the protons into the transverse plane. The pulse sequences during logging procedures are the same as laboratory measurements.

While the tool is moving through the borehole, the protons are either being aligned with the  $B_0$  field or tipped into the transverse plane. On tools that contain a magnet above and below the sensitive area, the extended magnet polarizes the protons before they enter the sensitive area of the tool. These protons are now ready to be tipped in the sensitive area of the tool. As these protons are being tipped, protons that have already been tipped leave the sensitive area of the tool.

Pulses of different frequencies are applied to the formation in order to measure protons in different sensitive regions (Figure 7). By applying pulses to the formation with different frequencies, quicker measurements can be obtained. The time between



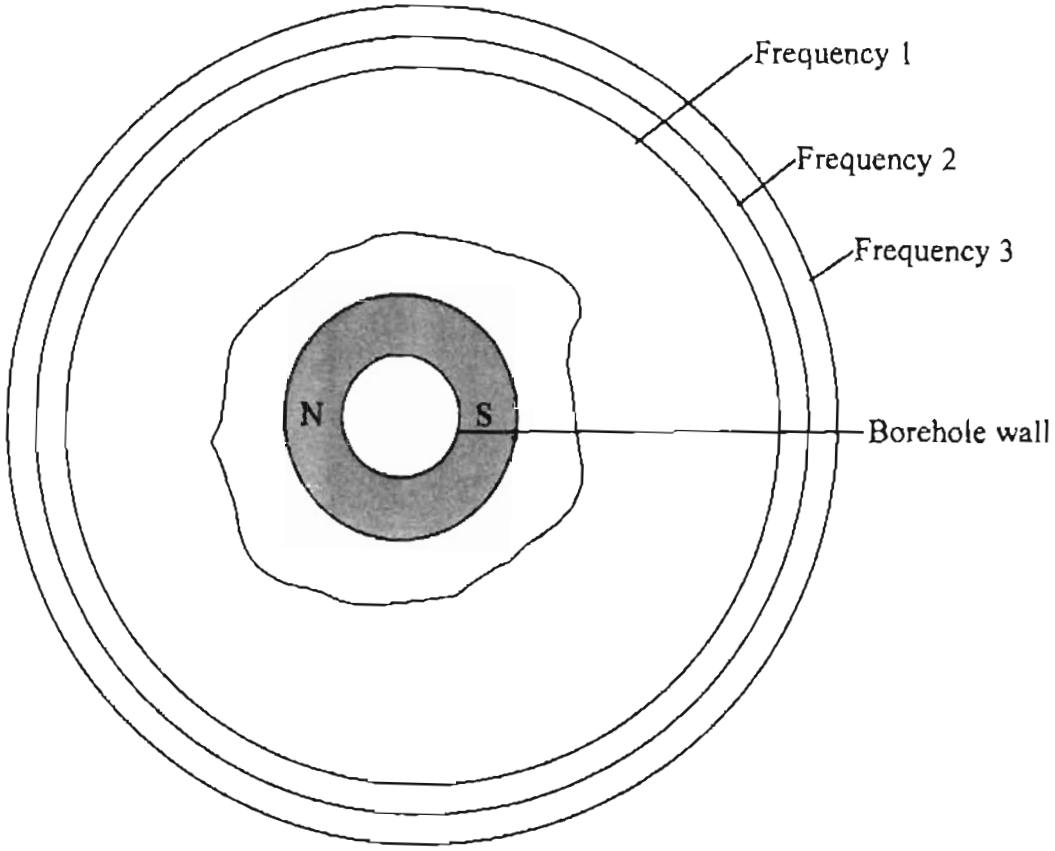


Figure 7. Multi-frequency NMR tool measurements (Modified after Coates et al., 1999)

frequencies is the echo train time, approximately 5 seconds, and the time between measurements at various frequencies is the time to repolarize (TW) at that frequency. If measurements of multi-frequencies are similar, the sensitive volumes are very close and the rocks being measured can be considered the same type of rock.

The logging speed can be increased when using multi-frequencies and the same signal to noise ratio can be maintained. When two frequencies are used, the polarization and measurement of protons is alternated. When frequency 1 is polarizing the protons, CPMG echo trains are be acquired from protons of frequency 2 (Figure 8).

The antenna on a commonly used tool, MRIL<sup>TM</sup>, is usually twenty-four inches long which determines the volume of the formation that is measured by each pulse sequence. A longer antenna will increase the logging speed, but the vertical resolution will decrease. The vertical resolution will equal the antenna length when the tool is stationary. As the tool moves through the borehole, the vertical resolution decreases at a rate that is proportional to the logging speed:

$$VR = L + V (TC * RA - TW) \quad (\text{Eqn. 12})$$

where VR is the vertical resolution, L is the length of the antenna, V is the logging speed, TC is the cycle time, RA is the running time, and TW is the polarization time.

The cycle time is proportional to the number of echoes and the echo spacing:

$$TC = TW + TE * NE \quad (\text{Eqn. 13})$$

where TE is the echo spacing and NE is the number of echoes

The depth of investigation into the formation is related to the field strength and Larmor frequency. The Larmor frequency is tuned to excite protons a certain depth into the formation (Figure 9). Figure 9 shows the sensitive volume, which is the depth of investigation, and how this volume relates to the frequency of  $B_0$ . If the frequency of the

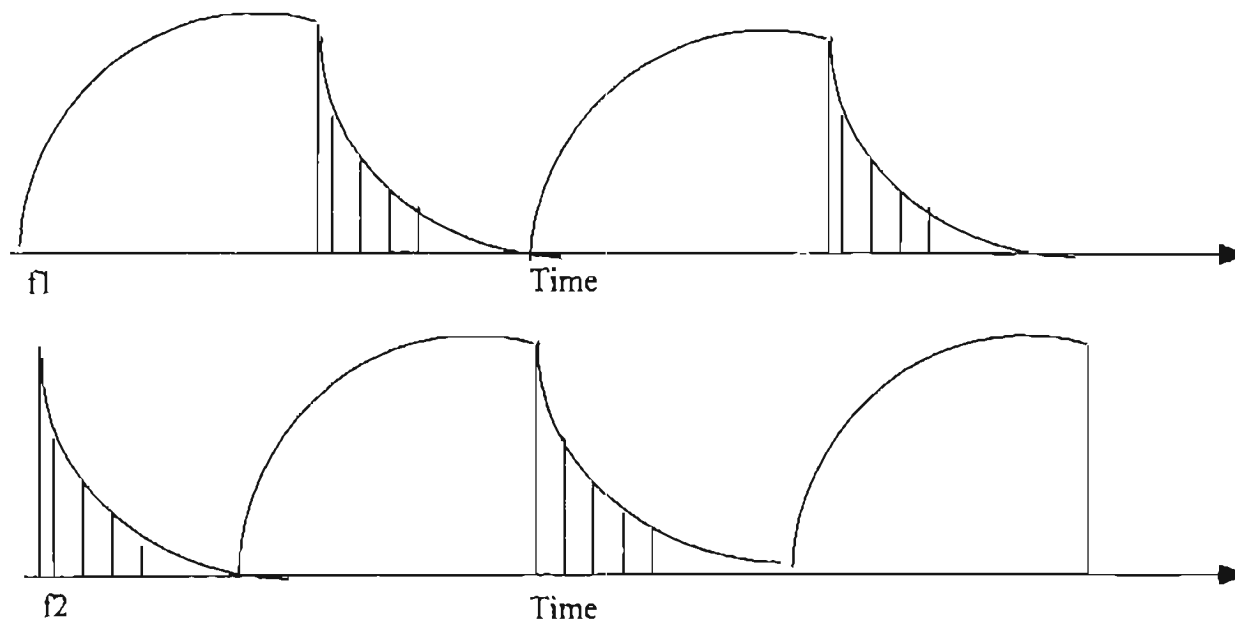


Figure 8. Alternating frequencies (Modified after Coates et al., 1999).

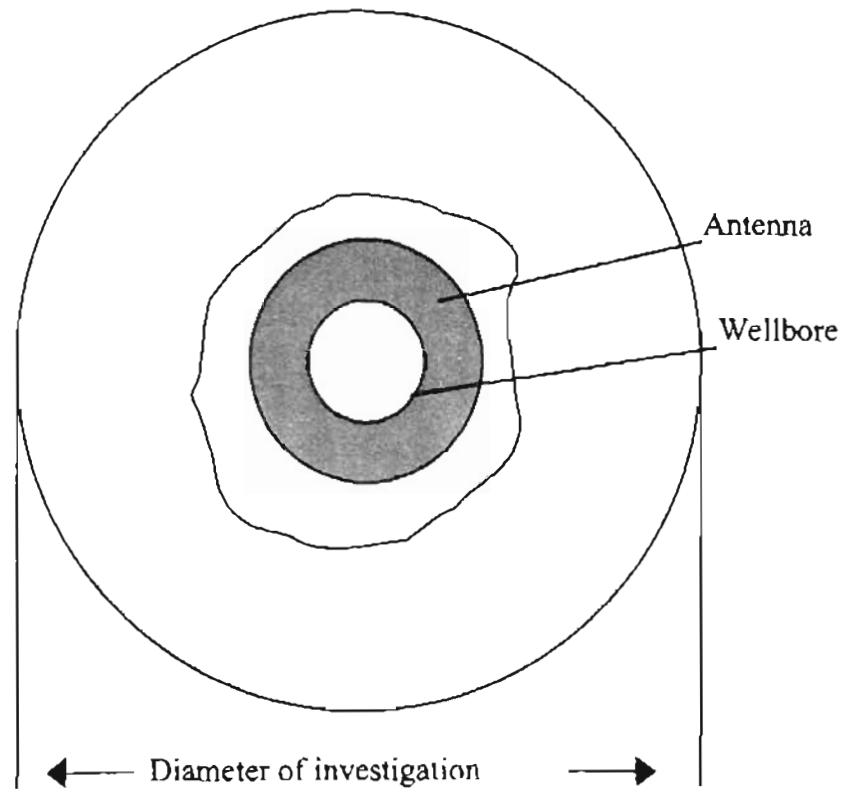


Figure 9. Schematic of diameter of NMR tool investigation (Modified after Coates et al., 1999)

$B_0$  field is decreased, the depth of investigation will decrease. The magnet's temperature also controls the depth of investigation. As the magnet gets hot the  $B_0$  field decreases and causes the depth of investigation to decrease.

If a washout intersects the sensitive area of the tool, the borehole fluids will cause the NMR porosity and the bound fluid volume to be overestimated. The fluid in the mud is hydrogen rich and the relaxation times of these protons are very fast because of the high surface area of the mud grains.

NMR signals are very weak and it is difficult to determine signal from noise. To correct for the signal-to-noise ratio several readings are stacked. By repeating an echo measurement the amplitude and position of the echo signal will remain the same. The noise is randomly distributed. Therefore by stacking and averaging several echoes the noise level is reduced.

The purpose of this study is to examine laboratory NMR responses in the Morrow Sandstone and to relate these responses to the microporosity systems in the reservoir interval. The analysis of the NMR relaxation distribution times will be correlated to Morrow rock properties, including pore types as viewed in thin section. This analysis will help geoscientists better use NMR data. In this study, permeability calculated from NMR data is compared to permeability as measured by conventional core analysis technique. By noting geologic reasons why the two techniques yield different estimates of permeability, geoscientists will be able to calculate permeability more accurately in the Morrow Sandstone in the study area.

## Chapter 2 – Core Descriptions

Cores evaluated in this study are from wells in Hemphill County, Texas (Bowers B1 and McQuiddy A1) and in Texas County, Oklahoma (Kaser #2R). The Morrow wells from Hemphill County, Texas are located on the northwest shelf of the Anadarko basin and are deeper than the other study well located on the edge of the basin in Texas County, Oklahoma (Figure 10).

The Bowers B1 interval of interest ranges from 13605' – 13631'. The zones of interest in the McQuiddy A1 are found from 11880' – 11887' and 13267' – 13355'. The zone of interest in the Kaser 2R well (Texas County, Oklahoma) ranges from 6240' – 6269'. The samples from these cores represent a range of lithologies.

The well logs available from the study wells include gamma ray logs, spontaneous potential (SP) logs, sonic log (interval transit time), and resistivity logs. The gamma ray log measures the amount of potassium, thorium, and uranium in the formation. Shales contain more potassium, thorium, and uranium than sandstones; therefore, the shales will have a higher gamma ray response or inflection to the right, than the sandstones. It is difficult to determine sand from shale by gamma ray response alone. Shaley sands contain a lot of clay that increases the gamma ray response. Therefore, the resistivity log is useful in determining sand from shale. The resistivity log measures the resistivity of the fluid in the formation. Hydrocarbons are more resistive than water and therefore will have a higher resistivity reading than the shales.

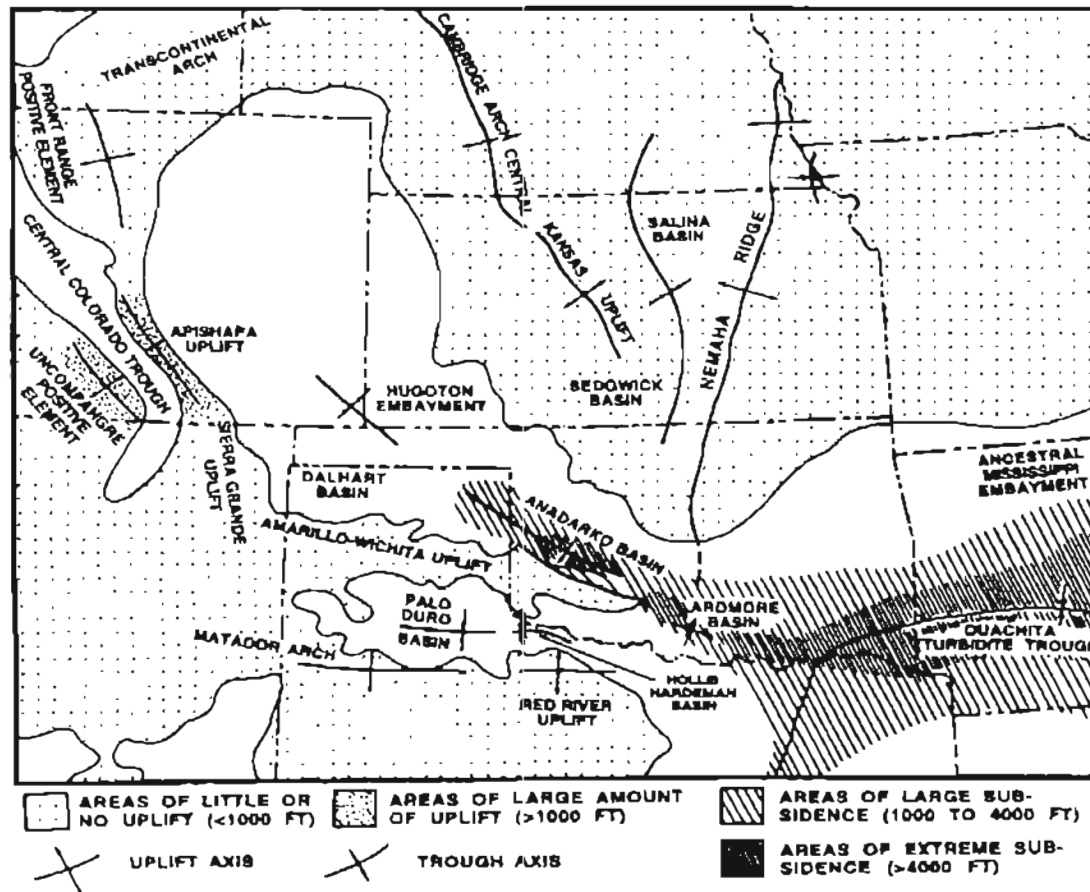


Figure 10. Paleogeography and structural features during Morrowan time (Puckette, 1996)

The SP log is used to determine the presence of impermeable beds (shale) from permeable beds (sand). The presence of shale in a sandy interval will cause a reduction (deflection to the right) in the SP. Shales have a fairly consistent SP response so the shale reading for a log is called the shale base line. Deflection from the shale base line is a measure of the sand content in the interval. Sand will deflect to the left of the shale base line.

The sonic log is a measure of interval transit time, which is a compressional sound wave traveling through the formation. The interval transit time is the reciprocal of the velocity. The interval transit time is dependent upon lithology and will be slower in shales than in sands. The presence of hydrocarbons in the formation will increase the interval transit time.

The Kaser well log (Figure 11) contains a gamma ray curve and a porosity log. The gamma ray log depicts sand between 6238' to 6263'. The porosity log for the Kaser well fluctuates between 16% to 30% between the interval of 6240' to 6267'. Figure 11 is the Kaser well log, showing the gamma ray log in the left track and the porosity log on the right.

The base of the Kaser interval (6269'-6262') is a black shale lithofacies that is overlain by 15' of a moderately sorted, fine to coarse grained, gray sandstone (following Folk's 1974 textural classification). The black shale is indicated on the Kaser well log (Figure 11) by the gamma ray deflection to the right that continues onto the left side of track 1. A one-foot thick black shale divides the 15' of sandstone, which was determined from the core description. The sandstone contains thinner intervals (4"-6") that fine upward from coarse grain size at the base to fine grain size at the top. Thin laminae of shale are scattered throughout the interval with more shale below the one-foot shale



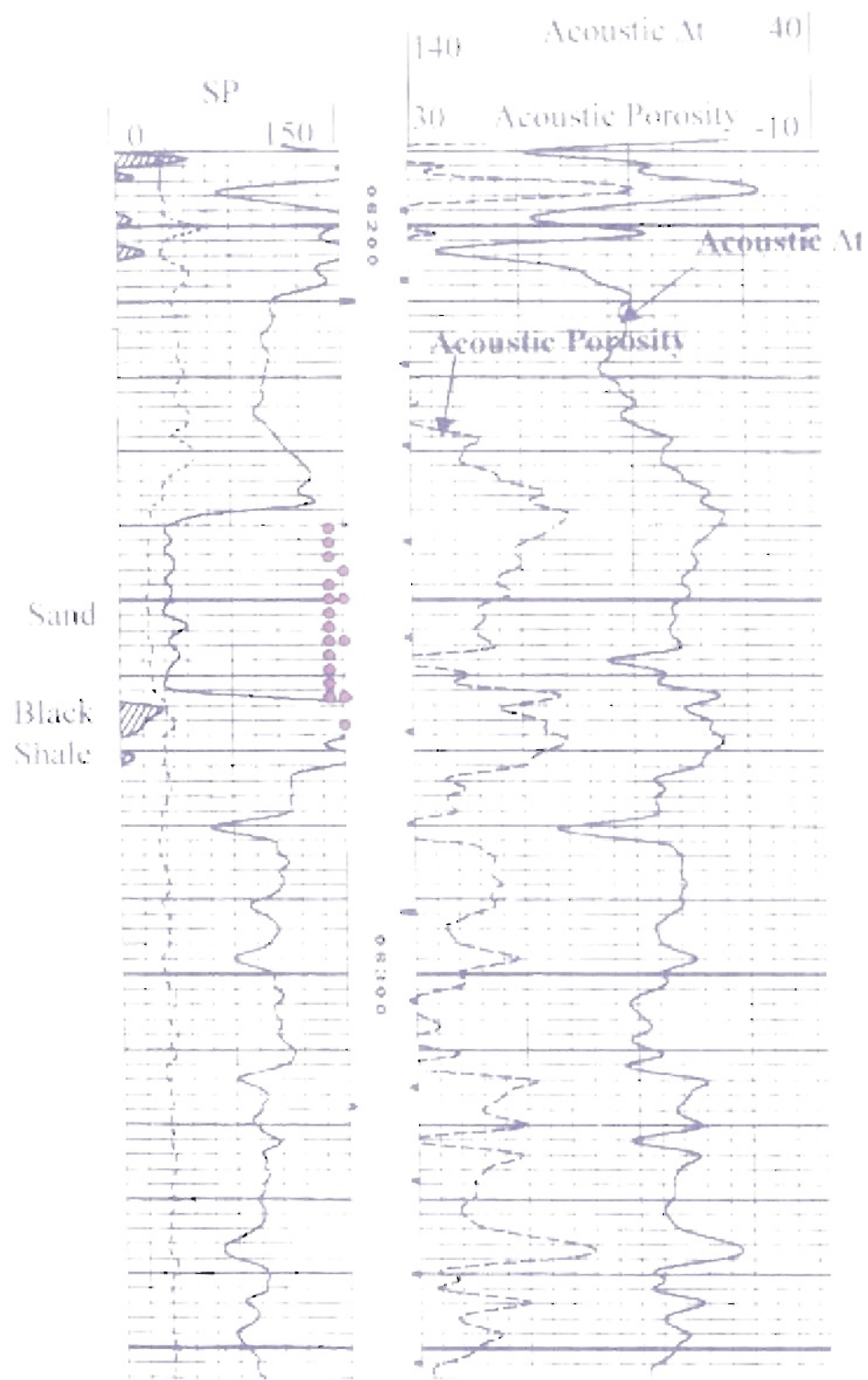


Figure 11. Kaser Log 6200' - 6300'

interval than above.

The overlying interval (6251' -- 6243') contains 9' of moderately sorted, gray sandstone. As with the lower interval just described, this interval contains fining-upward sequences, ranging in grain size from very-coarse sand at the base to very-fine sand at the top. The core also contains a one-foot interval (6248') of coarse-grained sand. Shale laminae, observed lower in the section, are absent from this interval. The top three feet of the Morrow in the Kaser is gray shale that contains hints of red and green color.

The base of the McQuiddy A1 (13303') has 9' of gray medium grained, moderately sorted sandstone, that is interbedded with dark gray to black shale. Contained in this interval are abundant shale nodules (shale rip-ups). The nodules are about one inch in length. This interval is overlain by 2' of gray, coarse grained, moderately sorted sandstone. This is overlain by 3' of gray, medium grained, moderately sorted sandstone. This interval is similar to the basal interval except that it is interbedded with shale laminae rather than shale beds. There are few shale nodules (rip-ups) present.

The upper 6' (13288'-13283') of the McQuiddy well is a gray, coarse to medium grained, moderately sorted sandstone. This interval is composed of two 3' thick fining-upward cycles. Thin shale laminae are present throughout this interval. Core plugs were taken at 13302', 13291', and 13288'. All the samples come from the fine sand portion of the fining upward sequence.

The upper section of the McQuiddy A1 (11886'- 11880') contains 5' of gray, coarse grained, well-sorted sandstone. This is overlain by 2' of gray medium grained sandstone. Within this 2' interval, thin shale laminae are present. The top foot of this section returns to the gray, coarse grained, well-sorted sandstone. Minor amounts of

shale laminae are present. Core plugs were taken at 11888' and 11886'.

The gamma ray log is in track 1 of the McQuiddy well log (Figure 12 and 13). At 11890', the gamma ray log is inflected to the left, indicating sandstone. From 11890' - 11850', the gamma ray shifts to the right, and is in the shape of a "Christmas Tree", indicating a fining-upward sequence. The resistivity log in track 2 records an increase in resistivity from 11890' - 11850'. Sandstones that contain hydrocarbons commonly record a higher resistivity than shales.

The gamma ray log for the deeper section of the McQuiddy well, 13300' - 13250', is inflected to the left, indicating sandstone. The resistivity curve for this same zone records a high resistivity reading.

The Bowers B1 core is unslabbed and lithology was difficult to describe. The basal interval of the Bowers B1 well consist of 17' (13631'-13615') of gray, coarse grained, well-sorted, siltstone. This is overlain by 10' of gray, fine-grained, well-sorted siltstone. Core plugs were taken from 13629' and 13624'.

The upper interval of the Bowers B1 (12820'-12800') is alternating, dark gray, very fine-grained sandstone and shale. The layers of sandstone are from 7 to 10' thick. As with the lower section of the Bowers, the core is still whole and sedimentary features were difficult to detect. A core plug was taken at 12807'.

The Bowers well log (Figure 14 and 15) contains a gamma ray. The gamma ray curve from 12900' - 12800' shows no variation over this interval. The resistivity curve from 12880' - 12870' shows a strong spike indicating sand. From 12830' - 12800' the resistivity curve contains spikes which indicate zones of sandstone.

The gamma ray log for the deeper section of the Bowers well (13660'-13630') shows a slight inflection to the left indicating a sandstone. The resistivity log for the

section shows a strong spike, also indicating the presence of sandstone that may contain hydrocarbons.

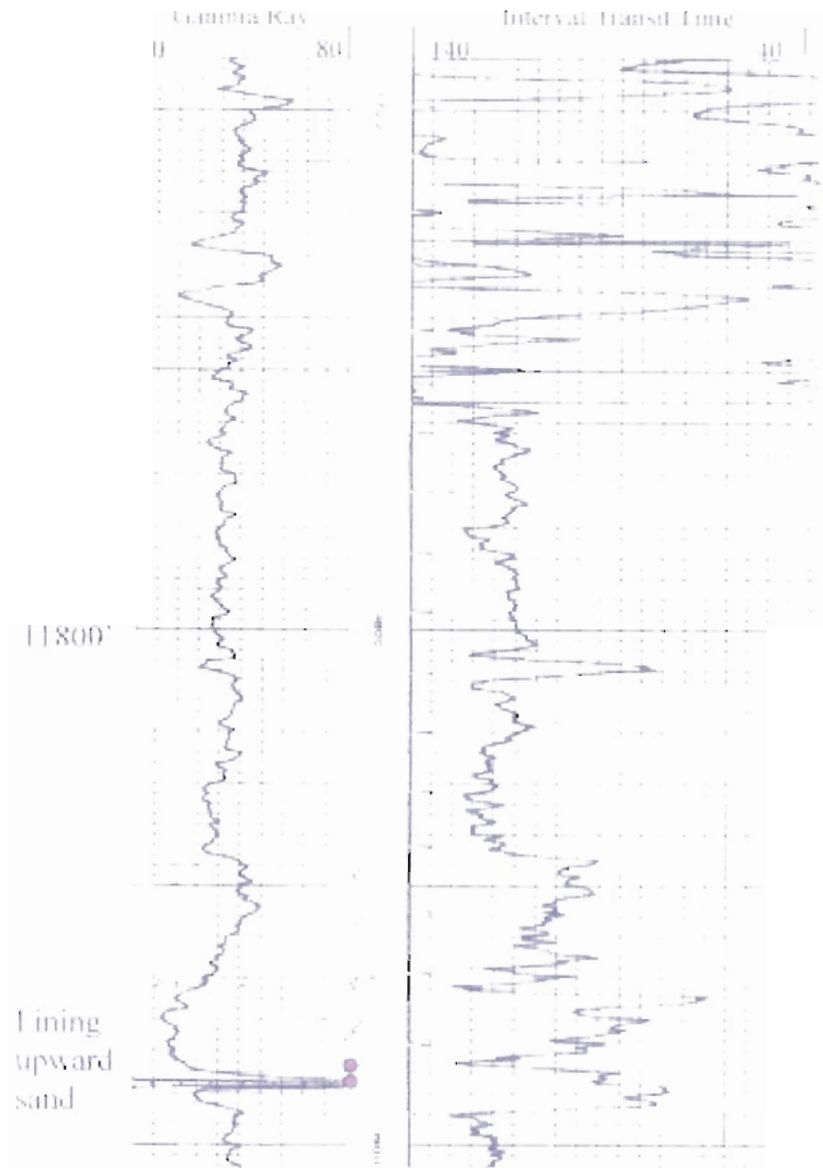


Figure 12 McQuiddy log 11700' - 11900'.

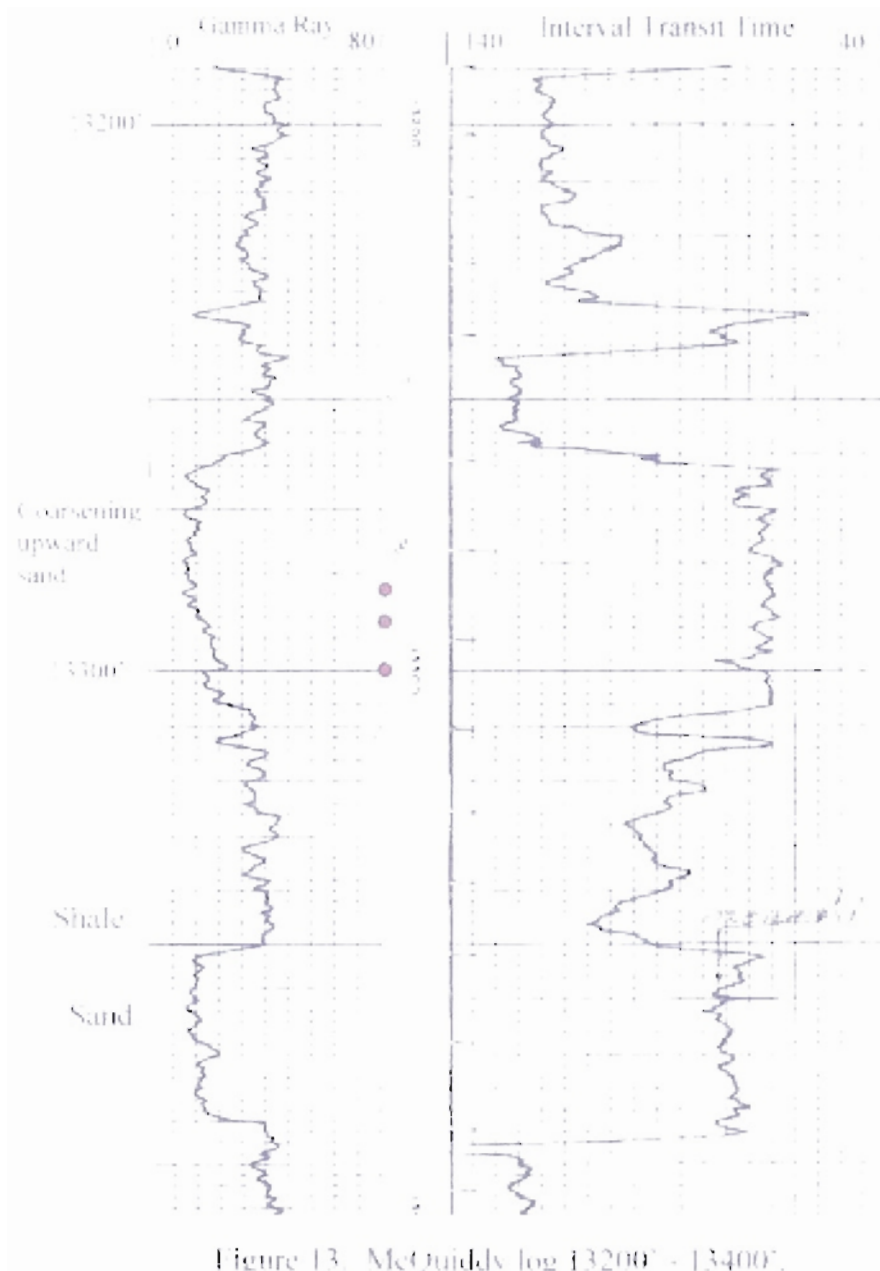


Figure 13. McQuiddy log 13200' - 13400'.

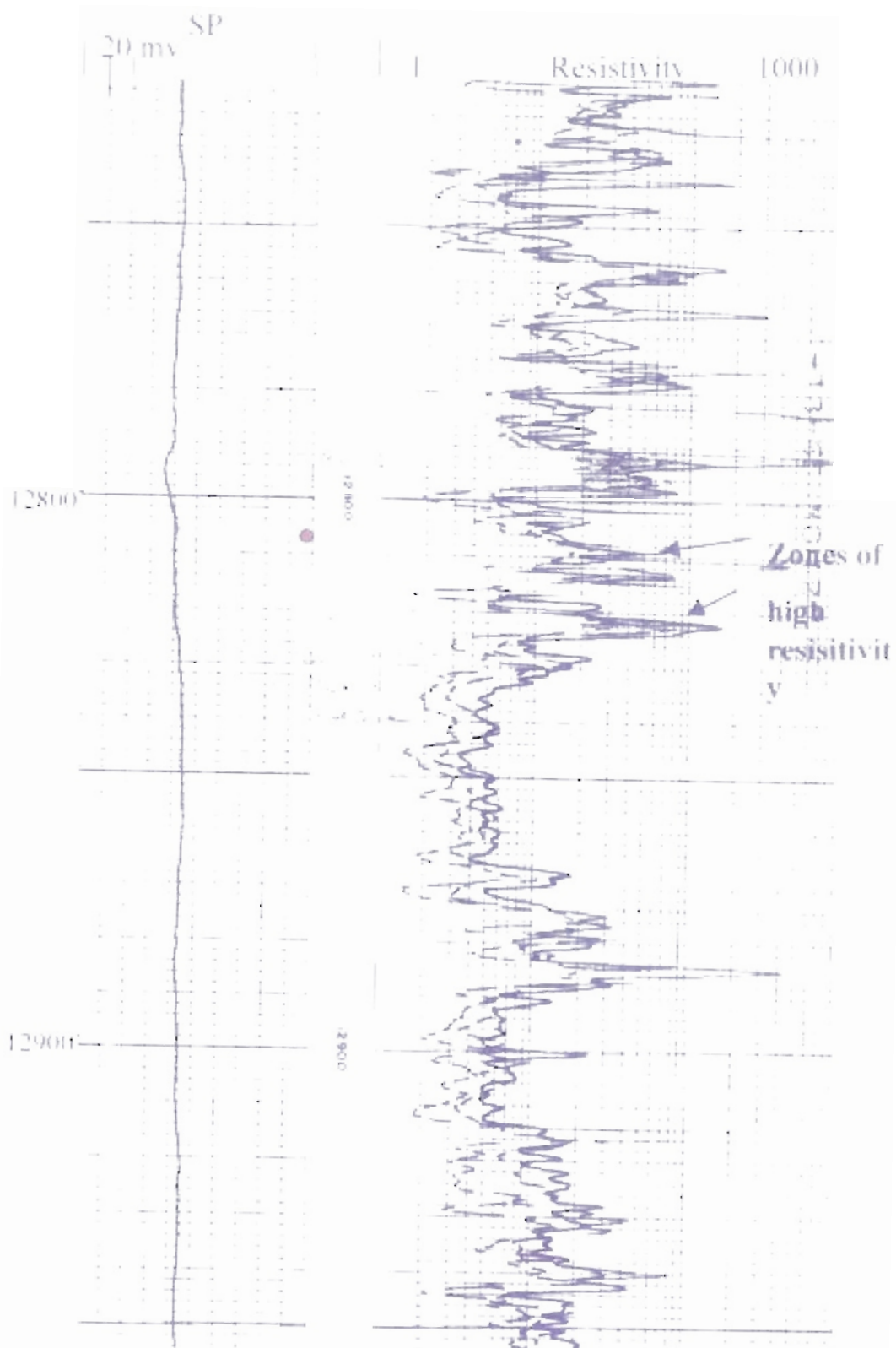


Figure 14. Bowers 12800' - 12900'

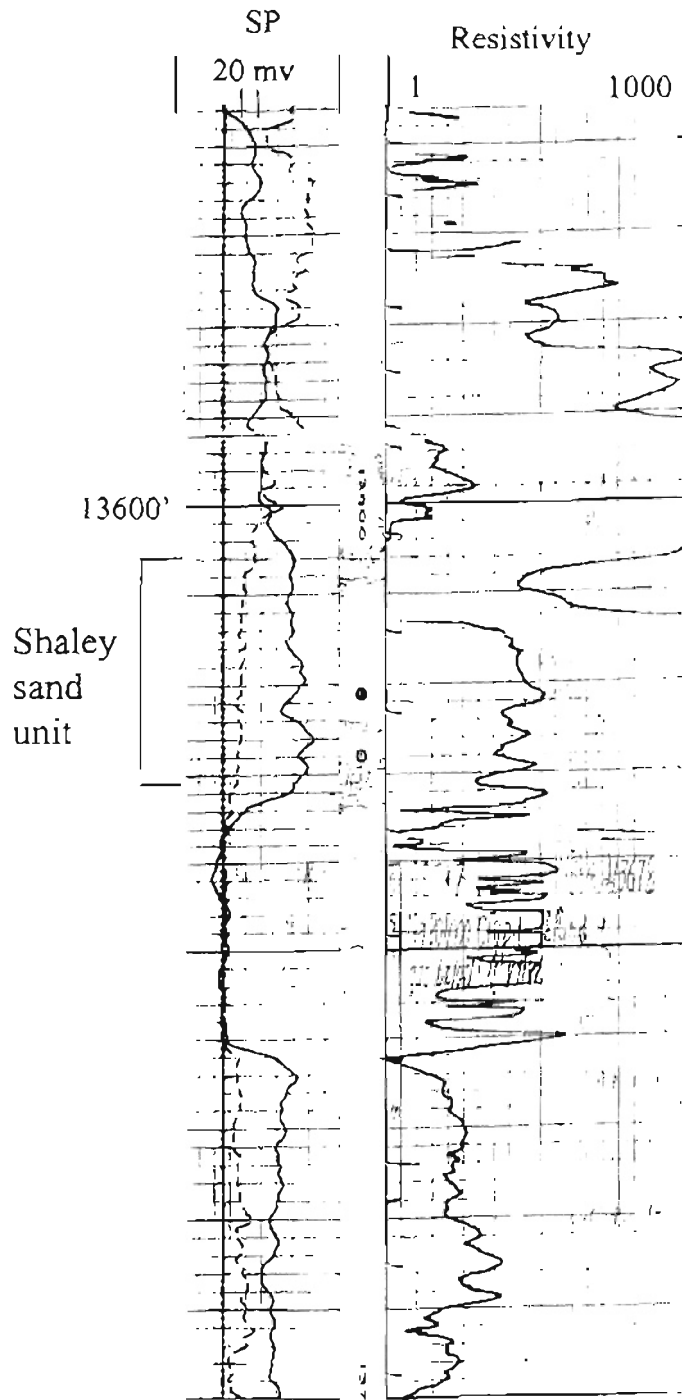


Figure 15. Bowers BI log,  
13600' - 13800'



## Chapter 3 - Methodology

### Sample Selection

The samples from the McQuiddy and Bowers wells were purposely selected from intervals of varied texture or grain size. The samples from the Kaser well in Texas County, Oklahoma were chosen from a well used in an earlier study by Phillips Petroleum Company (Caldwell, personal communication, 2000).

Core plugs were cut using a one and half-inch diameter bit. The bit was cooled with running tap water so that it would not overheat. The core plugs were air dried for 24 hours and placed in a Soxhlet cleaning unit. A Soxhlet is a distillation unit that uses alternating cycles of methanol and toluene to clean core plugs by removing any residual hydrocarbon. Once the samples were cleaned of hydrocarbons, they were dried at room temperature for 24 hours and placed in a vacuum for over 24 hours at 160° F. It is important to remove the water associated with clay or the porosity measurement will be under-estimated. Once the samples were dried they were placed in a humidity-controlled sample container to keep moisture constant. Trim ends were cut from these plugs for thin section preparation and MICP analysis.

### Core Analysis

The following procedures are standard core analysis methods. The samples were wrapped in Teflon and weighed in a closed balance. The closed balance was used to ensure air movement outside the balance does not interfere with the weighing of the

sample. The length and diameter of the samples were measured. These measurements were used to calculate bulk volume, a determination that is needed to calculate porosity and permeability of the samples. The samples were also weighed in mercury. The sample's bulk volume is determined by a standard mercury immersion method in which

$$V_b = W_{tHg} / (- T_{Hg} * 0.0013611 + 13.63837) \quad (\text{Eqn. 14})$$

where  $W_{tHg}$  is the weight of sample immersed in the mercury and  $T_{Hg}$  is the mercury temperature (unpublished Phillips Petroleum Company (PPCo) internal spreadsheet).

Note in Eqn. 14 that the temperature of the mercury is multiplied by a very small number.

Consequently, the equation simplifies to

$$V_b = W_{tHg} / 13.6 \quad (\text{Eqn. 15})$$

where  $V_b$  is the bulk volume in  $\text{cm}^3$ ,  $W_{tHg}$  is the weight of the mercury in grams and 13.6 is the density of mercury in  $\text{grams}/\text{cm}^3$ .

The porosity was determined using the Boyle's Law of gas expansion method (Dullien, 1992). The sample was placed in a container with a known volume and a known volume of gas pressure was applied. The change in the hydrostatic pressure ( $P_1$  and  $P_2$ ) was used in determining porosity. These pressure values were entered into a spreadsheet along with the length, diameter, and weight to calculate porosity. The porosity (in percentage form) was calculated in the PPCo spreadsheet by dividing the pore volume by the bulk volume. The pore volume is defined as:

$$V_p = V_b - V_g \quad (\text{Eqn. 16})$$

where  $V_p$  is the pore volume,  $V_b$  is the bulk volume and  $V_g$  is the measured grain volume (Dullien, 1992).

The permeability was determined by measuring the flow rate of gas (nitrogen) through the core plug at various pressure gradients in order to solve Darcy's Law

(Dullien, 1992). Darcy's Law is expressed as

$$Q = k \Delta P/L v \quad (\text{Eqn. 17})$$

where  $Q$  is the flow rate in  $\text{cm}^3/\text{s}$ ,  $\Delta P/L$  is the pressure gradient in  $\text{atm}/\text{cm}$ ,  $v$  is the viscosity of the fluid in centipoise, and  $k$  is the permeability. The gas flow measurements were entered into the PPCo spreadsheet and the permeability was calculated with the following expression:

$$k \text{ (length}^2\text{)} = 1000 (2 * CP \text{ (viscosity)} * \text{flow (cm}^3\text{/s)} * \text{pressure (atm)} * \text{diameter (cm)}) / \text{area (cm}^2\text{)} * (P1^2 - P2^2) \text{ (atm)} \quad (\text{Eqn. 18})$$

The units for the parameters in the above permeability equation are indicated by the terms in italics enclosed by parentheses following each of the variables. The unit of permeability will be in  $\text{cm}^2$ , which is equal to md.

#### NMR Measurement and Data Processing

To prepare the samples for NMR measurements the samples were placed in a vacuum cell to remove air and moisture. The samples were then saturated with a 3.3% NaCl solution while under vacuum. This step improves the filling of the smaller pores with brine. The saturated samples and the brine solution were placed in a closed bottle within a pressure cell and pressurized with oil up to 2000 pounds forcing the 3.3% NaCl solution into the pores. The samples remained stored in the 3.3% NaCl solution during the course of the study.

The NMR bench top spectrometer used in this experiment is a Maran-II made by Resonance Instruments Ltd. The Maran-II uses a 2.0 MHz resonance frequency to align hydrogen protons. The temperature is controlled at 35°C to maintain magnetic stability. A core sample was placed into a glass cylinder to align the sample with the magnetic field. The magnetic field applied to the sample is aligned along the  $B_0$  axis. The Maran-II

receiver coil has a sensitive zone that is approximately 1 to 1.5 inches in length. If the sample is only partially exposed to the magnetic fields, the NMR signal intensity, which is used to calculate porosity, will be underestimated.

The first NMR computer program used in the analysis procedure is called Free Induction Decay (FID). The FID program measures the proton decay after a single  $90^\circ$  pulse (Figure 16). From this single pulse and its decay, the parameters that are used in the CPMG and INVREC (inversion recovery) programs are determined. These parameters include the receiver gain, P90, P180, O1 and relaxation decay. The receiver gain (RG) parameter is the voltage gain of the system. At the beginning of a pulse sequence, a low-level signal is applied and the received signal is compared to the original signal. The gain compensates for the signal loss across the system.

The P90 parameter is the parameter that defines the time that a radio frequency pulse is applied in order to rotate the protons  $90^\circ$  from their original orientation. If the protons are originally precessing about the  $B_0$  field, the P90 pulse will rotate the protons to precess in the transverse field. The P180 parameter is the parameter that defines the time that a radio frequency pulse is applied. This pulse rotates the protons  $180^\circ$  from their original orientation.

The O1 parameter is the frequency offset of the spectrometer from the base frequency, which is approximately 2 MHz. Variations in temperature, magnet stability, etc. alter the strength of the magnet so that its resonance frequency is not exactly 2.0 MHz. Therefore, the offset tuning adjusts the resonance frequency in units of Hz. If the offset is less than 1000 Hz (or 1KHz), then the offset is within 1 part per thousand of the set signal frequency.

The relaxation decay, RD, is the time between the end of a scan and the beginning

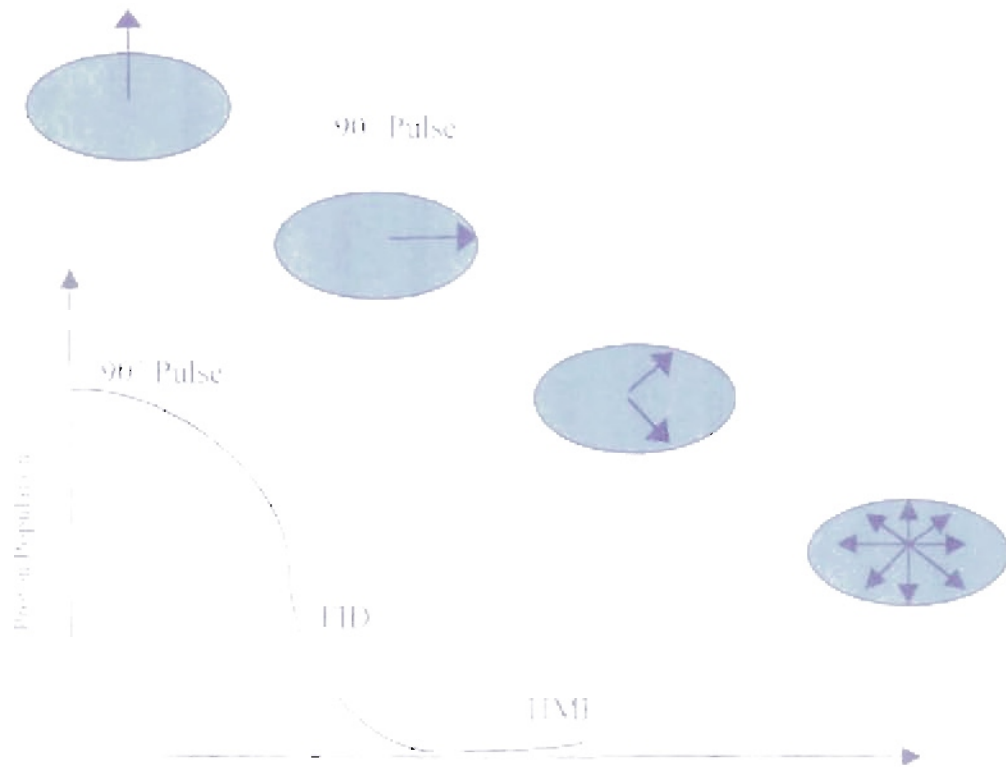


Figure 16. Diagram illustrating FID (Modified after Coates et al., 1999)

of the next  $90^\circ$  pulse. This time allows the magnetization of the sample to return to equilibrium before the next pulse. The RD is usually five times the  $T_1$ . These parameters are used in all relaxation experiments.

The following parameters are varied according to the character of the samples being measured: 1) number of scans, 2) the number of echoes, and 3) the pulse gap,  $\tau$ . The number of scans, NS, represents the number of complete pulsed experiments that are collected. More scans result in better quality data but the more scans you collect the longer the experiment takes. The number of echoes, NE, determines the length of each pulsed experiment in time. The more echoes collected, the longer the experiment time. The actual experiment time is calculated by multiplying the NE by the echo spacing,  $\tau$ . The experiment should have a length sufficient to allow all of the relaxation components to be measured. The  $\tau$  time needs to be chosen carefully; too fast inter-echo times will reduce the effect of diffusion on the CPMG measurement. If a  $\tau$  time is too long between echoes, part of the signal can be lost due to diffusion. The RD needs to be long enough to ensure proper polarization of protons before each CPMG pulse sequence. For the Morrow samples, 32 or 64 scans were applied. The number of echoes was 4096, and a  $\tau$  of  $300\mu\text{s}$  was used for these experiments. The CPMG pulse sequence was applied to the sample to measure the  $T_2$  relaxation times. From the CPMG pulse sequence, average  $T_2$  time and decay amplitudes were given.

The inversion recovery program, INVREC, applies a  $180^\circ$  pulse to align the protons  $180^\circ$  from  $B_0$  and then  $90^\circ$  pulses are applied. The inversion recovery program measures the average  $T_1$  time and the  $T_1$  decay.

The raw echo train data from  $T_1$  and  $T_2$  are transformed into a distribution of 30 single-exponential relaxation times. This is done by using a regularized nonlinear least

squares minimization procedure (Kenyon, 1997). The amplitudes from this minimizing procedure are plotted against time to produce the NMR distributions.

### Thin Sections

The thin section description of composition and texture is important in order to establish relationships among the petrographic properties, pore structure, and NMR measurements. The thin sections were prepared from the trim ends of the core plugs by Mineralogy Inc (Tulsa, OK). Blue epoxy was injected under a pressure of 1500 psi, to ensure that the epoxy entered all the smaller micro-pores. Samples with an average grain size of 4 mm or more were prepared as oversized thin sections and the samples with an average grain size less than 4 mm were prepared as standard thin sections. The samples were prepared as standard 30 microns thick thin sections.

A Zeiss petrographic microscope was used to observe the thin sections. The microscope contains a mechanical stage for use in point counting the petrographic thin sections. The microscope contains objectives of 2.5x, 10x, 16x and 30x magnification, and a graduated ocular (Figure 17). The ocular is fitted with a micrometer that is divided into ten increments; these increments are further divided into smaller subdivisions.

A nonstandard technique for point counting the thin sections was used. The technique is a modification of the Delesse (1847) method for measuring volume percentages based on area of minerals exposed on the surface of a thin section. The number of areas used to estimate composition per thin section was determined by using a grid size slightly smaller than the largest grain. For example, if the largest grain was 5 mm, then a grid size of 4 mm was used. For a grid size of 4 mm, a point count of 100 points was completed in each grid of the 4 mm square grids. A point count within a grid block consisted of estimating a "box" defined by the graduated ocular (Figure 18), ten

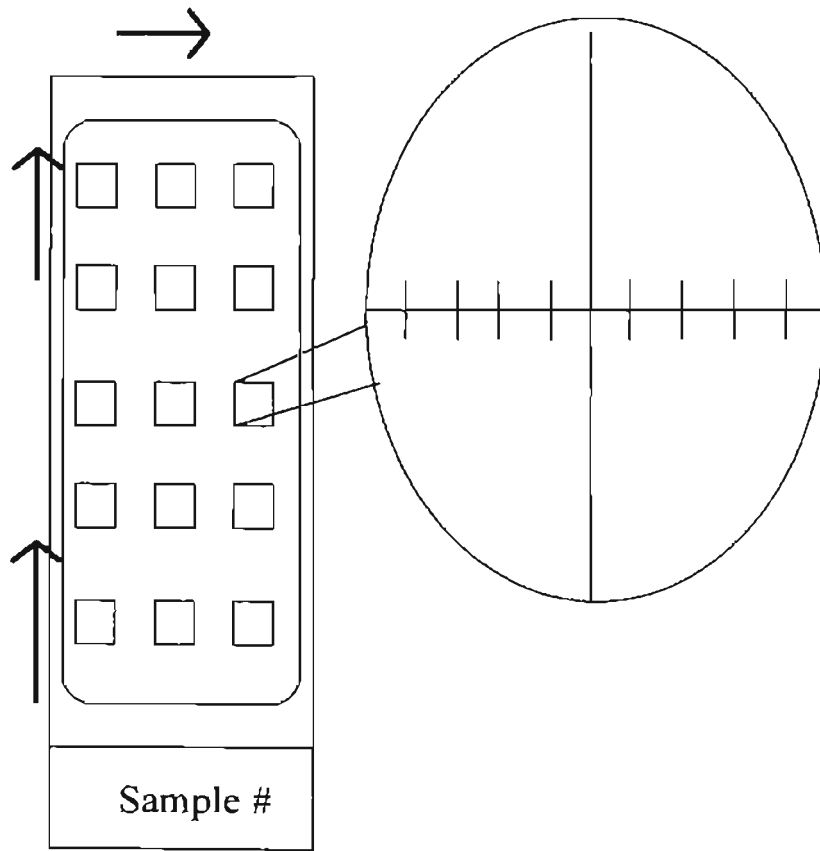


Figure 17. Sampling procedure and graduated ocular for point count analysis.



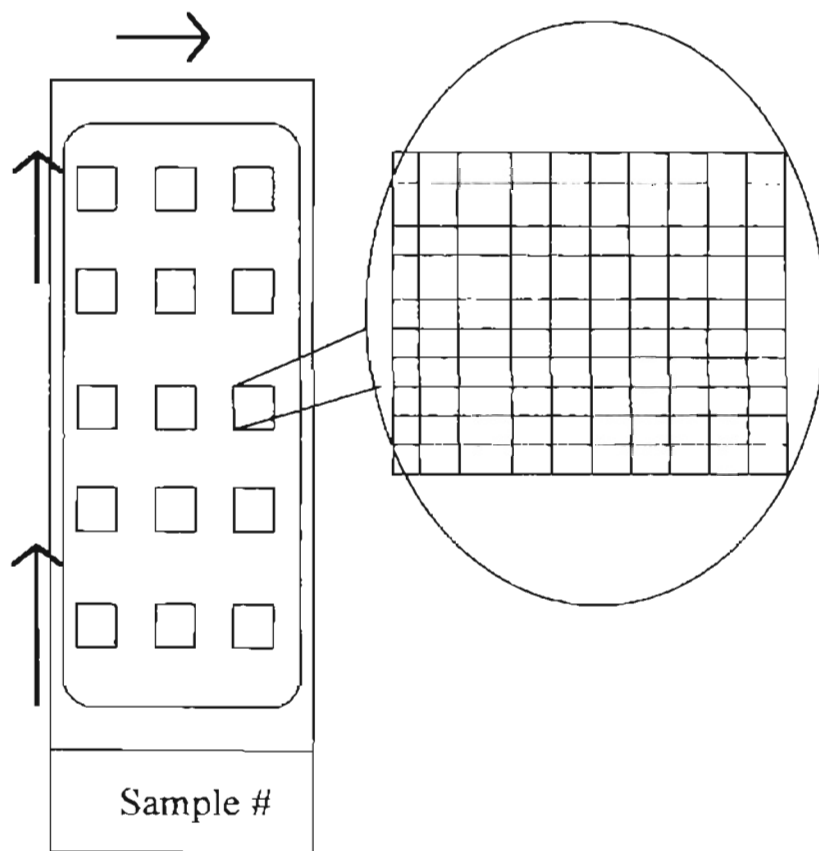


Figure 18. Diagram of "box" used for point counts.

squares down and ten squares across. By estimating and tabulating the mineral composition for each of the one hundred squares, the composition of each grid block area was determined. The type of grains, matrix, cement and pore space was determined for each slide. The values for the composition of the thin sections were normalized and entered into a spreadsheet. Appendix 1 contains the petrographic data.

The magnification used for measuring grain size was chosen based on a quick estimate of grain size. The fine-grained samples, like K 6240.6, a sample dominated by clay matrix and small grains, was counted using the 10x objective; the other slides were counted using the 2.5x objective. The grain sizes were measured using the calibrated increments on the crosshair ocular. For the 2.5x objective, it was determined that 25 of the small increments in the ocular equal one millimeter. As the crosshairs are approximately 4 mm in length, each increment in the micrometer was 0.04 mm (40 microns) in length (Figure 17). The grain sizes were measured at node points on a grid. To ensure an unbiased sampling of the grains, five contiguous or consecutive grains were counted. This approach prevents the grain size measurement from being biased to the larger grains (the eye may be attracted to large grains) (Figure 19). The grain sizes were measured and phi transformed in order to determine the sorting. The measurements were added to the final spreadsheet. Appendix 1 contains the grain size data.

### Mercury Pore Measurements

Mercury injection capillary pressure (MICP) is a measure of the amount of pressure required to force the non-wetting fluid phase (mercury) to displace the wetting phase (air) (Vavra, 1992). MICP data is obtained by injecting mercury into a clean sample with increasing pressure in pre-defined increments. Between each increase in pressure, equilibrium must be established; this can take from minutes to several hours.

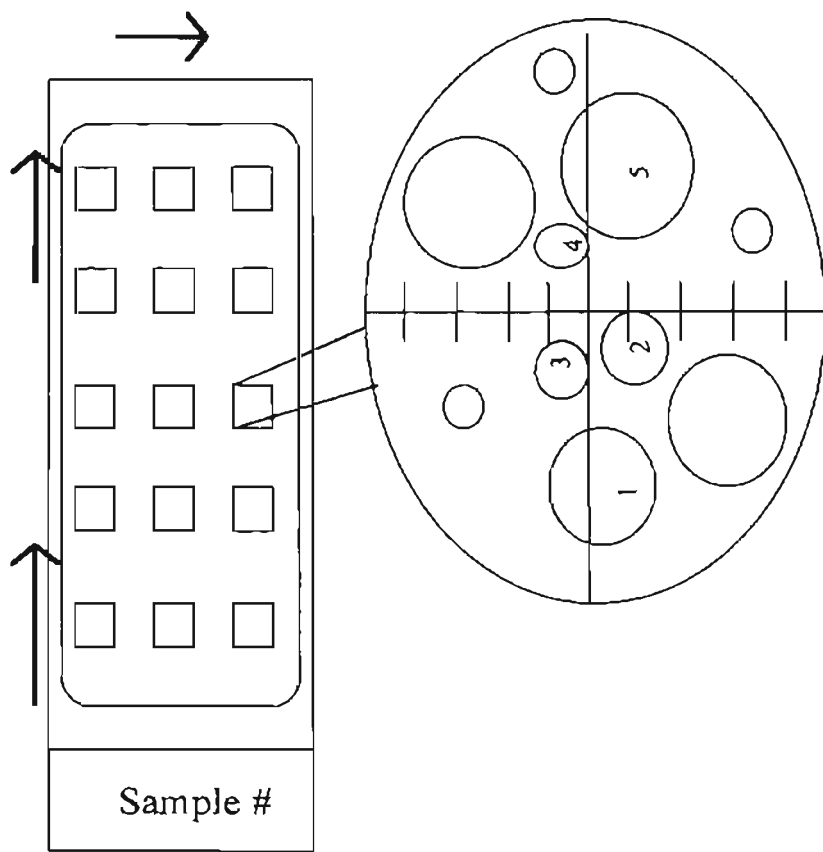


Figure 19. Grain size measuring procedure.

One hundred pressure steps between 0.5 and 60,000 psia are measured in the Morrow Sandstone.

The closure pressure is the pressure of mercury that fills the surface irregularities. The entry pressure is the pressure at which the mercury enters the pore throats after the surface irregularities are filled. The maximum saturation occurs when the pore volume is saturated with mercury. Figure 20 illustrates an example of a MICP curve. The minimum saturation pore volume is the pore volume that is unsaturated at maximum pressure. The equation for determining pore throat radius is

$$R = -2\gamma\theta/P_c \quad (\text{Eqn. 19})$$

where R is the pore radius,  $\gamma$  is the surface tension of 480 dyne/cm,  $\theta$  is the contact angle for air/mercury (140°), and  $P_c$  is the capillary pressure:

$$R = 107.6/P_c \quad (\text{Eqn. 20})$$

The above terms reduce to a constant (107.6) in the Laplace equation. The porosity from MICP is calculated by

$$\text{MICP } \phi = \text{volmax press} * \text{grn density} / (1 + (\text{volmax press} * \text{grn density})) * 100 \quad (\text{Eqn. 21})$$

where volmax press is the mercury volume at maximum pressure (cm<sup>3</sup>/g) and grn density is the grain density (2.65 g/cm<sup>3</sup>) (PPCo spreadsheet).

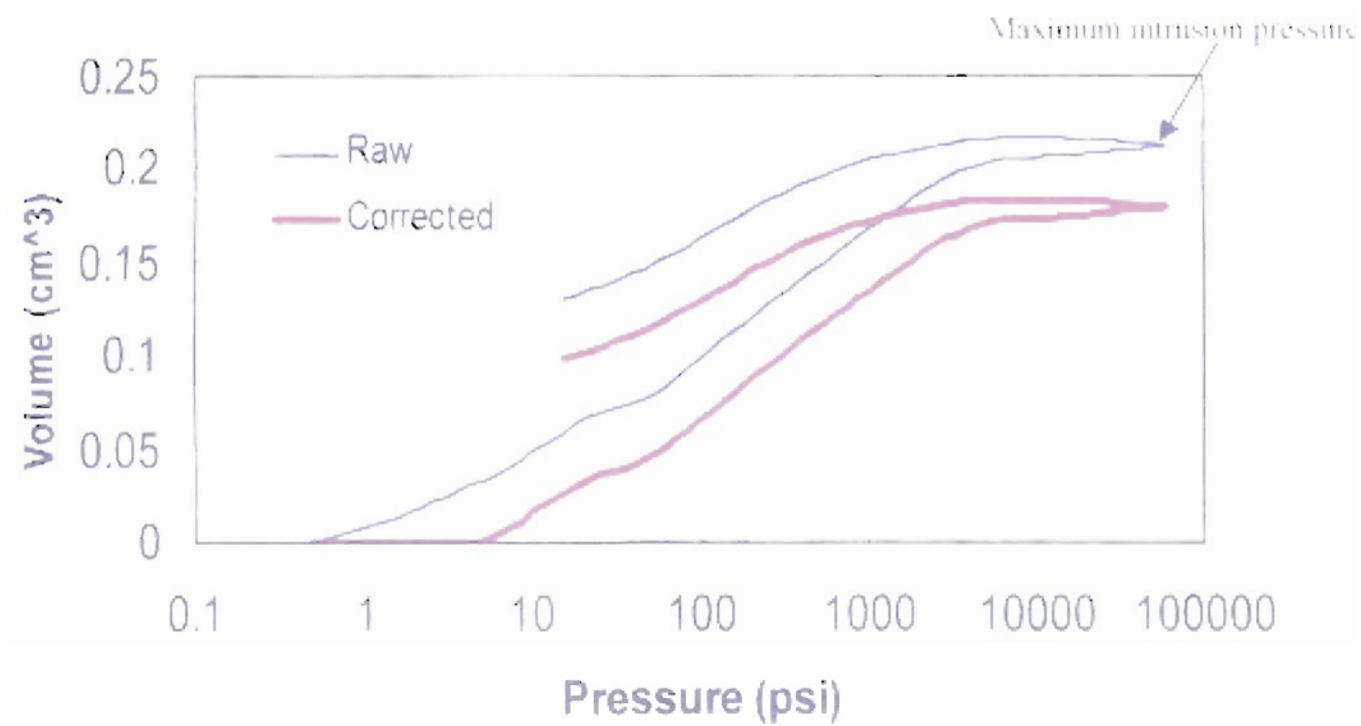


Figure 29. Example of MICP curve.

## Chapter 4 – Results

### NMR Curves

The NMR relaxation time distribution curves show the proportion of protons in pores of a given size vs. the corresponding decay-time constant associated with that pore size (Kenyon, 1997). The relaxation distributions are proportional to the area under the curve (porosity). Procedurally, a proportion of the porosity associated with a given size range can be correlated to the relaxation distribution in such a way that the given pore sizes correlate to a time range from the NMR relaxation distribution (Table 1). The times to length conversions are constant throughout the entire experiment (Figure 21). By taking the area under the curve for each relaxation time division, a percent of the total relaxation curve for each pore-size group can be calculated:

$$proportion = \frac{\sum_{i=j}^k Ai}{\sum_{i=1}^n Ai} \quad (Eqn. 22)$$

where the pore-size proportion is a fraction, n is the number of points in the distribution, j and k are less than n and represent the start and endpoints of the time interval for a range of pore-sizes. The percentages of each time division are used in describing the connection between the NMR curve and the petrography. The volume of each time group correlates to the volume of thin section porosity (Table 1).

The average  $T_2$  is a mean value and is not useful for describing the broad

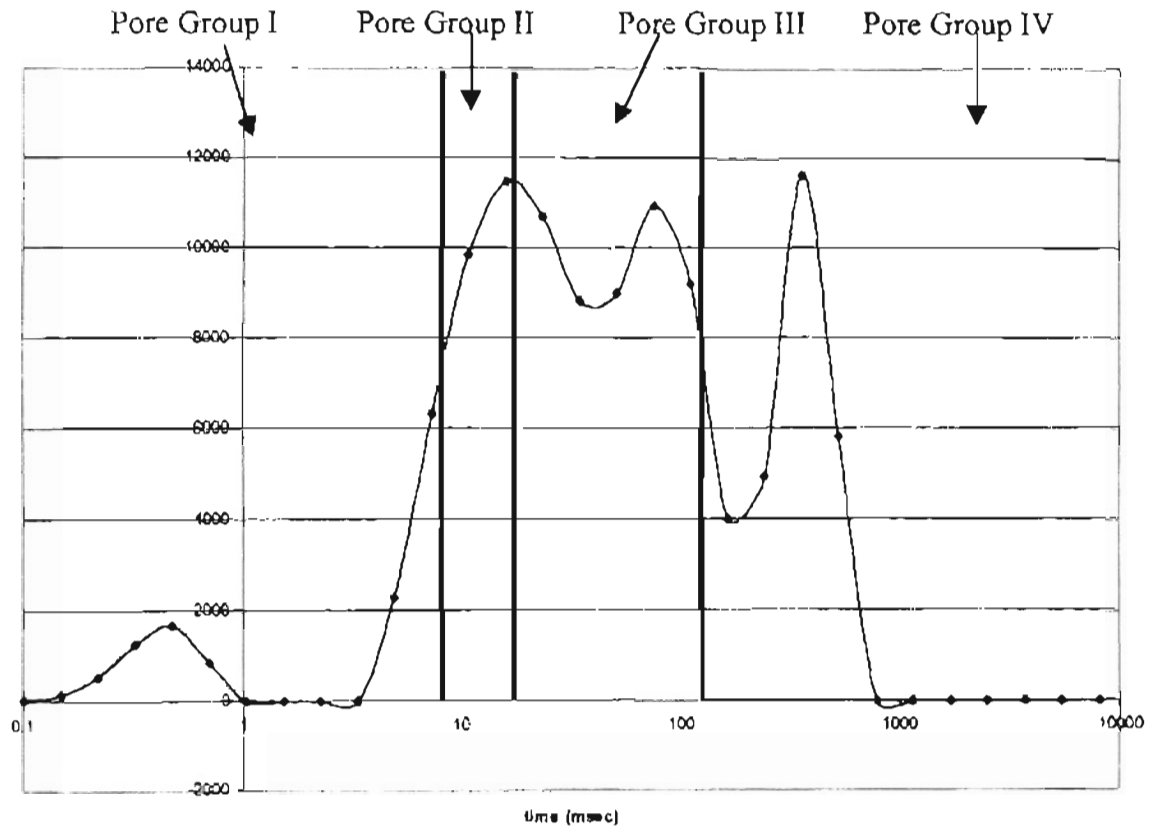


Figure 21. Diagram illustrating the relationship between the pore groups and NMR relaxation distribution times.

distribution of the relaxation curves. The mean  $T_2$  value is the time at which the transverse relaxation curve has decayed to within  $1/e$  of equilibrium (Howard et. al., 1993). The average  $T_2$  value weighs all the pore sizes with the same importance. Therefore the  $T_2$  times representing the micropores, which have little contribution to permeability, have the same importance as the  $T_2$  times representing the large pores, which contribute significantly to permeability. Consequently, the reason for applying a weighted  $T_2$  method is to place more emphasis on the larger pores.

Table 1. Assignment of relaxation times and petrographic pore types.

NMR Relaxation Time	Type of Pores
0.1 to 10 msec	Pores associated with clay
10 to 20 msec	Pores associated with dissolution of quartz and feldspar
20 to 100 msec	Primary porosity
100 to 1000 msec	Secondary porosity

The weighted  $T_2$  value used in this study is calculated using the proportion of total porosity for the time divisions discussed in the previous section above. The modal  $T_2$  for each time division is determined and multiplied by the fraction of that time division based on the total relaxation time. The weighted  $T_2$  is the sum of the  $T_2$  for each time group. Comparison reveals that the weighted  $T_2$  values are slower than the average  $T_2$  values (Figure 22) and the plot of the average  $T_2$  value vs. the weighted  $T_2$  value has an exponential relationship. The low permeability samples have a weighted  $T_2$  value and a



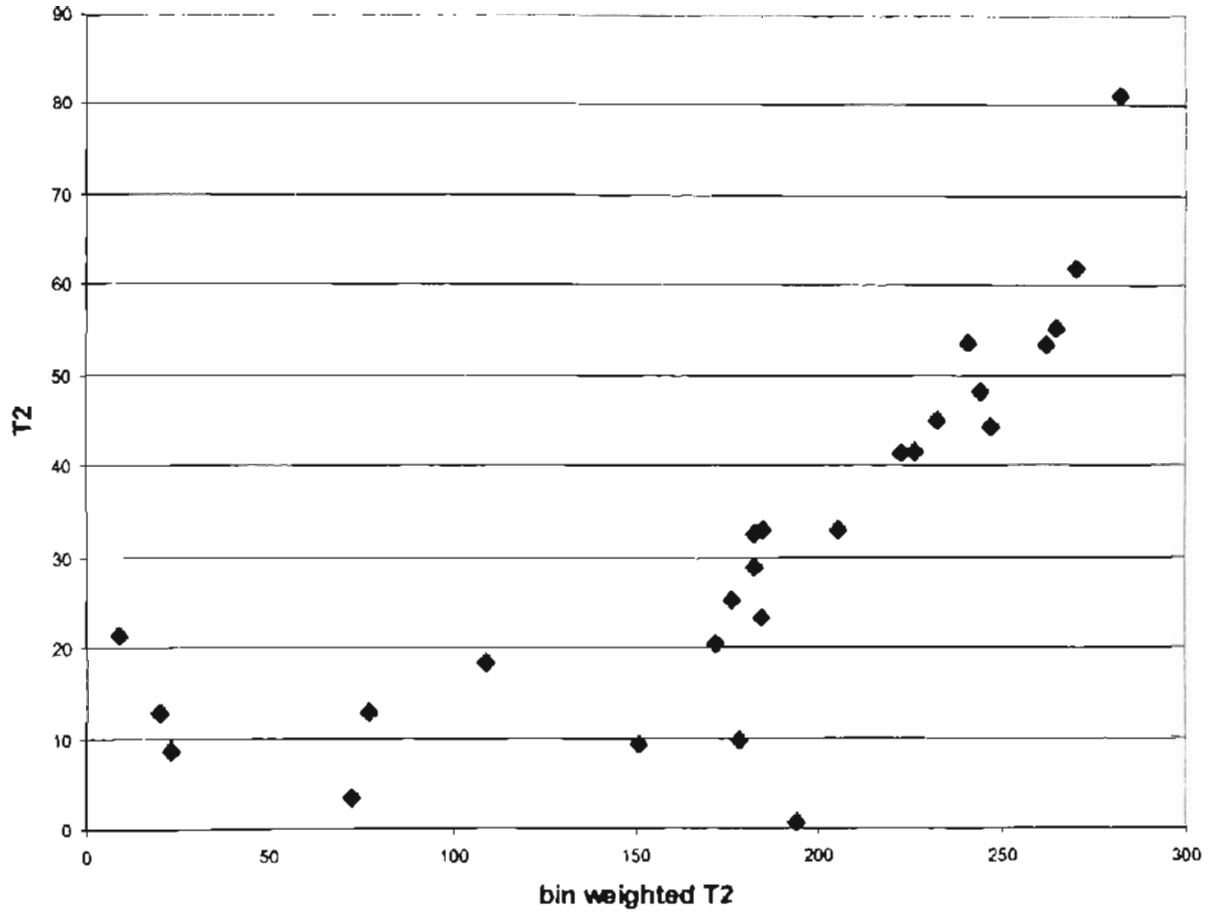


Figure 22. Weighted  $T_2$  vs average  $T_2$

mean  $T_2$  value comparable to each other since they contain a narrow distribution of small pores. In contrast the higher permeability samples display a greater difference between the weighted  $T_2$  value and the mean  $T_2$  value because the weighted  $T_2$  places more emphasis on the large pores than the small pores.

For example, sample K 6264.1 has a core porosity of 20%, NMR porosity of 19% and a core permeability of 85 md. Figure 23 is a thin section photo of sample K 6264.1 showing the clay and the large amount of porosity in the sample. The average  $T_2$  for this sample is 61 msec and the weighted  $T_2$  is 208 msec. Figure 24 shows the NMR relaxation distribution curve for sample K 6264.1. In terms of weighted  $T_2$ , 36% of the total relaxation is <100 msec or slow relaxation time (Figure 24). For this sample, the weighted  $T_2$  value better represents the pore-size range and its contribution to permeability than does the average  $T_2$  value.

As a second example, sample M 13288 is a quartz grain-rich sandstone that is quartz-cemented and has a core porosity of 4.5%, NMR porosity of 2.7% and core permeability of less than 1 md. The NMR porosity is lower than the core porosity due to the small pores that are below the detection limit of this NMR instrument. The detection limit of NMR instruments is based on their strength; a stronger instrument would be able to measure the smaller pores. Figure 25 is a thin section photo of sample M 13288. This thin section photo was taken in polarized light. The percentage of the NMR curve that represents fast relaxation times (<10 msec) is 68% (Figure 26). Therefore, a properly weighted  $T_2$  value will portray the large percentage of fast relaxation times, while also taking into account the slow relaxation times (32% of total). The average  $T_2$  for this sample is 8.6 msec while the weighted  $T_2$  is 23 msec. Both the average  $T_2$  and the weighted  $T_2$  for this sample are relatively fast. For low porosity/low permeability samples

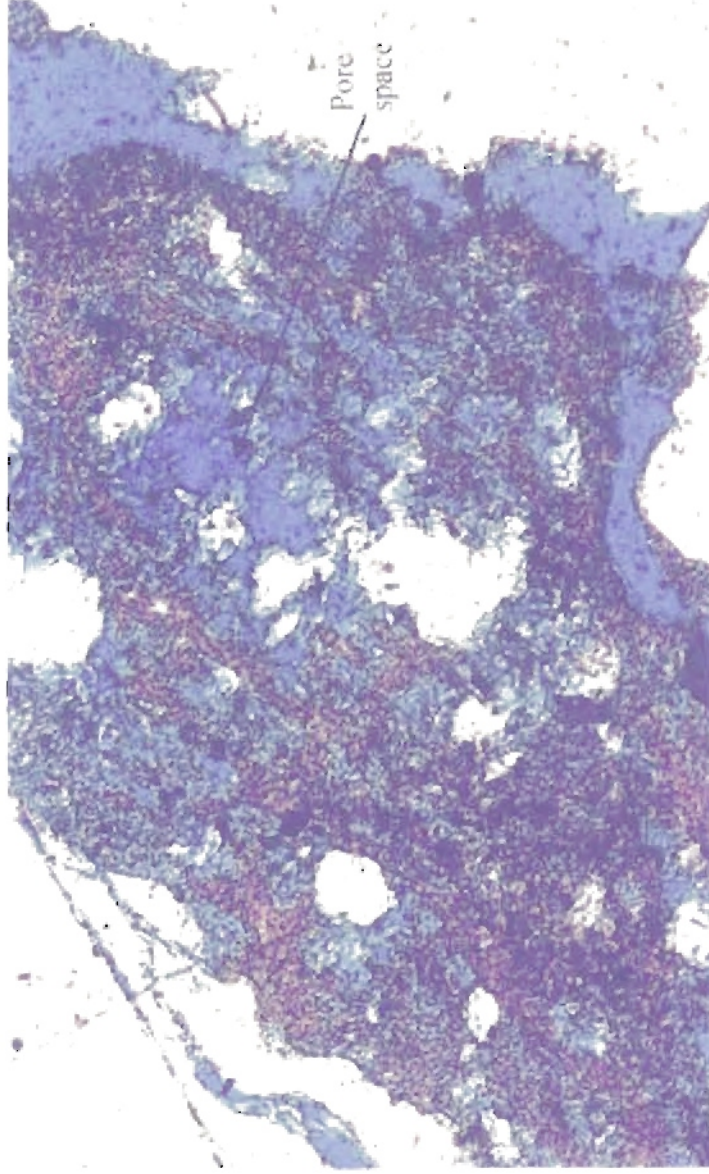


Figure 2.3: Picture of K 6264.1. demonstrating voids in clay. The pore space is in blue.

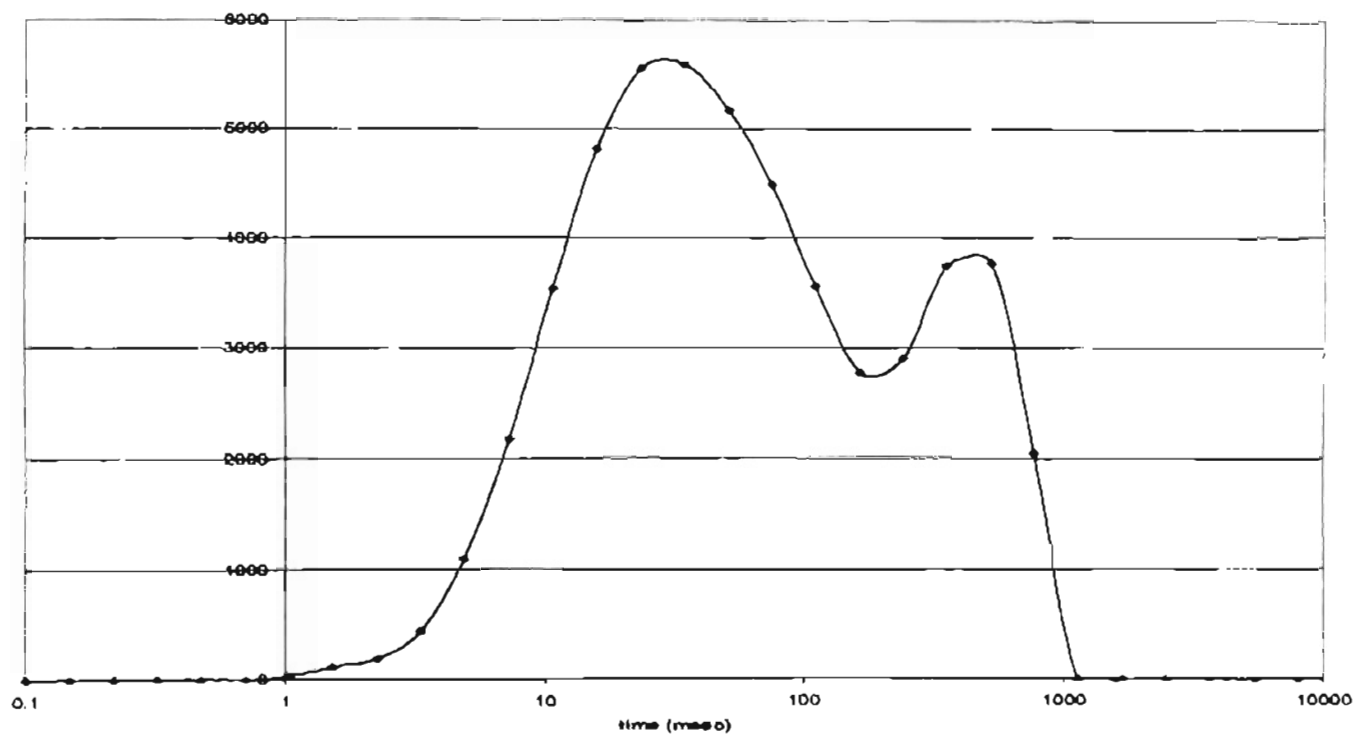


Figure 24. NMR Curve for sample 6264.1

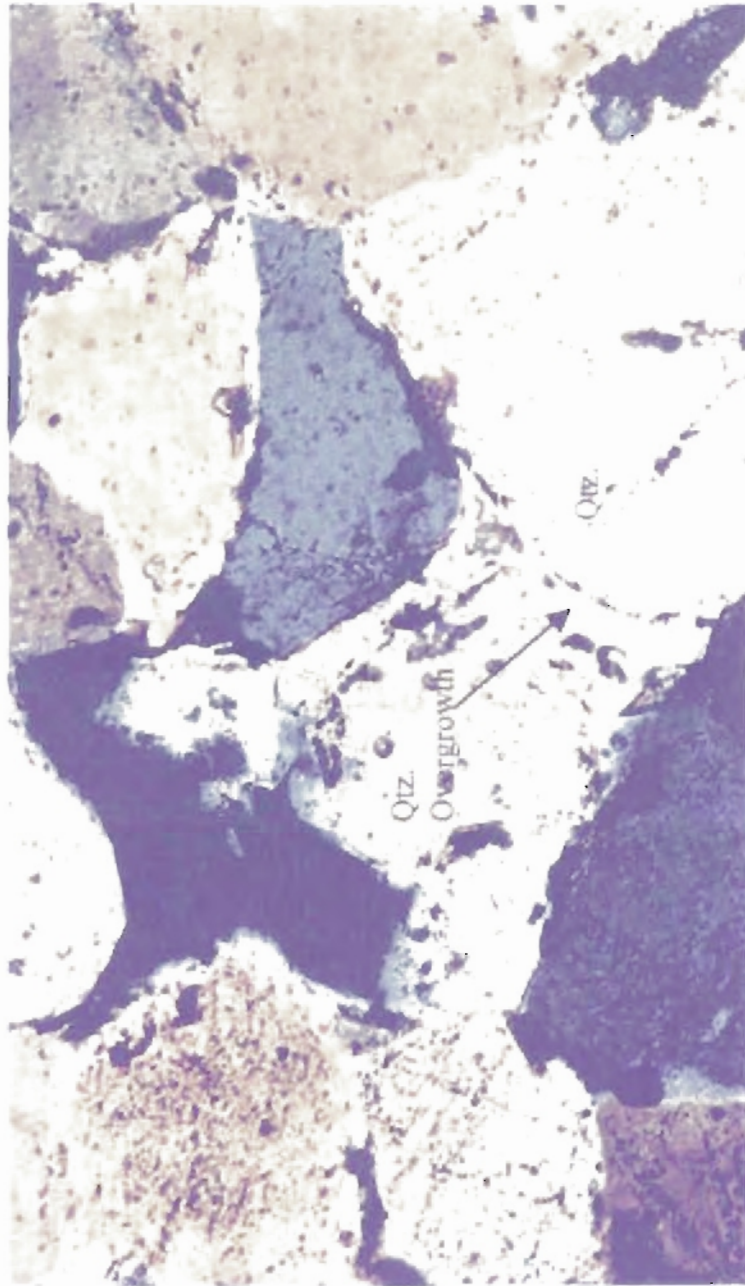


Figure 25 Thin section photo of sample M13288

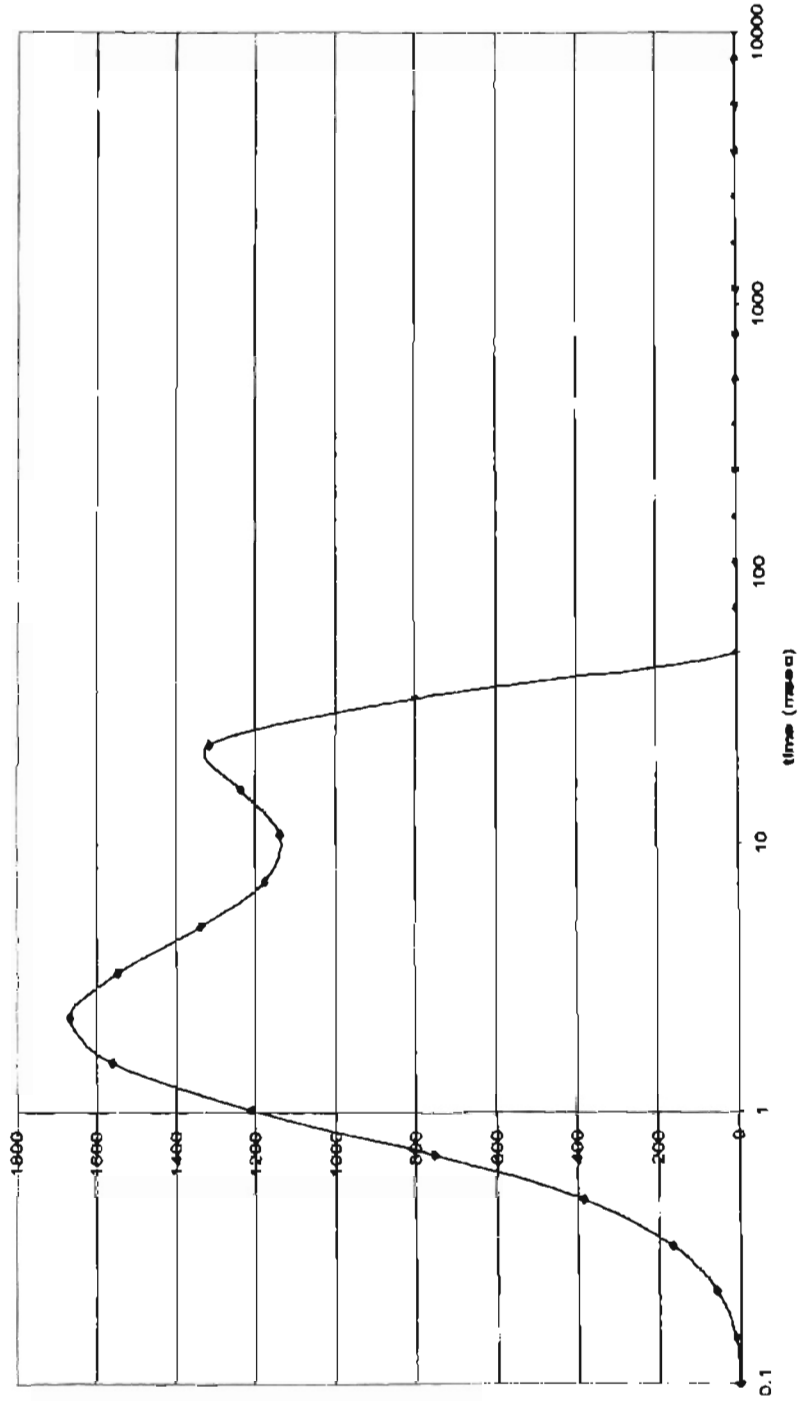


Figure 26. Sample M 13288 NMR curve

such as this one, the average  $T_2$  and weighted  $T_2$  times are similar. However, the weighted  $T_2$  procedure, described above is still applied to the low porosity samples in order to be procedurally consistent with the correction applied to the higher porosity/permeability samples.

Petrography and Core Analysis Data

The Morrow Sandstone samples in this study are divided into three distinct populations based on their position on the porosity vs. permeability cross-plot (Figure 27 and Table 2). These populations are subjective groups and based on visual inspection of the data. Statistical tests were not used to classify the data into the populations. Appendix 2 contains a brief summary of the relationship between the petrographic and relaxation distribution of each sample. The following discussion focuses on the relaxation distribution times for each of the porosity-permeability populations (Figure 21).

Table 2. Porosity-Permeability Populations

Population		Samples
High porosity/high permeability		K 6252, K 6256.6, K 6264.1, K6259.8
Intermediate porosity/medium permeability		K 6243.1, K 6245.1, K 6246, K 6249A, K 6249B, K6250.8, K 6253.4, K 6257.1, K 6261, K 6263, K 6266, K 6266.4,
Low porosity/low permeability	Plotted	M 11886, M 11888
	Not Plotted	K 6240.6, K 6267.1, M 13288, M 13291, B 12807, B13624, B 13629

Permeability measurements were difficult to obtain on many of the samples in Population 3 due to the fact that the permeability is less than 1 md. The samples that are

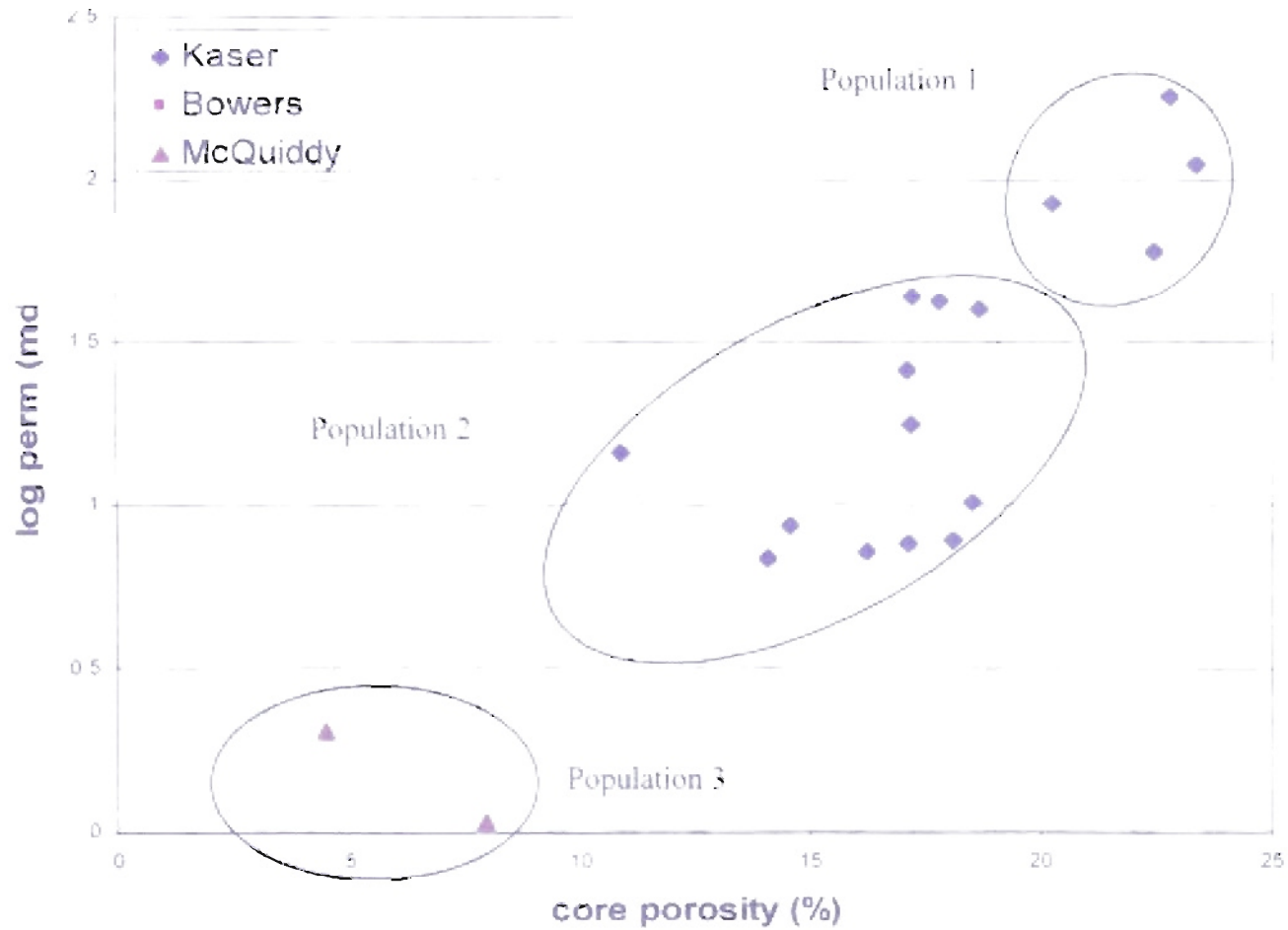


Figure 27. Core porosity vs log core permeability



not plotted on Figure 27 (see Table 2) are the samples that have a permeability of less than 1 md.

The porosity for each sample within a population is divided into four pore-size groups. NMR does not classify pores according to type (i.e. secondary or primary) but instead classifies pores according to size. Pores of the same size could have been derived from different processes. For this thesis, the dominant type of porosity occurring in each pore group is described. The first pore-size group, Pore Group I, is dominated by porosity associated with visible clay clusters of chlorite and kaolinite. The average pore size for this group is 40 microns. The porosity associated with dissolution of quartz and feldspar is the dominant type of porosity found in the second pore-size group, Pore Group II. These are pores that occur within grains. The average pore size for this group is around 120 microns. Primary porosity is defined as the intergranular pores found between the framework grains. The pore size of primary porosity for this study is around 120 to 150 microns. This is the dominant type of pore composing Pore Group III. The fourth pore group, with a mean pore-size of 400 microns, is formed through complete dissolution (secondary porosity) of framework grains. Both Pore Group II and IV contain secondary porosity. Pore Group II is distinguished from Pore Group IV in that the original mineral outline is visible in Pore Group II. These voids are the pore spaces within the circumference of the mineral being dissolved. The original mineral outline is not visible in Pore Group IV. Some of the porosity in Pore Group IV, though interpreted to be secondary porosity in origin, may contain primary, preserved or enhanced porosity.

The first population contains samples that have high porosity and high permeability (Figure 27). These samples have core porosity greater than 20% and core permeability greater than 60 md. The high porosity-/high permeability-sandstone

population is characterized by:

- 1) a quartz grain content (about 60%) that has an average grain size of about 400 microns,
- 2) a high kaolinite content, (about 9%) found mainly filling the secondary pore space (leached grains) and enhanced primary porosity
- 3) a high chlorite content, (7.5%) found surrounding the quartz grains and as clusters in the secondary porosity. Voids occur within the clusters of chloritic clay where fossils or minerals have dissolved (Figure 28).

The samples also contain 3.5% or less of quartz overgrowths and less than 1% heavy minerals, muscovite, biotite, siderite, organic matter, and rock fragments. (See Appendix 2 for a complete description of each sample.)

The dominant type of porosity found in the high porosity/high permeability population is from Group IV. Pore Group IV comprises 35% to 50% of the total optical porosity (TOP). The diameter of the pores is between 200 to 500 microns. The pores contain clay, and minor amounts of heavy minerals, muscovite, biotite, siderite, organic matter, and rock fragments.

Pore Group III comprises between 19% to 33% of TOP for the high porosity/high permeability population. This pore group tends to be volumetrically smaller than Pore Group IV because of the quartz overgrowths that fill the primary pores. The average diameter of the pores is 120 microns. The primary pores contain less clay than the secondary pores.

Pore Group I comprises between 5% to 33% of TOP. The average pore diameter for this group is 40 microns. The voids contained within the clusters of clay can be as large as 100 microns. Figure 28 is a thin section photo of K 6246.1 that illustrates the

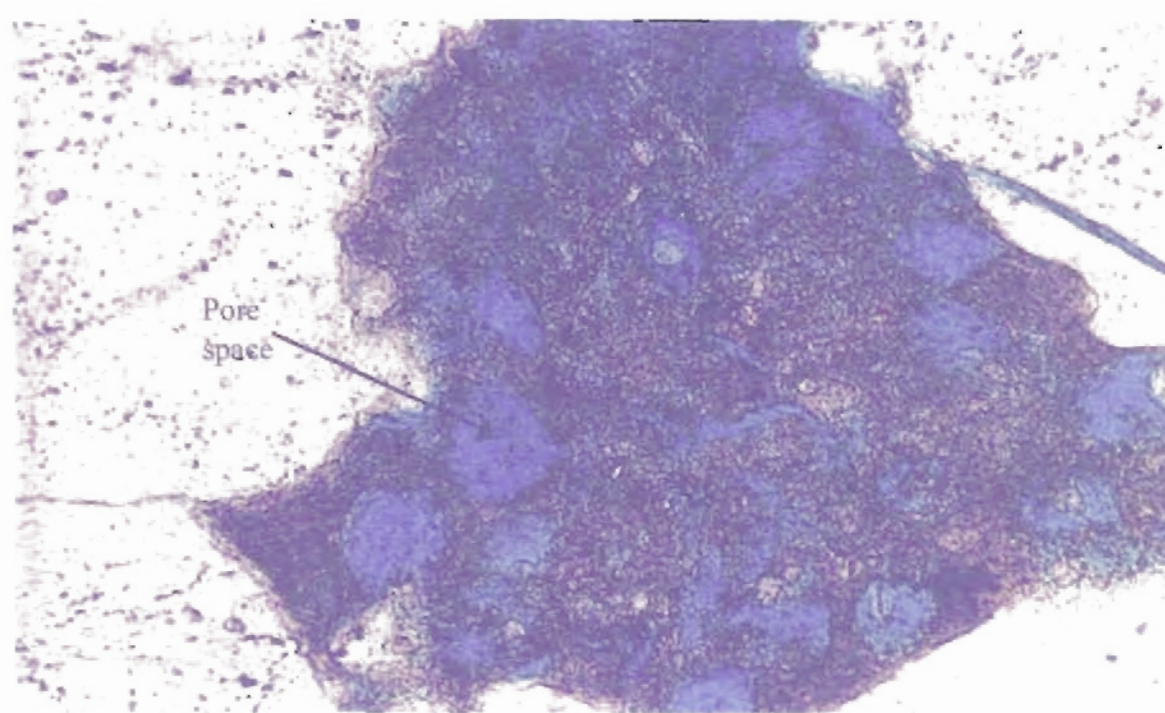


Figure 28. Thin section photo of sample K 6246.1 demonstrating the voids within clay. The porosity is in blue.

voids in the clay formed from dissolution of unstable minerals.

Pore Group II averages 15% of the TOP. The average pore size associated with this pore group is 120 microns. Appendix 2 contains the amounts of the different porosity types for each sample in this population.

Table 3. Table showing the correlations between porosity and NMR distributions.

SAMPLE	CORE POROSITY	NMR POROSITY	% of NMR Distribution in Pore Group			
			Group I	Group II	Group III	Group IV
K6240.6	7.27	5.63	79.71	3.00	7.68	9.60
K6243.1	10.86	16.93	39.01	19.44	13.36	28.11
K6245.1	16.25	17.29	37.64	19.13	21.01	22.23
K6246	17.20	14.52	26.40	21.64	26.89	25.07
K6249A	14.56	11.68	28.81	17.27	26.80	27.11
K6249B	17.14	17.09	29.89	20.08	26.74	23.29
K6250.8	17.80	16.98	23.22	18.12	25.96	32.69
K6252	22.76	23.49	18.51	18.11	24.12	39.26
K6253.4	18.51	17.70	30.31	21.75	25.67	22.27
K6256.6	23.31	23.24	14.11	21.69	28.88	35.31
K6257.1	18.65	18.90	14.05	18.49	35.16	32.26
K6259.8	22.42	20.86	12.77	12.88	38.67	35.67
K6261	17.09	17.82	11.92	19.49	36.05	32.54
K6263	18.11	17.48	16.76	22.98	38.28	21.98
K6264.1	20.22	19.97	7.83	16.05	39.99	36.14
K6266	17.17	18.13	15.40	24.84	37.49	22.28
K6266.4	14.07	15.65	13.16	20.25	38.14	28.46
K6267.1	9.61	10.71	23.95	35.93	29.91	10.22
B12807	0.51	1.02	63.88	15.17	12.18	8.78
B13624	0.48	0.92	92.90	7.10	0.00	0.00
B13629	9.03	9.93	51.21	8.90	15.06	24.83
M11886	4.47	15.68	26.46	17.17	24.95	31.42
M11888	7.93	9.36	17.32	16.49	20.30	45.89
M13288	4.53	2.68	68.76	16.52	14.72	0.00
M13291	-0.57	3.51	58.94	8.22	12.07	20.77
M13202	2.27	1.05	73.10	1.43	25.47	0.00

The total area under the relaxation distribution curve for the high porosity/ permeability population compares favorably with TOP (Figure 21). The percentages of the NMR relaxation distribution for each individual sample are shown in Table 3. The relaxation distribution between 0.1 to 10 msec corresponds to Pore Group I. For this

population, the percentage of the NMR relaxation distribution that correlates to Pore Group I comprises about 13% of the relaxation distribution. Pore Group II corresponds to the 10 to 20 msec portion of the relaxation distribution. This pore group comprises about 17% of the total distribution. Pore Group III correlates to the 20 to 100 msec portion of the relaxation distribution. Pore Group III can be attributed for about 34% of the total relaxation distribution for this population. Pore Group IV is associated with the 100 to 1000 msec portion of the relaxation distribution, and accounts for 36% of the total relaxation distribution.

The second population of samples has slightly lower porosity and permeability values. The porosity values range between 8% to 20% and the permeability values range from 10 to 40 md (Table 2).

The mineralogy of this population of litharenites is dominated by

- 1) a quartz (about 60%) grain content with an average grain size of 700 to 1400 microns, (medium to coarse sand).
- 2) chlorite, (about 7% of the sample) found surrounding the quartz, calcite, and dolomite grains. Chlorite is also found as clusters filling the secondary porosity.
- 3) kaolinite, (6% of the total mineralogy) mainly found filling the secondary porosity.
- 4) minor amounts of calcite and dolomite, calcite varies from less than 1% to 10% of the total composition. Dolomite comprises between less than 1% to 5% of the composition.
- 5) quartz overgrowths (less than 1% to 3% of the total composition).
- 6) less than 1% of rock fragments, heavy minerals, siderite, biotite, and

muscovite.

The dominant type of porosity for the intermediate porosity/medium permeability population is Pore Group IV. Pore Group IV comprises about 36% of the TOP with an average pore diameter between 200 to 500 microns. The porosity associated with pore Group I comprises about 20% of the TOP. The largest pores associated with this pore group are 40 microns in diameter. The porosity associated with Pore Group II comprises about 30% of the TOP, with an average pore diameter of less than 120 microns. Pore Group III comprises about 19% of the TOP having an average pore diameter of 120 microns.

As with the first population discussed, the total area under the relaxation distribution curve compares favorably with the second population as well. The percentage of the NMR relaxation distribution for each sample is shown in Table 3. The porosity associated with Pore Group I corresponds to the 0.1 to 10-msec portion of the relaxation distribution (which is about 33% of the total distribution). The portion of the relaxation distribution that is associated with Pore Group II is between 10 to 20 msec. This portion of the relaxation distribution comprises about 27% of the total relaxation distribution. Pore Group III is associated with the 20 to 100 msec portion of the relaxation distribution (comprises about 25% of the total distribution). Pore Group IV is associated with the 100 to 1000 msec portion of the relaxation distribution (which is about 27% of the total distribution).

The third distinct reservoir-quality population consists of low porosity and low permeability samples. The porosity values are less than 8% and the permeability is less than 3 md (Figure 27). Within this population the samples contains two distinct lithologies. As determined by thin-section petrography, the first lithology is a siltstone

composed of clay matrix and less than 30% quartz grains (samples K 6240.6, B 13624 and B 13629) and the second lithology is a fine- to coarse-grain sandstone that contains a significant amount of pore-filling cement. The siltstone contains subrounded quartz grains that have an average diameter of 70 microns. The only visible porosity found in these thin sections is porosity associated with clay.

The samples in the third population (minus the siltstones) are dominated by:

- 1) quartz (approximately 70-80%) grains that have an average grain size of 200 to 400 microns.
- 2) three types of cement (each type comprises between 2% to 10% of the samples) quartz overgrowths (about 6%), calcite cement (about 4%- though one sample contains 48%) dolomite cement (about 2.5%) of the total composition.
- 3) less than 1% muscovite, biotite, fossils and rock fragments.

Pore Group IV dominates the TOP in this group of sandstones (about 75%). Pore Group III is almost absent in these samples. A few samples contain small amounts of Pore Group I and Pore Group II. The porosity values for each of these samples are shown in Table 3.

Pore Group I is associated with the 0.1 to 10-msec portion of the relaxation distribution and accounts for 29% to 93% of the total distribution (Table 3). Pore Group II corresponds to the 10 to 20 msec portion of the relaxation distribution (about 9.5% of the total NMR distribution). Pore Group III corresponds to the 20 to 100 msec portion of the NMR relaxation distribution (about 16% of the total distribution). Pore Group IV corresponds to the 100 to 1000 msec portion of the relaxation distribution. This corresponds to about 23% of the total distribution.

## Porosity Relationships

The unique populations that are observed in the core porosity vs. core permeability plots are also noticeable as distinct populations in the core porosity vs. NMR porosity plot (Figure 29). The plot of porosity vs. NMR porosity yields a strong correlation between the two porosity measurements ( $r = 0.92$ ). The  $r$ -value is referred to as a correlation coefficient. The higher the absolute value of the correlation coefficient, the stronger the linear relationship between the variable pairs on the cross-plot. The  $r$ -values can range from  $-1.0$  to  $1.0$ . A negative  $r$ -value indicates an inverse relationship and a positive  $r$ -value suggests a positive relationship. The core porosity measured by a Boyles' Law gas porosimeter measures the pore volume by determining differences in gas volume at pressure. In contrast, the NMR porosity "counts" the hydrogen protons that fill the same pore volume. In a fully water-saturated sample, all the pores will contain water. Since the water contains hydrogen atoms, all the pores will be measured during a NMR measurement.

The porosity-permeability populations are also present in a plot of core porosity vs. MICP porosity (Figure 30). The populations are more obvious at low and intermediate porosity values. At high core porosity values, the MICP porosity is much less than the core porosity. The  $r$ -value for the core porosity v. MICP porosity is  $0.9$ , which is slightly less than the NMR porosity plot. The low MICP readings observed in the high porosity samples might be due to a number of factors, though in this case the error is probably due to problems in the estimation of closure pressure (Figure 30). Closure pressure is subtracted from the MICP porosity to correct for "non-porosity" irregularities in the sample chip. The "non-porosity" irregularities are natural surface irregularities that are produced when the sample chip is prepared for measurement.



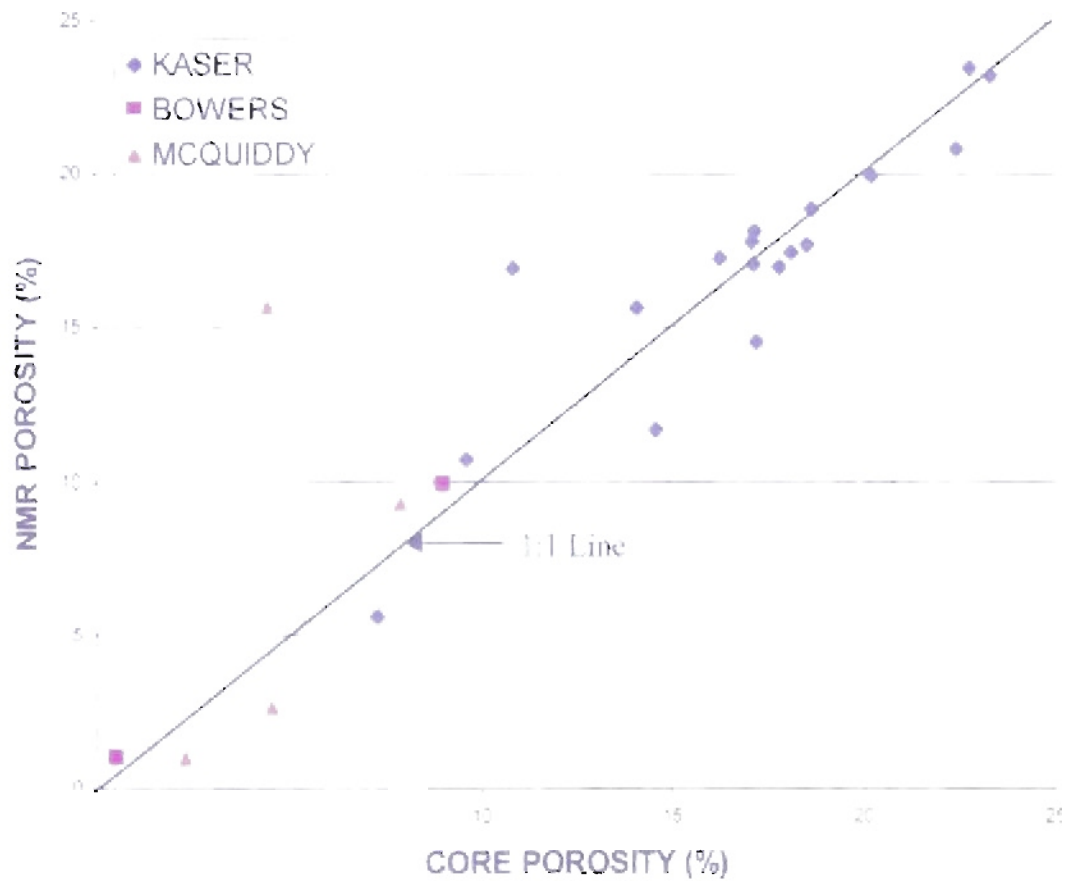


Figure 29 Core porosity vs NMR porosity

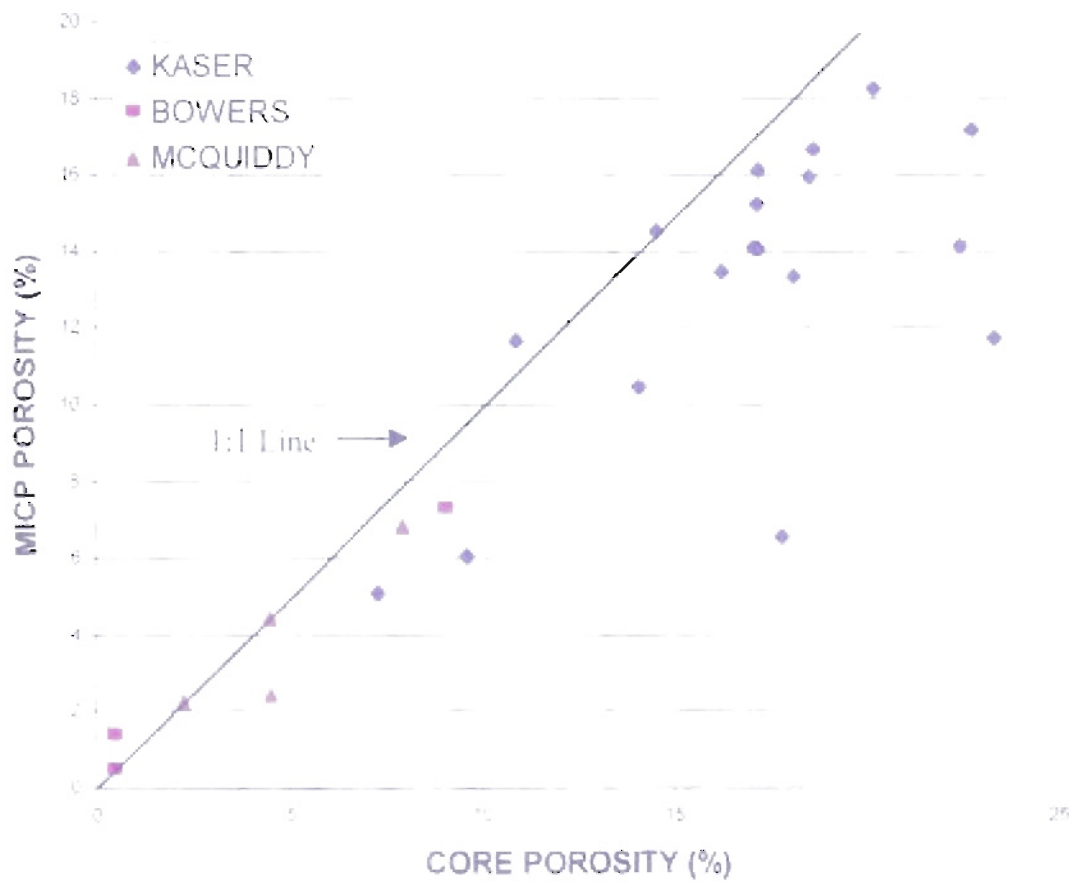


Figure 30 Core porosity vs MICP porosity

## T<sub>2</sub> Cutoff

The T<sub>2</sub> cutoff distinguishes the movable fluids from the irreducible water within a sample. The T<sub>2</sub> cutoff can vary within a single lithology (Coates, 1999) if a portion of the stratigraphic section is finer grained or contains more clay or cement than the rest of the section. The increase in clay or cement will decrease the T<sub>2</sub> cutoff. Centrifuged samples are used to determine the water content at irreducible water saturation (S<sub>wi</sub>). After centrifuging the sample, the water remaining is the irreducible water. The NMR measurement is made on the centrifuged samples. The S<sub>wi</sub> T<sub>2</sub> cutoff is defined as the slowest relaxation time on the S<sub>wi</sub> relaxation distribution. The Kaser samples were centrifuged for two hours at 5000 rpm in order to determine the T<sub>2</sub> cutoff. The S<sub>wi</sub> cutoffs range from 4.9 msec to 74 msec (Figure 31). The majority of the S<sub>wi</sub> cutoffs in this study are around 33 msec, which is a finding consistent with other research for sandstones (Kenyon, 1997). When calculating permeability in this study, the 33-msec cutoff is used.

The amount of bound fluid can be determined by taking the proportion of the NMR curve that is faster than the cutoff. Sample K 6240.6 has a S<sub>wi</sub> cutoff at 4.9 msec; the percentage of bound fluid is 77%. Figure 32 is the S<sub>wi</sub> relaxation curve for sample K 6240.6. When the 33-msec cutoff is applied, the percentage of bound fluid increases to 84%. The increase in bound fluid inferred to be present in the sample based on a 33-msec cutoff would affect the outcome of the calculated permeability. The increase in bound fluid estimated from this technique will result in permeability calculations that are lower than the measured permeability.

Sample K 6249A has a S<sub>wi</sub> cutoff at 74 msec. At a cutoff of 74 msec, the percentage of bound fluid is 73%. This bound fluid estimate is lowered to 53% when the

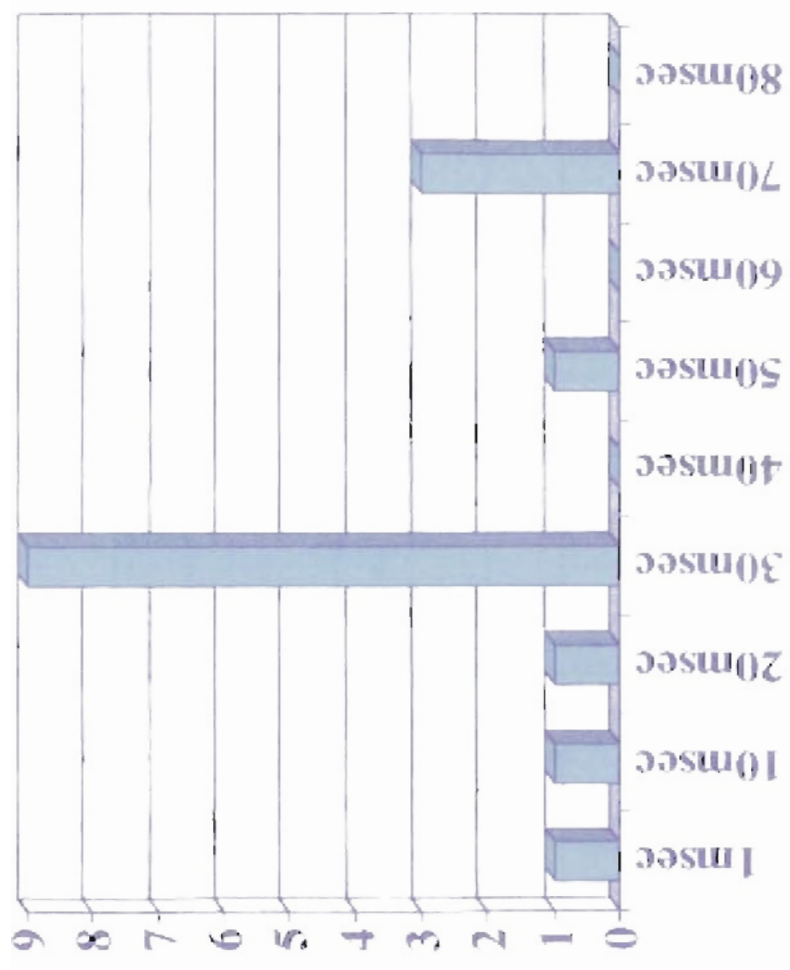


Figure 31 Histogram showing distribution of SWI cutoff times, with 30msec being the mode.

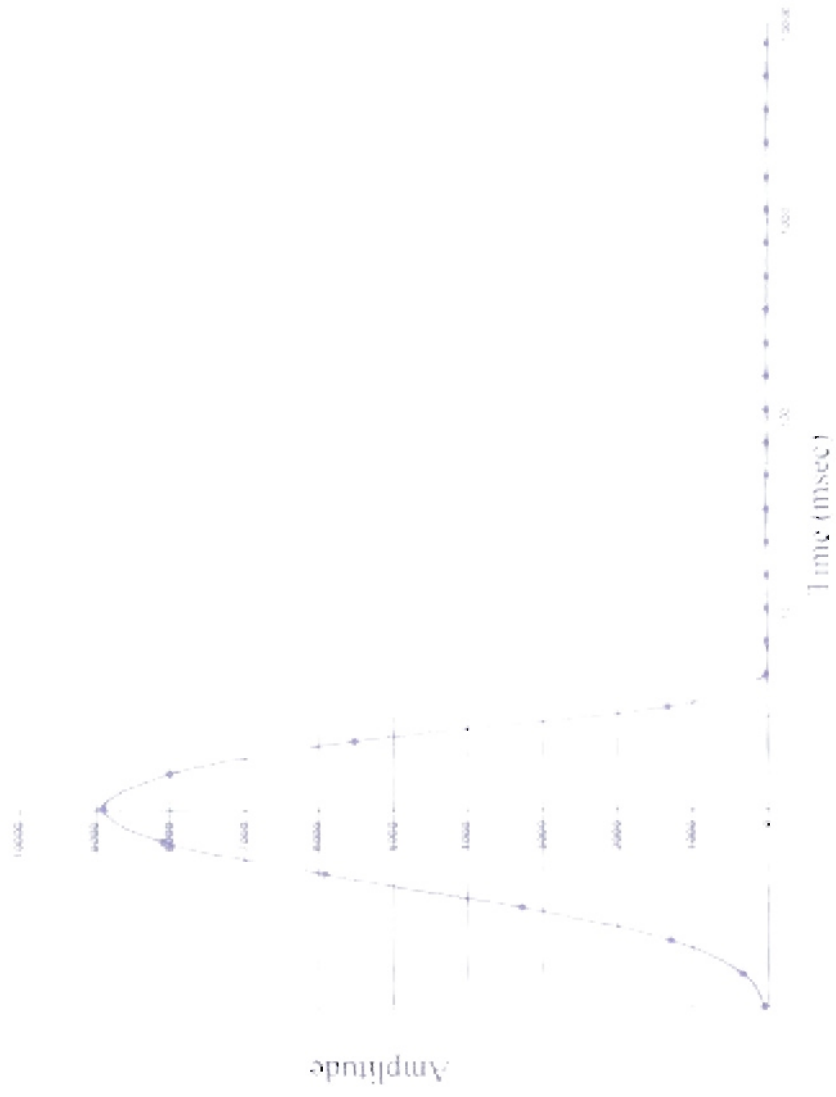


Figure 3.2 K 6240 6 Swi curve

cutoff time is decreased to 33 msec. Figure 33 shows the Swi relaxation curve for sample K 6249A. The net result in a lower BVI will also affect the outcome of the calculated permeability, resulting in estimates that maybe larger than measured permeability.

### Coates-Timur Permeability Results

There are several “versions” of the Coates-Timur equation; the one used in this thesis is the “original” Numar version. In this study, when using recommended default values for the Coates-Timur (C-T) equation shown below, calculated permeability values are lower than the core permeability.

$$k = (\phi/10)^4 * (FFI/BVI)^2 \quad (\text{Eqn. 23})$$

where  $\phi$  is the NMR porosity in percent and FFI/BVI is the T<sub>2</sub> cutoff time that best matches the Swi value (Figure 34). The standard equation using Swi parameters also calculates permeability lower than the standard equation using FFI/BVI ratio at 33 msec (Figure 35). In order to improve the fit of calculated permeability with measured permeability, a "guess and check method" was used to adjust the exponents. When the b-variable was being “adjusted” the a- and c-variables were held constant. The final equation, which yields a "best-fit" to the measured Swi permeability, is:

$$k = (\phi/9)^{5.5} * (FFI/BVI)^{1.5} \quad (\text{Eqn. 24})$$

Figure 36 shows a calculated Swi permeability vs. core permeability cross-plot using the above equation. The large amount of scatter within the FFI/BVI ratio for the Swi data set makes it difficult to calculate a permeability this is in agreement with the measured core-analysis permeability. For this reason, the FFI/BVI value is determined using the 33 msec cutoff.

The comparisons from this thesis show that the Coates-Timur permeability equation calculates permeability values that are lower than observed for the measured core

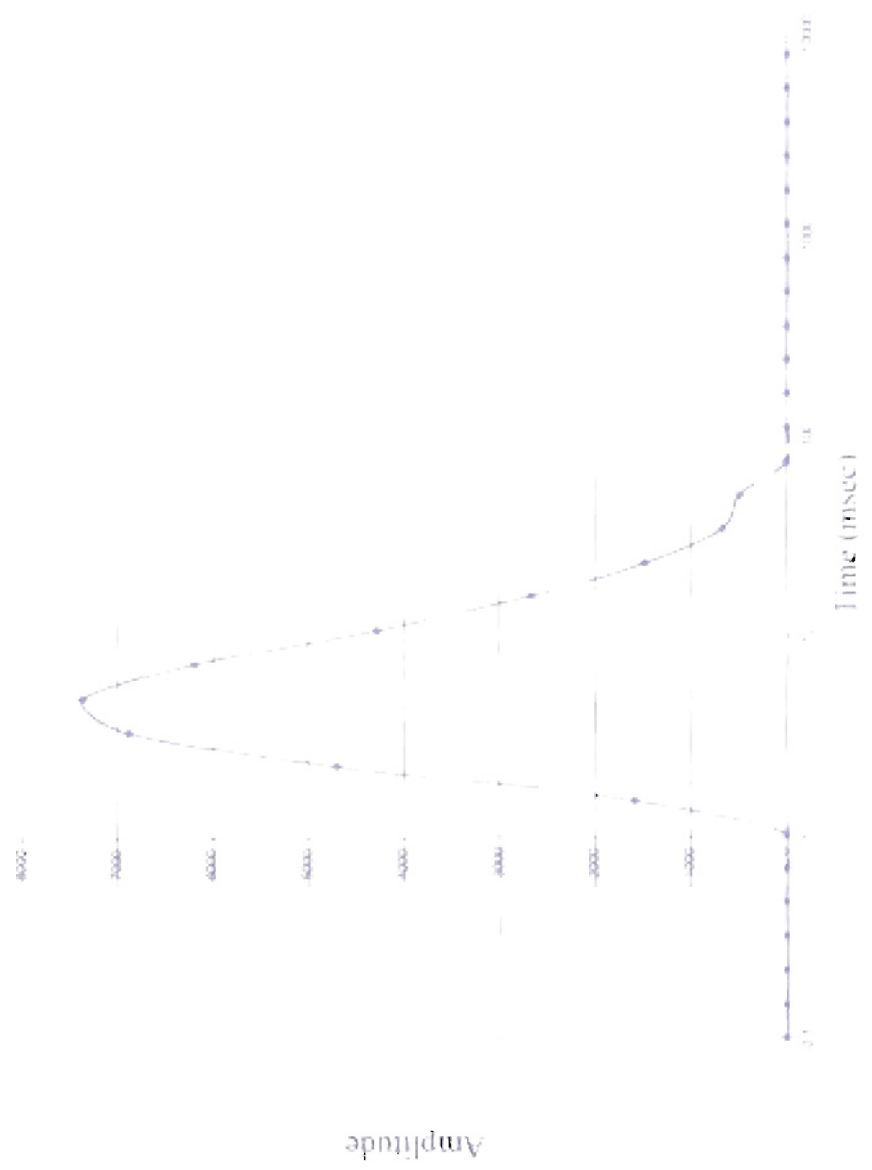


Figure 33 - K 62.49A Swi curve

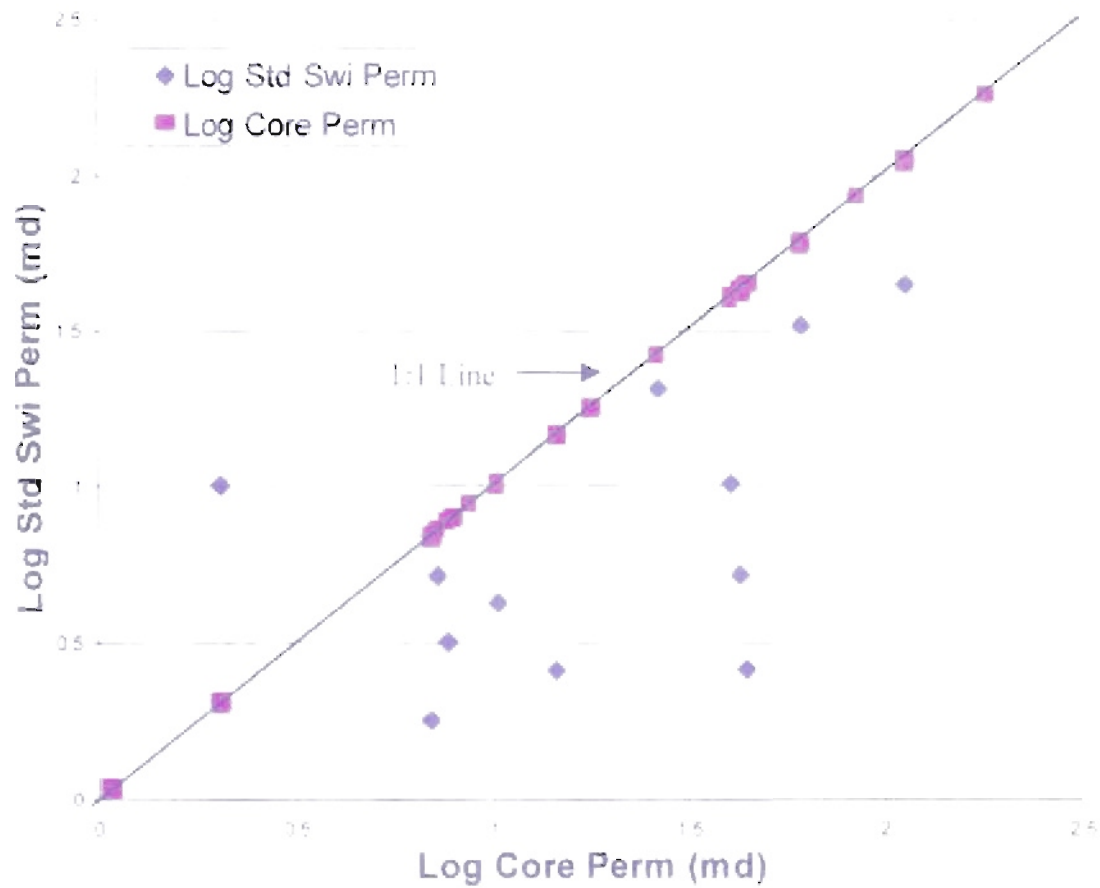


Figure 34. Core permeability vs Std Swi permeability



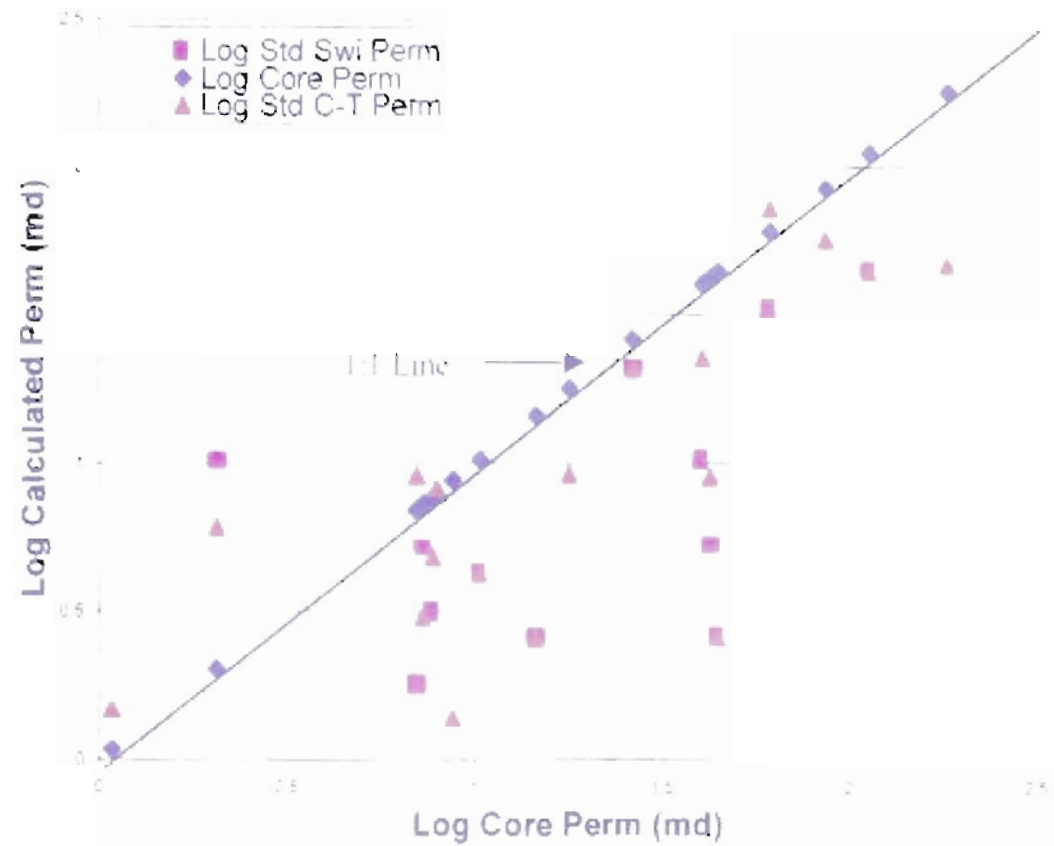


Figure 75 Core permeability vs Std Swi permeability and Std C-T permeability

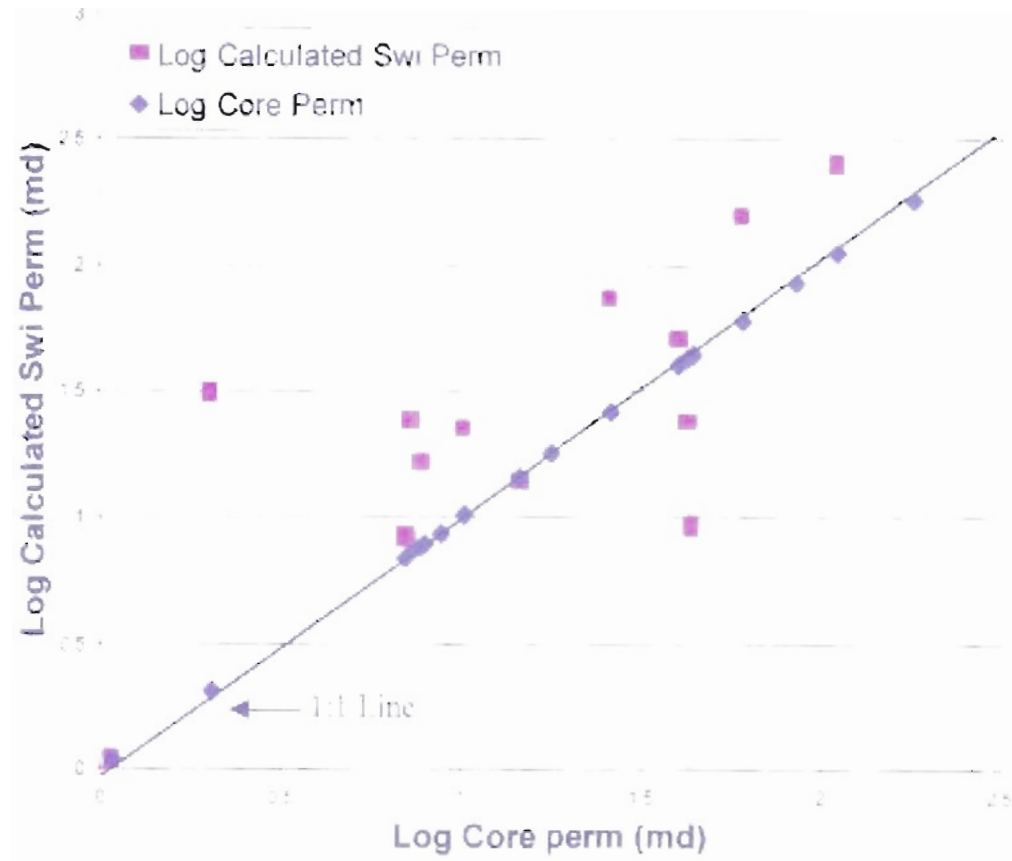


Figure 36 Core permeability vs Calculated Swi permeability

permeability. Figure 37 is a plot of the standard C-T equation using the default parameters. In order for the C-T permeability to agree with the core permeability the a-, b- and c-variables must be adjusted until the calculated permeability correlates as close in agreement with the core permeability as possible.

The r-value is an approximation of how strong the correlation is between the calculated and the core permeability. A simple comparison of r-values does not necessarily provide the best answer. Therefore, the use of graphs and visual inspections of the results are needed. The calculated permeability and the core permeability with the highest r-values were graphed in order to determine which values for a-, b- and c provide a permeability estimate that is closest to core permeability (Figure 38). Figure 38 illustrates how two equations can have the same r-value, of 0.89, yet one equation is visually closer to the core permeability than the other. The equation

$$k = (\phi/8.7)^{5.6} * (FFI/BVI)^{1.1} \quad (\text{Eqn. 25})$$

calculates a permeability that corresponds to the highest r-value, but visually it does not correspond closely with the core permeability. The equation

$$k = (\phi/9.5)^5 * (FFI/BVI)^1 \quad (\text{Eqn. 26})$$

visually correlates closer to the core permeability, even though it has the same r-value of 0.89 as Equation 25. For the Coates-Timur equation to correlate well with the core permeability in the Morrow Sandstones, the a-value is adjusted to be about 9.5, the b-value is adjusted to about 5, and the c-value is determined to be around 1 (Figure 39).

### SDR Permeability Results

In contrast to the C-T comparison made above, the SDR standard equation calculates permeability values that are higher than the measured core permeability. As with the C-T discussion, the a-, b- and c-variables in the SDR equation must be varied in

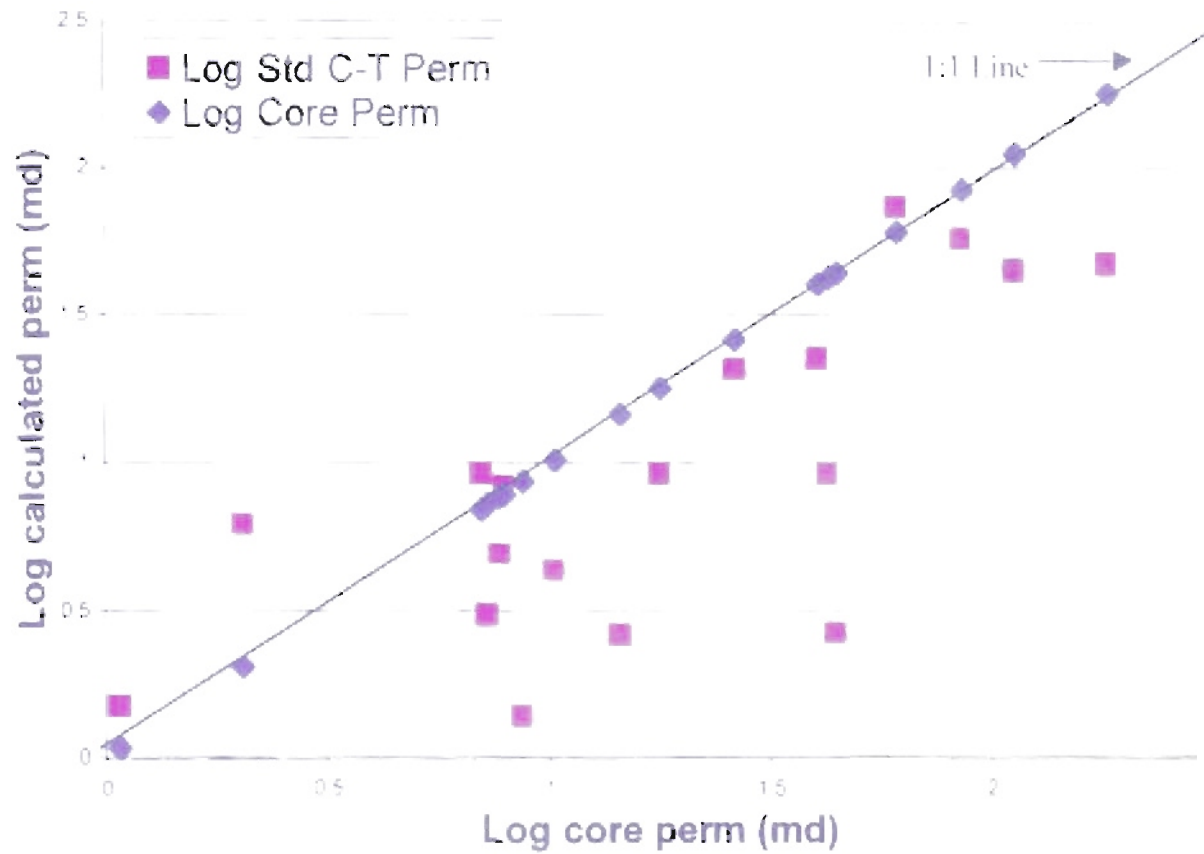


Figure 37. Core permeability vs Std C-T permeability

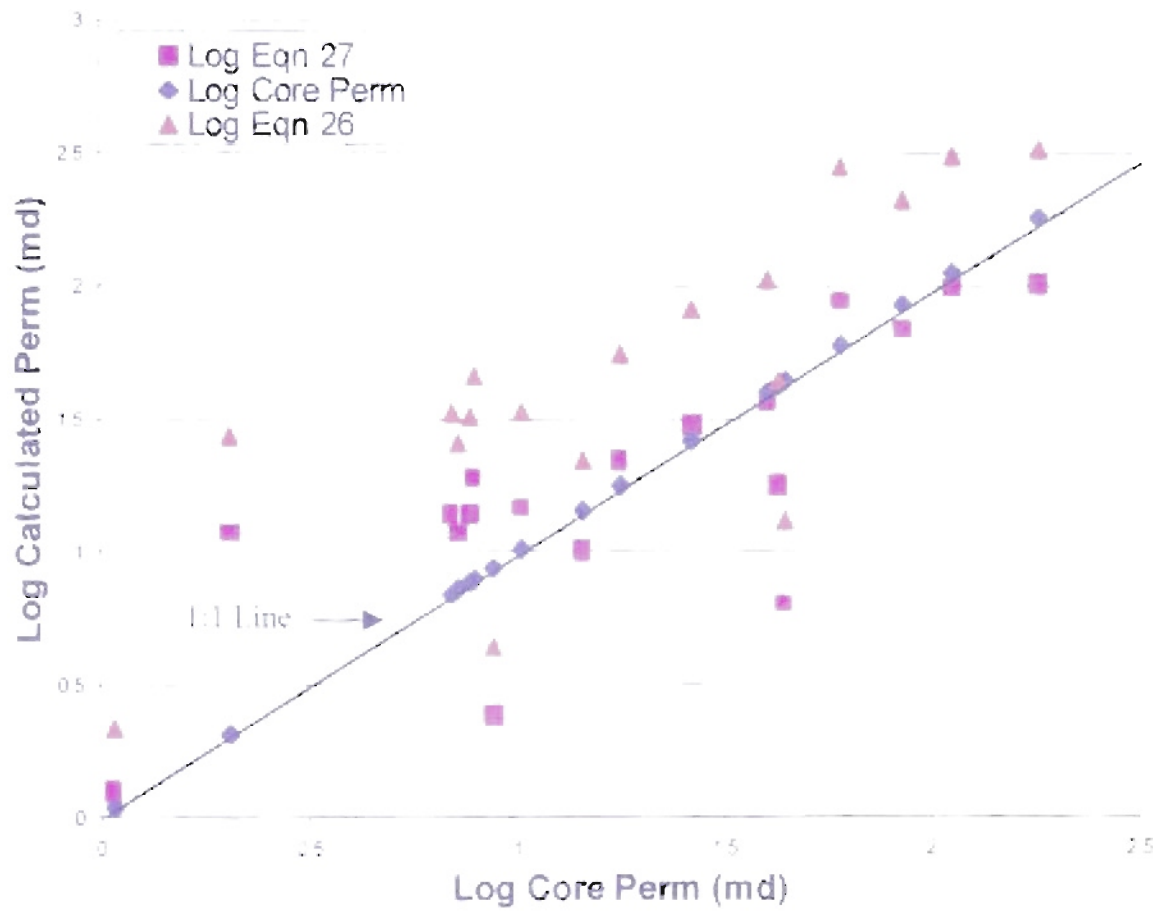


Figure 38. Core permeability vs Eqn 26 and Eqn 27

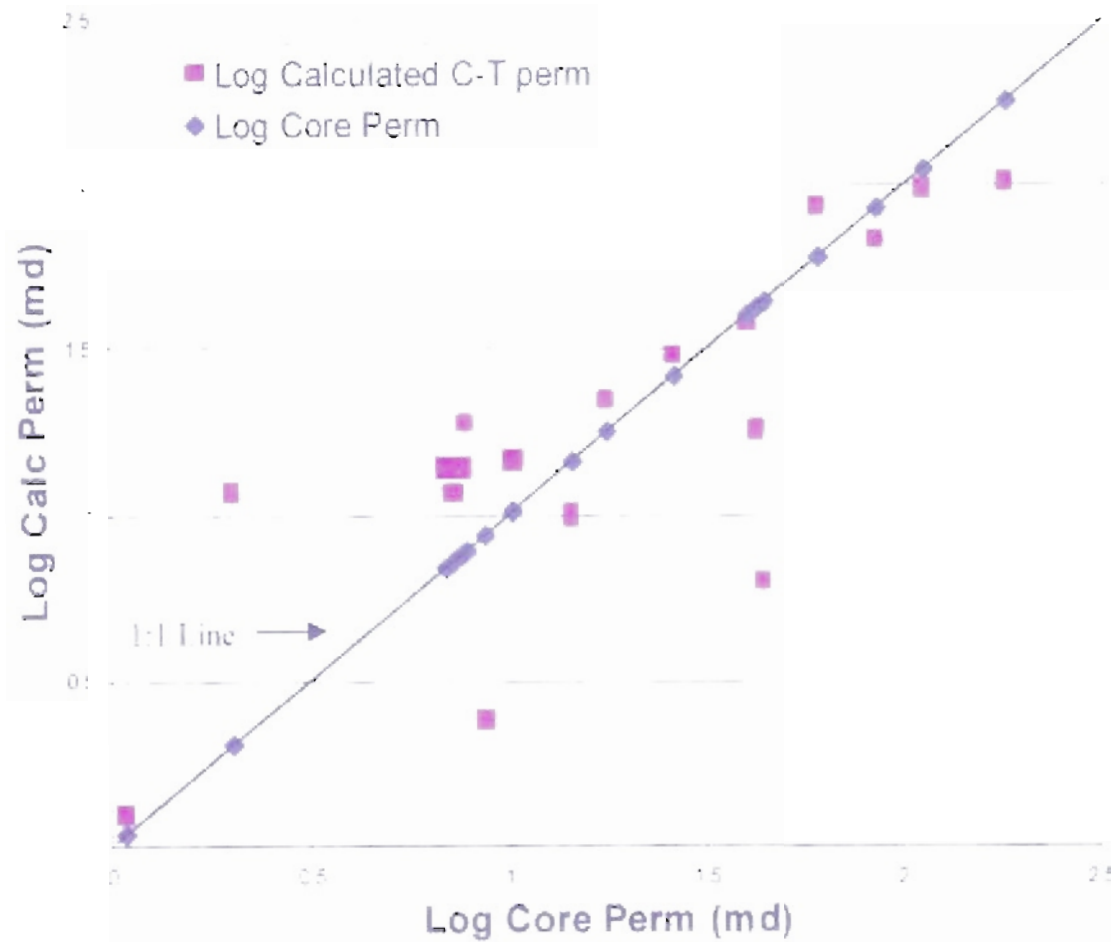


Figure 39 Core permeability vs Calculated C-T permeability

order to find a better fit to the measured data. Recall the standard SDR equation from Chapter 1:

$$k = 4 * \phi^4 * T_2^2 \quad (\text{Eqn. 27})$$

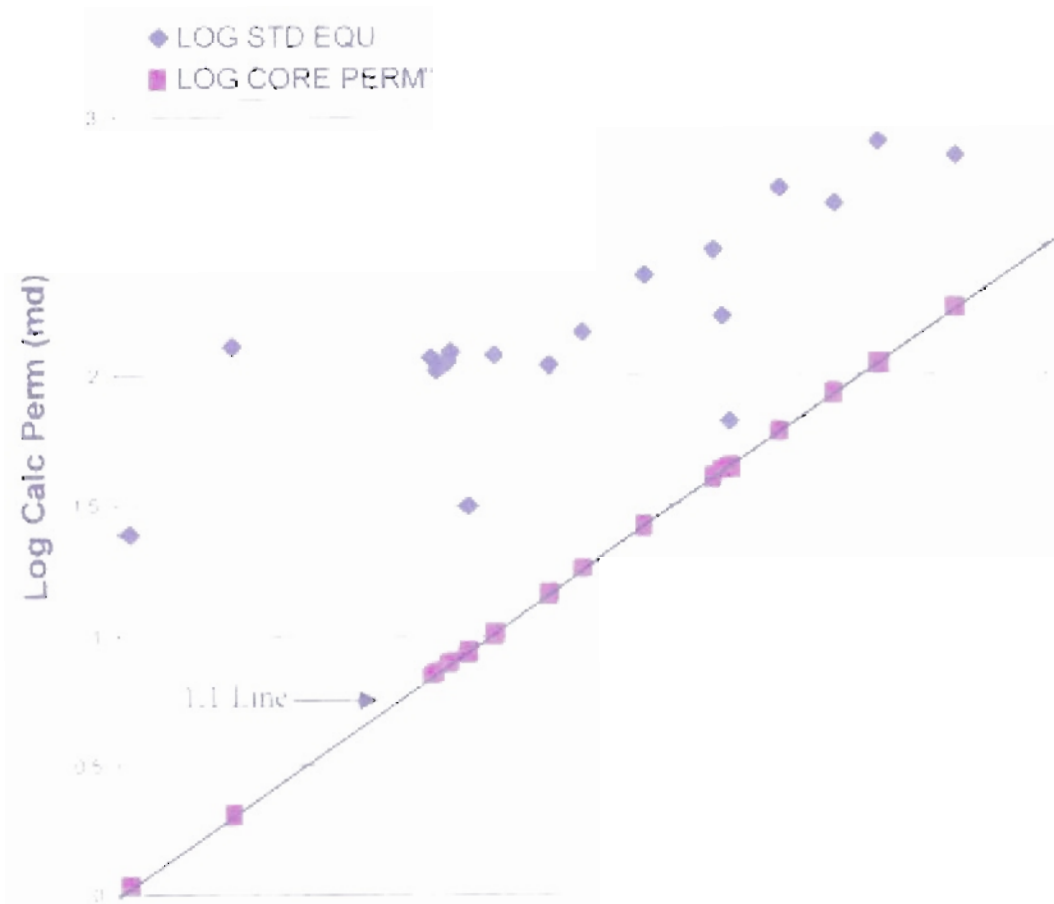
Since the porosity is in fractional form, the b-variable should be increased in order to decrease the calculated permeability, when compared to the standard equation. As with the C-T permeability calculations above, the “guess and check” method is applied to determine the variables that yield the closest calculated permeability to core permeability. Figure 40 is a plot of the log of the core permeability vs. calculated SDR permeability using the standard equation.

The weighted  $T_2$  value is used in this equation since the weighted value better represents the sample's pore system than does the average  $T_2$ . The  $T_2$  value for all the samples ranges from 70 msec to 260 msec. The  $T_2$  component of Equation 27 increases exponentially for the large  $T_2$  values when the c-variable is increased. The c-variable was also decreased in order to lower the calculated permeability. The c-variable is decreased in small stepwise increments since larger decreases tend to lower the calculated permeability too much. While the c-variable is being decreased, the a- and b-variables are held constant. To further decrease the calculated permeability value, the a-variable is slightly decreased also.

Figure 41 illustrates that the following equation yields permeability values that are closer to the measured core permeability.

$$K = 4.5 * \phi^{4.55} * T_2^{1.82} \quad (\text{Eqn. 28})$$

For the SDR equation the a-, b- and c-variables can vary slightly from the recommendations in Equation 28 and similar results will be achieved.



Log Core Perm (md)

Figure 40 Core permeability vs Std SDR permeability



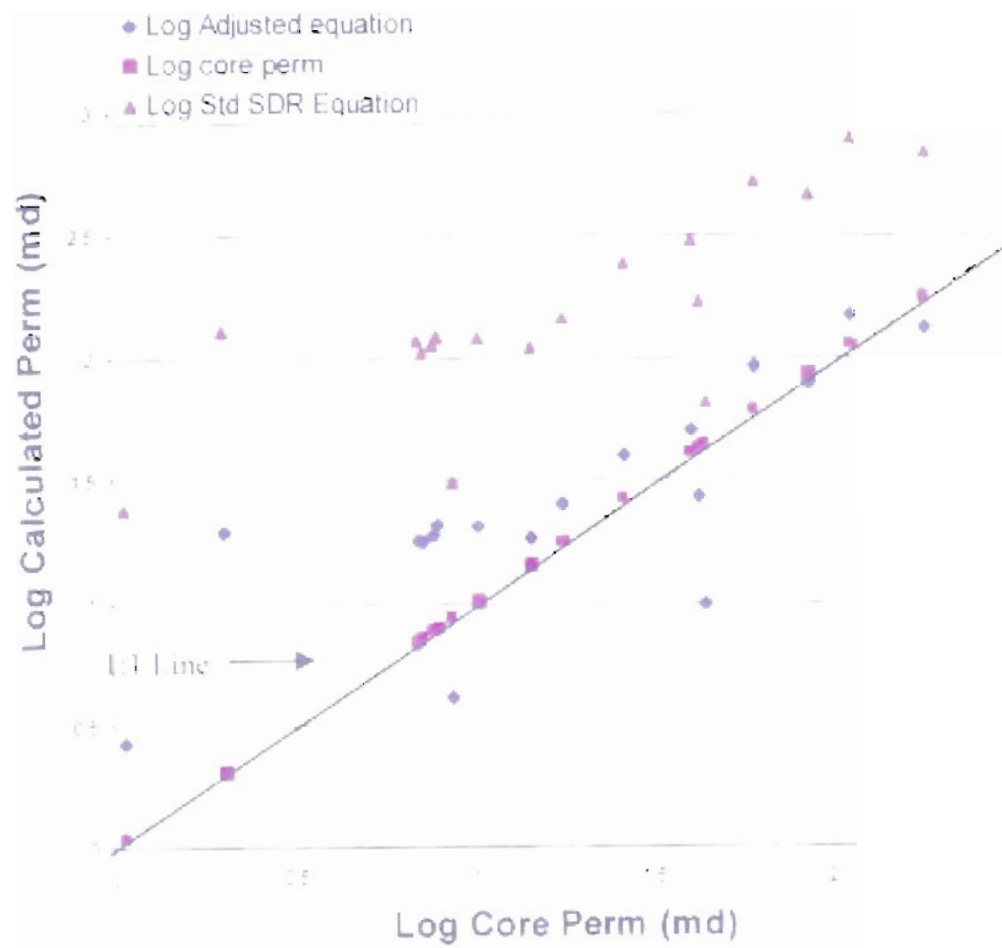


Figure 41 Core permeability vs Calculated SDR permeability

## Chapter 5 - Conclusions

Following are the main observations and recommendations about the use of NMR logging in the Morrow Formation reservoirs:

- 1) Data analysis suggests that NMR porosity correlates more strongly with core porosity than with porosity determined by mercury-injection capillary pressure (MICP). The MICP porosity does not correlate well with NMR response because of instrument error or because of measurement (human) bias in determining the closure pressure, or both.
- 2) The strong correlation between NMR porosity and core analysis porosity ( $r = 0.89?$ ) suggests the two techniques are measuring similar attributes of the rocks and provides strong support for the use of NMR in reservoir characterization.
- 3) The NMR relaxation curve for a given time range corresponds closely with sandstone pore sizes. By assigning pore sizes to NMR time ranges, a geoscientist is better able to determine the proportion of pore types in the formation of interest. The proportions of pore sizes and pore types determine the permeability of the formation through relationship to pore throat sizes.
- 4) Some of the deeply buried sandstones in this study have low porosity for different reasons; some samples have low porosity due to compaction of abundant clay matrix, while other matrix-free samples have low porosity due to abundant quartz cement. NMR response cannot distinguish between these two varieties of low porosity

sandstone. As a rule, these two varieties of sandstone will occur in different depositional environments in the Morrow Formation.

- 5) The 33-msec  $T_2$  cutoff is used to define the boundary between bound-fluids and free-fluids in this data set (an industry convention). The cutoff, which is used to determine  $S_{wi}$ , yields  $S_{wi}$  estimates for the Morrow data set with a large amount of scatter. The scatter is probably because the data were collected from three wells spread over a large geographic area. The amount of variation would probably decrease if the calibration data had been restricted to one field with similar geologic conditions.
- 6) Permeability Calculations - Two different equations were used to calculate permeability from the NMR data:

a. Coates - Timur Equation

The 33-msec  $T_2$  cutoff is used in the Coates-Timur equation. The default equation (Equ 23 in text) yields a permeability estimate that is less than the core permeability. By adjusting the exponents, the equation becomes:

$$K = (\phi/9.5)^5 * (FFI/BVI)^4$$

This adjusted equation gives calculated permeability estimates that are more closely aligned with the core permeability measurements ( $r = ?$ ).

b. SDR Equation

In this thesis, the weighted  $T_2$  method is used as input to the SDR permeability equation rather than using the average  $T_2$  value. The weighted  $T_2$  value better represents the relative importance of different pore sizes (and hence, pore throat sizes) for controlling permeability in sandstones. In contrast to the Coates-Timur equation discussed above, the default SDR equation (Equ 27 in text) yields

permeability estimates that are higher than the core permeability. By adjusting the exponents, the equation becomes:

$$K = 4.5 * \phi^{4.55} * T_2^{-1.82}$$

This adjusted equation gives calculated permeability estimates that are more closely aligned with the core permeability measurements ( $r = ?$ ).

It is not clear why the two techniques (Timur-Coates and SDR) give such different results relative to standard core-analysis permeability.

- 7) Relative to core analysis, the NMR technique provides very good estimates of reservoir porosity (as discussed above under #2). However, the estimates of reservoir permeability are not in good agreement with the core analysis permeability. This may suggest that this thesis experiment has problems with estimates of  $S_{wi}$ . Another option is that the equations used for estimating permeability from NMR data (modifications of the Carmen-Cozeny (sp?) equation) are not appropriate models to use for describing the controls on permeability in a granular media. This explanation may be particularly true if the media has been deeply buried and diagenetically altered.
- 8) As demonstrated by this thesis, a successful NMR logging program in a new area requires careful calibration of the tool with the local rock properties. The calibration is best performed with samples directly from the penetrated formation (samples from conventional core, sidewall core, or cuttings).
- 9) Service companies will calibrate the NMR tool with the local rock properties. The local rock properties reflect the geologic conditions at a position in a basin. Consequently, NMR logging without careful calibration to a formation may be of

limited value in an exploration setting unless the controls on the regional rock properties are the same from location to location within the basin. For example, changes in geology might require that each field or each depositional environment within a small area be calibrated to the NMR log. The process of calibrating the NMR tool is similar to the procedures outlined in this thesis.

- 10) NMR logging data can provide valuable input (porosity and permeability) to the building of reservoir models (reservoir simulation or geologic facies models) if the NMR logs are carefully calibrated to the rocks.

## APPENDIX 1







mono. qtz	size	poly. qtz	size	clay	size	para/clay	size	heavy min	size	flint	size	poro/dss	size	calcite	size	dolomite	size	secondary por	size	primary porosity	size	rock frag	sum	kaolinite	size
58		10		21		5		0		5		1		0		0		0		0		0	0	0	
52		23		8		4		0		8		3		1		0		2		0		0	0	0	
65		7		18		4		0		2		0		2		0		0		0		0	0	0	
38		30		10		8		0		2		0		2		1		1		0		0	0	0	
55		3		14		7		0		17		0		3		0		0		0		0	0	0	
40		41		13		4		0		8		0		2		0		0		0		0	0	0	
51		10		11		4		0		20		1		3		0		0		0		0	0	0	
39		17		9		5		0		73		2		1		2		0		0		0	0	0	
59		15		7		2		0		11		1		1		1		0		0		0	0	0	
71		0		15		4		0		8		1		1		1		1		0		0	0	0	
60		0		8		4		0		3		2		1		0		1		0		0	0	0	
71		0		10		3		0		12		3		1		0		0		0		0	0	0	
61		30		8		7		0		0		0		0		0		0		0		0	0	0	
sum														sum											
4992	38.3	440	11.5	754	0.2	247	0.04	19	0.04	390	7.1	83	0.12	217	1.8	344	2.4	298	1	50	0.2	54	1.4	2	
avg														avg											
63.2	1.3	5.8	0.8	9.3	0.0	3.1	0.0	0.2	0.0	4.9	0.4	1.1	0.1	2.7	0.4	4.4	0.3	3.8	0.3	0.7	0.2	0.7	0.0	0.0	
total sum																									
7897.0																									
normalized														normalized											
63.2		5.8		9.3		3.1		0.2		4.9		1.1		2.7		4.4		3.8		0.7		0.7		0.0	

w0244 1		millimeters				2.5 mg																									
#/no	qz	size	poly qz	size	clay	size	muscovite	size	por/c clay	size	glauconite	size	plag	size	heavy min	size	Dist	size	por/foss	qz overgrow	size	calcite	size	dolomite	size	secondary por	size	primary porosity	size		
73	1		0	0	8	0.04	0		4	0.04			0					1	0.04		2		4	1	0	0.8	3	0.04	0	0.04	
63	1.3		0	0	0		0		4				0		0		1	1	1		2		8	1.2	4		6		5		
67	1		8	1	6		0		4				0		0		3	1.2	1		2		0	0.6	3		3		1		
58	1		12	1.2	11		0		3				0		0		3		1				7	0.8	2		2		1		
58	0.5		0	0	12		0		7				0		1	0.3	18		4				1	1.4	1		0		0		
63	0.8		0	0	8		0		4				0		0		4		3				5		1		7		4		
61	0.6		0	0	10		0		6				1		0		5		1				4		4		3		6		
56	0.8		0	0	4		0		3				0		0		5		2				10		6		7		2		
63	0.8		1	0.8	10		0		1				0		0		3		0				10		5		3		4		
76	1		0	0	12		0		1				0		0		1		0				3		0		3		2		
58	1		12	0.8	12		0		2				0		0		3		2				1		1		10		1		
75	1		0	0	4		1	0.02	1				0		0		1		0				4		0		8		2		
61	1		0	0	7		0		3				0		0		3		0				7		6		13		2		
64	1.1		8	1.4	6		0		3				0		0		1		1				2		1		11		0		
54	1		0	0	9		0		1				0		0		6		6				7		12		1		2		
56	0.9		4	0	12		0		3				0		0		10		1				4		5		3		2		
75			3	0	8		0		3				0		0		1		1				1		1		4		0		
35			10	0	15		0		2				0		0		10		7				3		4		13		1		
67			0	0	8		0		1				0		0		3		1				0		2		7		0		
sum																															
1143	15		56	5.2	177	0.04	1	0.02	56	0.04	1	0	1	0	2	0.3	60	2.24	33	0.04	8	0	06	5.2	89	0.8	106	0.04	35	0.04	
average																															
67.3	0.9		2.9	0.3	9.3	0.0	0.1	0.0	2.9	0.0	1.0	#DIV/0!	0.1	#DIV/0!	0.1	0.3	4.2	0.7	1.7	0.0	2.0	0.0	5.1	1.0	3.8	0.8	5.6	0.0	1.8	0.0	
total sum																															
1902																															
normalized																															
67.2			2.9		9.3		0.1		2.9		0.1		0.1		0.1		4.2		1.7		0.3		5.0		3.8		5.6		1.8		















#0256.6		7.5 mm																		Secondary		Primary																	
Mono	size	Poly	size	Ca-silica	size	Dolomite	size	Keokano	size	Clay	size	Porcelain	size	Diss.	size	Por/diss	size	porosity	size	porosity	size	Qtz over	size	Heavy min	size	organics	size	Carbonate	size	Illite	size	Biotite	size	Andersite	size				
80	1	5	0.7	2	0.2	0		7	0.2	7	0.4	2	0.2	7	0.2	1	0.1	2	0.2	3	0.2	3		0		0		1	0.4	0	0	0	0	0					
81	0.5	8		1		0		3	0.8	9		3		5		2		4		2		3		0		0		0	0	0	0	0	1	0					
56	0.8	8		0		0		1	1.1	9		4		8		2		5		4		2		0		0		0	0	0	0	0	3	0					
54	0.5	5		0		0		7	1.0	10		3		6		2		6		2		4		0		0		0	0	0	2	0	3	0					
59	0.7	7		1		2	0.1	6	7	5		5		5		2		2		1		2		0		0		0	0	0	1	0	0	0					
55	1	7		1		0		8	9	4		5		1		7		2		3		3		0		0		0	0	0	0	0	0	0					
51	1.2	8		1		1		4	9	8		8		2		5		2		2		2		0		1	0.1	0	2	0	0	0	0	0					
83		8		0		0		3	8	8		4		8		3		5		0		2		0		0		0	0	0	0	0	0	0	0				
48		5		0		0		14	1.1	3		7		7		4		5		2		3		0		0		0	0	0	0	0	0	0	0				
35		8		0		0		12	7	2		9		5		8		10		2		2		0		0		0	0	0	0	0	0	0	0				
36		8		0		0		12	1.1	3		10		4		8		2		2		2		1	0.1	0		1	0	0	0	0	0	0	0				
56		3		0		0		8	8	2		8		4		2		2		2		3		0		0		0	0	0	0	0	0	2	0				
37		6		0		2		12	1.2	4		7		2		7		0		0		2		0		0		1	0	0	0	0	0	2	0				
57		5		1		0		14	8	1		8		2		3		1		2		3		0		0		0	0	0	1	0	0	0	0				
58		3		2		0		8	1.1	2		8		2		1		2		2		2		0		0		0	0	1	0	0	0	0	0				
54		5		0		0		9	9	3		10		3		1		3		2		2		0		0		0	0	0	0	0	0	0	0				
81		8		0		0		5	1.0	2		4		3		5		3		1		1		0		1		0	0	0	0	0	0	0	0				
57		4		0		0		8	1.4	1		5		2		3		4		2		2		0		0		0	1	0	0	0	0	0	0				
59		3		0		0		5	9	1		8		2		8		4		2		8		0		0		0	0	0	0	0	0	0	0	0			
58		2		1		0		3	1.0	2		10		1		8		3		3		3		0		0		0	0	0	0	0	0	0	0	0			
82		0		1		0		9	9	0		2		5		1		8		3		2		0		0		0	0	0	0	0	0	0	0	0			
83		2		0		1		7	9	2		5		2		3		3		3		3		0		0		1	0	0	0	0	0	0	0	0			
80		2		1		0		9	9	1		5		1		4		4		3		3		0		0		0	0	0	1	0	0	0	0	0			
52		3		2		3		4	1.0	3		7		2		6		4		3		3		0		0		0	1	0	0	0	0	0	0	0			
81		6		0		0		4	8	2		5		2		8		0		3		3		0		0		0	0	0	0	0	0	0	0	0			
82		2		0		0		9	9	1		8		1		8		1		2		2		0		0		0	2	0	0	0	0	0	0	0			
55		8		0		0		10	1.1	2		8		2		2		2		2		3		0		0		1	0	0	0	0	0	0	0	0			
48		7		0		0		12	1.6	1		6		1		3		3		3		3		0		0		0	0	0	0	0	0	0	0	0			
86		1		1		0		8	1.2	1		5		1		8		3		4		4		0		0		0	0	0	0	0	0	0	0	0			
54		8		3		0		11	1.4	1		8		4		4		4		2		3		0		0		0	1	0	0	0	0	0	0	0			
58		0		0		3		7	1.0	2		7		2		7		1		2		2		0		0		0	0	0	0	0	0	0	0	0			
87		0		0		3		8	7	1		5		2		3		2		2		1		0		0		0	0	0	0	0	0	0	0	0			
sum																																							
1830.0	5.4	144.0	0.7	19.0	0.2	19.0	0.1	254.0	0.8	308.0	0.4	77.0	0.2	72.0	0.2	75.0	0.1	152.0	0.2	82.0	0.2	83.0	0.0	1.0	0.1	3.0	0.1	5.0	0.4	8.0	0.0	6.0	0.0	12.0	0.0	0.0			
average																																							
55.5	0.8	4.4	0.7	0.8	0.2	0.0	0.1	7.7	0.4	9.3	0.4	2.3	0.2	8.7	0.2	2.3	0.1	4.8	0.2	7.5	0.2	2.5	0.0	0.0	0.1	0.1	0.1	0.2	0.4	0.2	0.0	0.2	0.0	0.4	0.0				
total sum																																							
3299.0																																							
normalized																																							
55.5		4.4		0.8		0.0		7.7		9.3		2.3		8.7		2.3		4.8		7.5		2.5		0.0		0.1		0.2		0.2		0.2		0.4		0.0			

k0257 1		2.5 mag												Porosity		Secondary		Primary												Heavy											
Vono	size	Poly	size	Calcite	size	Dolo	size	Kaolinite	size	Clay	size	clay	size	Qtz	size	dis	size	porosity	size	porosity	size	Qtz over	size	glauconite	size	min	size	organics	size	plag	size	carbon	size	lite	size	biofr	size	siderite	size		
53	1.7		10 0.8	1	0.2	0	0.0	11	1	8	0.4	3	0.1	3	0.5	1	0.1	4	0.1	1	0.1	3	0.1	0	0	0	0	0	0	0	0	0	0	0	0	0	0	0	0	0	
47	1.1		15 1.8	1	0	0	0	10	0.8	4	1	1	0	8	3	0	0	6	0	1	0	4	0	0	0	0	0	0	0	0	0	0	0	0	0	0	0	0	0	0	
58	1		3 0.5	1	0	0	0	18	5	1	1	1	0	6	5	0	0	2	0	2	0	2	0	0	0	0	0	0	0	0	0	0	0	0	0	0	0	0	0	0	
48	0.5		3 0.4	1	0	0	0	7	5	1	1	1	0	17	7	0	0	5	0	1	0	2	0	0	0	0	0	0	0	0	0	0	0	0	0	0	0	0	0	0	
53	0.8		8 0.8	1	1	0	0	8	4	2	1	1	0	7	3	0	0	5	0	2	0	3	0	0	0	0	0	0	0	0	0	0	0	0	0	0	0	0	0	0	
54	0.5		3 1.4	0	0	0	0	8	8	1	1	1	0	8	3	0	0	4	0	2	0	2	0	0	0	0	0	0	0	0	0	0	0	0	0	0	0	0	0	0	
54	0.4		15 0.8	0	0	0	0	2	5	0	0	0	0	10	7	0	0	2	0	3	0	2	0	0	0	0	0	0	0	0	0	0	0	0	0	0	0	0	0	0	
43	0.6		3	3	4	3	0	0	4	1	1	1	0	20	6	0	0	3	0	1	0	3	0	0	0	0	0	0	0	0	0	0	0	0	0	0	0	0	0	0	
83	1.8		7	6	0	0	5	7	2	2	2	2	0	6	2	0	0	2	0	2	0	2	0	0	0	0	0	1	0.2	0	1	0	0	0	0	0	0	0	0		
55	0.0		5	0	0	0	9	8	4	7	4	3	0	7	4	0	0	3	0	1	0	2	0	0	0	0	0	0	0	0	0	0	0	0	0	0	0	0	0		
77			5	0	0	0	2	4	1	2	0	0	0	2	0	0	0	3	0	1	0	4	0	0	0	0	0	0	0	0	0	0	0	0	0	0	0	0	0	0	
58			2	0	0	0	7	1	0	0	0	0	0	20	5	0	0	5	0	1	0	2	0	0	0	0	0	0	0	0	0	0	0	0	0	0	0	0	0	0	
82			10	1	0	0	7	4	1	0	1	0	0	0	2	0	0	3	0	0	0	1	0	0	0	0	0	0	0	0	0	0	0	0	0	0	0	0	0	0	
48			20	2	5	8	5	1	7	2	2	2	0	4	1	0	0	4	0	1	0	2	0	0	0	0	0	0	0	0	0	0	0	0	0	0	0	0	0	0	
88			15	0	0	0	2	3	1	5	2	1	0	5	2	0	0	1	0	1	0	2	0	0	0	0	0	0	0	0	0	0	0	0	0	0	0	0	0	0	
86			5	0	0	0	10	5	2	5	2	1	0	5	2	0	0	1	0	0	0	1	0	0	0	0	0	0	0	0	0	0	0	0	0	0	0	0	0	0	
72			3	0	0	0	3	4	2	4	1	1	0	4	1	0	0	2	0	1	0	2	0	0	0	0	0	0	0	0	0	0	0	0	0	0	0	0	0	0	
59			3	1	0	0	17	8	1	0	0	0	0	6	0	0	0	3	0	0	0	1	0	0	0	0	0	0	0	0	0	0	0	0	0	0	0	0	0	0	
82			2	1	2	1	16	2	1	0	0	0	0	8	2	0	0	3	0	0	0	1	0	0	0	0	0	0	0	0	0	0	0	0	0	0	0	0	0	0	
47			0	0	1	0	6	4	1	10	5	0	0	3	0	0	0	0	2	0	0	0	0	0	0	0	0	0	0	0	0	0	0	0	0	0	0	0	0	0	
71			2	0	2	9	3	1	0	2	2	0	0	6	2	0	0	0	0	1	0	0	0	0	0	0	0	0	0	0	0	0	0	0	0	0	0	0	0	0	
51			0	1	2	4	3	2	27	5	4	0	0	0	0	0	0	0	0	0	0	0	0	0	0	0	0	0	0	0	0	0	0	0	0	0	0	0	0	0	
73			10	0	0	0	4	3	2	2	0	0	0	2	0	0	0	3	0	1	0	2	0	0	0	0	0	0	0	0	0	0	0	0	0	0	0	0	0	0	
81			5	2	4	9	3	0	4	1	6	2	0	0	1	0	0	0	2	0	2	0	2	0	0	0	0	0	0	0	0	0	0	0	0	0	0	0	0	0	
72			0	0	0	20	2	0	2	0	2	0	0	2	0	0	0	0	0	0	0	1	0	0	0	0	0	0	0	0	0	0	0	0	0	0	0	0	0	0	
80			4	1	5	2	1	0	2	0	2	0	0	1	0	0	0	1	0	2	0	2	0	0	0	0	0	0	0	0	0	0	0	0	0	0	0	0	0	0	
72			0	0	1	3	8	1	10	3	1	0	0	0	1	0	0	0	0	0	0	1	0	0	0	0	0	0	0	0	0	0	0	0	0	0	0	0	0	0	
86			5	0	0	5	4	1	4	1	2	0	0	0	1	0	0	0	0	0	0	0	0	0	0	0	0	0	0	0	0	0	0	0	0	0	0	0	0	0	
62			5	0	0	25	1	0	2	0	0	0	0	0	0	0	0	0	1	0	0	0	0	0	0	0	0	0	0	0	0	0	0	0	0	0	0	0	0	0	
78			0	0	0	6	2	0	13	3	0	0	0	0	0	0	0	0	0	0	0	0	0	0	0	0	0	0	0	0	0	0	0	0	0	0	0	0	0	0	
88			5	0	0	3	10	1	4	2	1	0	0	2	0	0	0	0	0	0	0	2	0	0	0	0	0	0	0	0	0	0	0	0	0	0	0	0	0	0	
81			3	0	0	0	4	0	8	2	0	0	0	0	0	0	0	0	0	0	0	1	0	0	0	0	0	0	0	0	0	0	0	0	0	0	0	0	0	0	
sum																																									
1979.0	8.4	178.0	6.3	17.0	0.2	27.0	0.6	258.0	1.8	141.0	0.4	35.0	0.1	270.0	0.8	81.0	0.1	84.0	0.1	30.0	0.1	38.0	0.1	1.0	0.0	1.0	0.0	1.0	0.4	1.0	0.2	17.0	1.2	8.0	0.1	2.0	0.0	1.0	0.0		
average	61.8	9.9	5.8	0.9	0.5	0.2	0.8	8.0	0.9	4.4	0.4	1.1	0.1	8.4	0.8	2.5	0.1	2.8	0.1	0.9	0.1	1.3	0.1	0.0	0.0	0.0	0.0	0.0	0.4	0.0	0.2	0.4	0.6	0.3	0.1	0.1	0.0	0.0	0.0		
total sum	3185.0																																								
normalized	62.1		5.8		0.5		0.8		8.0		4.4		1.1		5.5		2.5		2.8		0.8		1.9		0.0		0.0		0.0		0.4		0.3		0.1		0.0		0.0		

Mond		Poly		Calcite		Dolo		Kaolinite		Clay		Porphy clay		Dens		Porosity		Secondary		Primary		Oz over		glauconite		Heavy min		organics		carbonate		muscovite		Illite		siltstone		sandstone		rock	
size	size	size	size	size	size	size	size	size	size	size	size	size	size	size	size	size	size	size	size	size	size	size	size	size	size	size	size	size	size	size	size	size	size	size	size	size	size	size	size	size	
57	0.1	2	0.4	1	0.1	1	0.1	15	0.4	5	0.4	1	0.1	5	0.4	2	0.1	3	0.8	2	0.1	1	0.1	0		3	0.4	0		0		0		2		0		0			
48	0.8	10	0.8	3		3		0	0.2	5		2		8		3		11	0.2	4		3		1	0.2	2		0		0		1		0		0		0			
52	0.3	3	0.4	3		5		2		1		0		7		2		11		4		4		0		0		0		0		1	0.1	0		0		0			
65	0.4	2		1		1		2		3		1		4		2		11		4		4		0		0		0		0		0		0		0		0			
56	0.4	4		1		3		3		2		1		8		4		9		5		3		0		1		0		0		0		0		0		0			
57	0.3	3		3		3		2		1		1		9		3		12		5		4		1		1		0		0		0		0		0		0			
55	0.5	8		1		1		6		2		0		7		5		8		8		3		0		0		0		0		0		0		0		0			
49	3	2		5		20		1		1		1		8		2		0		5		4		0		1		0		0		0		0		0		0			
54	0	4		8		7		2		1		1		8		2		8		4		4		0		0		0		0		0		0		0		0			
49	4	1		2		1.6		1		1		1		5		1		13		2		3		0		2		0		0		0		0		0		0			
57	2	0		1		8		7		1		1		4		2		8		8		3		0		1		0		0		0		0		0		0			
53	0	2		3		9		4		2		0		4		4		7		4		4		0		0		0		0		0		0		0		0			
57	8	1		3		4		3		1		1		4		3		10		4		4		0		0		0		0		0		0		0		0			
64	5	1		3		3		1		0		0		5		2		8		3		5		0		0		0		0		0		0		0		0			
87	3	0		3		3		0		0		3		2		1		0		4		3		0		1		1	0.2	0		0		0		0		0			
87	0	1		0		11		8		2		2		7		1		1		2		3		0		2		0		0		0		0		0		0			
65	0	0		3		4		8		0		5		1		10		3		3		0		0		0		0		0		0		0		0		0			
58	3	0		2		9		3		1		0		6		2		11		4		4		0		0		0		0		0		0		0		0			
56	0	0		1		2		2		1		0		8		0		10		8		4		0		1		0		0		0		0		0		0			
50	2	1		2		8		3		1		0		2		9		9		9		4		0		1		0		0		0		0		0		0			
52	3	0		0		7		3		0		0		8		3		9		7		3		0		1		0		0		1		0		0		0			
68	0	1		2		3		1		0		4		2		7		9		4		0		0		1		0		0		0		0		0		0		3	0.2
54	2	3		1		8		2		0		4		1		0		11		5		0		0		0		0		0		0		0		0		0			
54	0	2		3		20		1		0		4		4		4		10		7		4		0		1		0		0		0		0		0		0			
82	0	2		1		8		1		0		4		2		12		4		4		0		0		0		0		0		0		0		0		0			
52	3	2		1		6		1		0		7		2		14		5		5		0		0		1		0		0		0		0		0		0			
40	8	1		1		10		3		0		8		3		10		8		4		0		0		0		1		0		0		0		0		0			
52	2	0		1		6		1		0		8		3		12		6		5		0		0		0		0		0		0		0		0		1			
56	0	1		3		5		1		1		7		4		13		3		5		0		0		0		0		0		0		0		0		0		4	
46	1	4		1		4		3		1		11		1		10		10		4		0		0		0		1	0.4	0		1		0		0		0			
37	0	2		5		13		8		1		7		1		10		9		5		0		1		0		0		0		1		0		0		0			
45	0	1		3		5		8		2		7		1		10		4		3		0		0		8		1		0		2		0		0		1			
57	13	1		0		8		8		1		2		0		0		8		7		2		0		0		0		0		0		0		0		0		3	
60	2	7		0		4		3		1		5		1		8		8		4		0		3		0		0		0		0		1		0		1		0	
60	1	2		3		5		1		0		8		2		0		0		4		0		0		0		0		0		0		0		0		1		0	
87	0	0		0		0		3		1		2		1		18		5		2		0		0		0		1		0		2		0		0		0		1	
68	0	0		2		4		2		0		8		1		11		4		3		2		0		0		0		0		0		0		0		0		1	
50	3	1		2		14		2		0		8		3		10		2		4		0		1		0		0		0		0		0		0		0		0	
54	2	1		0		12		3		0		4		1		7		10		3		0		1		0		0		0		0		0		0		0		0	
59	3	0		1		7		3		0		6		2		7		8		2		0		0		0		0		0		0		0		0		0		0	
50	0	2		8		19		1		0		3		2		5		10		2		0		0		0		0		0		0		0		0		0		0	
sum																																									
2275.0	2.8	101.0	1.6	59.0	0.1	20.0	0.1	297.0	0.8	123.0	0.4	29.0	0.1	234.0	0.4	85.0	0.1	354.0	1.0	241.0	0.1	148.0	0.1	4.0	0.2	26.0	0.4	4.0	0.2	3.0	0.8	2.6	0.1	10.0	0.0	1.0	0.0	14.0	0.2		
ave/8 po																																									
55.5	0.4	2.5	0.5	1.4	0.1	2.2	0.1	7.2	0.4	3.0	0.4	0.7	0.1	5.7	0.4	2.3	0.1	8.8	0.5	5.9	0.1	3.8	0.1	0.1	0.2	0.7	0.4	0.1	0.2	0.1	0.4	0.0	0.1	0.2	0.0	0.0	0.0	0.3	0.2		
total sum																																									
4114.0																																									
normalized																																									
55.3		2.3		1.4		2.2		7.2		3.0		0.7		5.7		2.3		8.8		5.9		3.8		0.1		0.7		0.1		0.1		0.0		0.2		0.0		0.3		0.2	

wt%		2.5 mag																																				
Mono	size	Poly	size	Calcite	size	Dolomite	size	Kaolinite	size	Clay	size	Porosity	size	Diss	size	Porosity	size	Secondary porosity	size	Primary porosity	size	Otr over	size	Heavy min	size	organics	size	plaq	size	carbonate	size	lime	size	biofilm	size	rock frag	size	
42	0.6	8	0.8	1	0.2	4	0.2	10	0.8	12	0.8	1	0.1	9	0.6	4	0.1	5	0.2	0	0.1	1	0.1	0	0	0	0	0	0	0	0	0	0	0	0	2	0.5	
41	0.8	4	0.3	3		0		4		10		2		8	0.2	1		4		1		2		0		0		0		0		0		0		0		
40	0.8	9	0.8	1		2		2		8		2		5		1		4		0		2		2	0.4	0		0		0		0		0		0		
41	0.6	4	0.8	2		0		3		13		2		3		1		5		4		1		0		0		0		0		0		0		0		
45	0.4	2	0.6	0		4		4		5		1		5		2		2		3		3		0		0		0		0		0		0		0		
58	0.0	3	1	0		3		4		6		2		7		3		5		3		2		0		0		0		0		0		0		0		
54	0.6	5	0.8	0		0		10		0		1		9		3		1		1		2		0		3		0		1		0		0		0		
50	0.7	5	0.5	0		0		11		9		3		10		3		3		0		3		0		0		0		2		0		0		1	0.4	
53	0.8	2	0.6	2		0		16		5		1		8		4		4		0		2		0		1		0		0		0		0		3	0.4	
46	0.9	8	1	1		0		10		11		5		12		2		1		10		0		0		0		0		0		0		0		0		
63	1	3	1	1		0		6		10		4		8		2		1		0		0		0		1		0		0		1		0		0		
37	1	8	1	1		0		17		0		2		18		3		0		0		1		0		0		0		0		0		0		0		
33	0.8	15	2	2		0		17		8		2		7		2		1		1		3		0		0		0		0		0		0		0		
40	1	0	1	1		1		5		7		2		8		3		4		3		4		0		2		0		0		0		0		0		
64	1.3	4	0	0		0		11		0		2		4		2		0		1		4		0		2		0		0		0		0		0		
64	1	0	0	0		1		0		9		3		15		3		1		1		1		0		0		0		2		0		0		0		
64	1	2	1	1		1		0		8		0		0		0		7		5		5		0		2		0		0		2		0		0		
40	1	1	1	1		2		6		8		2		5		1		4		4		4		0		1		0		0		3		0		0		
50	2	7	1	1		1		0		4		1		13		3		4		2		5		0		0		0		1		0		0		0		
70	3	0	0	0		1		2		3		1		5		1		4		0		3		0		3		0		0		2		0		0		
62	0	0	0	0		3		2		7		0		11		3		4		1		4		0		0		0		0		1		0		0		
52	3	1	1	0		0		3		8		3		11		2		0		0		7		0		1		0		0		0		0		0		
50	0	0	1	2		2		17		3		2		12		3		2		3		2		0		1		0		0		4		0		0		
65	3	3	3	3		3		8		3		1		3		2		0		2		3		0		0		0		0		2		0		0		
56	4	0	0	1		1		21		5		1		2		0		3		0		3		0		0		0		1		1		0		1		
52	10	0	0	1		7		2		1		1		10		3		8		0		4		0		0		0		0		2		0		13	1	
58	2	0	0	0		0		8		3		3		2		0		0		2		5		0		0		0		1		0		0		0		
59	10	0	0	0		13		3		3		1		4		2		1		0		3		0		0		0		0		0		0		0		
36	5	2	2	2		20		3		3		2		19		4		0		2		4		0		1		0		0		0		0		0		
57	15	5	4	4		5		1		0		0		8		3		0		2		3		0		1		0		0		0		0		0		
55	0	25	3	3		8		1		0		0		2		1		8		1		2		0		1		0		0		0		0		0		
54	15	13	7	3		7		3		1		0		8		1		4		0		1		0		7		0		0		0		0		0		
20	25	7	3	8		3		8		3		0		10		2		4		0		1		0		12		1		0		0		0		4		
46	0	12	5	4		5		4		1		0		20		2		5		0		0		0		2		0		0		3		0		0		
72	0	15	3	2		3		2		3		1		0		0		2		0		1		0		0		0		1		0		0		0		
sum	1017	12.6	101.0	5.9	97.0	0.2	74.0	0.2	282.0	0.8	203.0	0.0	54.0	0.1	282.0	0.8	71.0	0.1	103.0	0.2	43.0	0.1	95.0	0.1	2.0	0.4	41.0	1.0	4.0	0.4	10.0	0.4	23.0	0.0	1.0	0.0	24.0	2.3
average	54.8	0.8	5.3	0.7	2.8	0.2	2.1	0.2	8.1	0.8	5.6	0.8	1.5	0.1	8.1	0.4	2.0	0.1	2.9	0.2	1.2	0.1	2.7	0.1	0.1	0.4	1.2	1.0	0.1	0.4	0.3	0.4	0.7	0.0	0.0	0.0	0.7	0.8
total sum	3517	0																																				
normalized	54.5		5.4		2.8		2.1		8.0		5.8		1.5		8.0		2.0		2.9		1.2		2.7		0.1		1.2		0.1		0.3		0.7		0.0		0.7	





k0266		2.5 mm																																					
Mono	size	Poly	size	Calcite	size	Dolomite	size	Kaolinite	size	Clay	size	Poroclay	size	Olss	size	Poroidss	size	Secondary porosity	size	Primary porosity	size	Oils over	size	organics	size	plag	size	carbonate	size	muscovite	size	rock frag	size		size				
54	0.7	10	1	8	0.5	3	0.3	6	0.4	5	0.2	0	0	1	0.6	0	0	2	0.4	1	0.2	3	0	3	0.2	1	0.2	4	0.4	0	0	0	0	0	0	0			
62	0.6	5	0.3	1		2		3		7		1	0.1	8	0.2	1	0.1	4	0.2	1	0.2	4	0	0	0	2	0	0	0	0	0	0	0	0	0	0			
54	0.4	8	0.4	2		9		2		13		0		7		0		3	0.2	2		3	0	0	0	0	0	0	0	0	0	0	0	0	0	0			
73	1	0		2		4		14		1		0		2		1		2		0		1	0	0	0	0	0	0	0	0	0	0	0	0	0	0			
67	1.2	5	0.5	1		3		5		8		1		5		1		3		0		4	0	0	0	2	0.7	0	0	0	0	0	0	0	0	0			
77	1	0		3		6		4		3		1		5		1		0		1		3	0	0	0	0	0	0	0	0	0	0	0	0	0	0			
53	0.6	0		4		8		15		8		1		6		2		4		2		0	0	0	0	0	0	0	0	0	0	0	0	0	0	0			
46	0.6	15		2		9		13		5		1		5		1		2		0		1	0	0	0	0	0	0	0	0	0	0	0	0	0	0			
81	10	1		8		9		9		0		0		5		1		4		0		3	0	0	0	0	0	0	0	0	0	0	0	0	0	0			
52	10	1		1		1		23		2		0		4		1		1		1		3	0	0	0	0	0	0	0	0	0	0	0	0	0	0			
84	5	0		4		4		10		2		1		4		2		0		2		4	0	0	0	1	0	0	0	0	0	0	0	0	0	0			
85	7	1		2		1		6		1		1		3		1		2		0		3	0	0	0	2	0	0	0	0	0	0	0	0	0	0			
60	3	4		3		2		10		1		1		7		1		2		0		4	0	0	0	1	0	0	0	0	0	0	0	0	0	0			
49	15	0		7		7		7		7		0		3		0		3		1		5	0	0	0	0	0	0	0	0	0	0	0	0	0	0			
58	10	0		3		1		1		7		1		7		2		2		2		3	0	0	0	3	0	0	0	0	0	0	0	0	0	0	0		
72	0	1		1		4		5		5		1		5		2		2		1		5	0	0	0	2	0	0	0	0	0	0	0	0	0	0	0		
74	2	1		2		3		7		7		0		3		1		3		1		1	0	0	0	1	0	0	0	0	0	0	0	0	0	0			
57	5	5		7		14		3		0		0		2		1		2		1		3	0	0	0	2	0	0	0	0	0	0	0	0	0	0	0		
58	5	3		10		4		4		0		0		3		2		1		1		3	0	0	0	0	0	0	0	0	0	0	0	0	0	0	0		
71	5	2		3		4		2		1		1		2		1		1		2		5	0	0	0	1	0	0	0	0	0	0	0	0	0	0	0		
83	8	1		7		5		3		2		2		4		2		1		2		4	0	0	0	1	0	0	0	0	0	0	0	0	0	0	0		
71	7	2		1		4		3		1		1		6		1		1		1		2	0	0	0	0	0	0	0	0	0	0	0	0	0	0	0		
80	0	1		7		8		3		1		1		4		1		3		1		3	0	0	0	0	0	0	0	0	0	0	0	0	0	0	0		
50	5	14		6		9		6		0		0		7		1		0		1		2	0	0	0	11	0	0	0	0	0	0	0	0	0	0	0		
88	5	2		0		0		0		0		1		10		2		1		0		2	0	0	0	0	0	0	0	0	0	0	0	0	0	0	0		
sum																																							
1535	0.63	141.0	2.2	60.8	0.5	115.0	0.3	170.0	0.4	129.0	0.2	16.0	0.1	121.0	0.8	29.0	0.1	49.0	0.8	24.0	0.2	74.0	0.0	18.0	0.9	1.0	0.2	20.0	0.4	2.0	0.3	7.0	0.4						
average																																							
81.4	0.8	5.6	0.6	2.4	0.5	4.8	0.3	7.0	0.4	3.2	0.2	0.8	0.1	4.8	0.4	1.2	0.1	2.0	0.3	1.0	0.2	3.0	0.0	0.7	0.3	0.0	0.2	0.9	0.4	0.1	0.3	0.3	0.4						
total sum																																							
2517	0																																						
normalized																																							
81.0		5.8		2.4		4.8		7.0		5.1		0.8		4.8		1.2		1.9		1.0		2.8		0.7		1.0		0.8		0.1		0.3							

x0266.4		7.1 mg		Calcite		Dolomite		Keokite		Clay		Poroclay		Ox		Porofoss		Secondary		Primary		Qtz over		organica		silica		carbonate		illite		blotite		rock frag		Calcite		dolo		fossil	
Mono	size	Poly	size	(replacing qtz)	size	(replacing qtz)	size	size	size	size	size	size	size	size	size	size	porosity	size	porosity	size	size	size	size	size	size	size	size	size	size	size	size	size	size	size	size	size	size	size	size		
23	1.1	1	0.2	0	0	0	0	0	1	0.8	0	0	0	4	0.8	0	0.1	1	0.2	0	0.1	0	0	0	0	0	0	0	0	0	0	0	0	0	0	0	0	0	0		
36	1.2	0		3	0.2		0	0.2						18		2		1		0		2	0.1	0		0	0	0	0	0	0	0	0	0	0	0	0	0	0		
38	0.8	7	0.8	0		7		12	0.4	3	0.2	2	0.1	9		2		0		0		1		0		0	0	0	0	0	0	0	0	0	0	0	0	0	0		
36	0.8	10	0.8	0		0		0		1	0.4	0		4		1		0		0		3		0		0	0	0	0	0	0	0	0	0	0	0	0	0	0		
22	0.8	13		0		0		2	0.2	3		1		5		1		1		1		2		0		0	0	0	0	0	0	0	0	0	0	0	0	0	0		
19	0.8	10		3		11		3		1		0		15		2		1		0		1		0		0	0.8	0	0	0	0	0	0	0	0	0	0	0	0		
57	1	0		2		2		7		1		0		0		0		2		0		2		0		3	0	0	0	0	0	0	0	0	0	0	0	0	0		
63	0.8	8		0		0		7		2		0		0		0		1		1		3		0		0	0	0	0	0	0	0	0	0	0	0	0	0	0		
47	0.8	0		0		0		12		8		2		4		1		8		0		4		0		0	0	2	0	0	0	0	0	0	0	0	0	0	0		
47	0.5	10		0		1		4		4		1		3		2		4		4		3		0		0	0	0	0	0	0	0	0	0	0	0	0	0	0		
38	2			0		8		12		2		1		5		1		8		0		3		0		1	0	0	1	0	0	0	0	0	0	0	0	0	0		
48	7	0		0		0		8		4		1		5		2		4		1		3		0		0	0	0	0	0	0	0	0	0	0	0	0	0	0		
48	5	0		0		0		12		5		1		4		1		3		1		4		0		1	0	0	0	0	0	0	0	0	0	0	0	0	0		
50	3	0		0		0		5		5		1		10		3		1		2		3		0		1	0	0	0	0	0	0	0	0	0	0	0	0	0		
44	8	0		0		0		8		8		2		7		2		0		2		4		0		1	0	0	1	0	0	0	0	0	0	0	0	0	0		
53	0	0		0		0		5		8		1		11		3		3		0		3		0		2	0	0	2	0	0	0	0	0	0	0	0	0	0		
45	5	0		0		0		8		10		2		9		3		2		2		3		0		2	0	0	2	0	0	0	0	0	0	0	0	0	0		
58	2	2		1		10		7		1		1		5		2		2		1		2		0		4	0	0	0	0	0	0	0	0	0	0	0	0	0	0	
40	3	0		4		10		8		0		4		4		2		1		1		3		0		3	0	0	2	0	0	0	0	0	0	0	0	0	0		
81	5	0		0		4		3		0		3		0		1		0		4		3		0		1	0.3	0	0	0	0	0	0	0	0	0	0	0	0	0	
54	0	0		0		0		13		4		1		7		2		2		4		4		0		8	0.4	0	1	0	0	0	0	0	0	0	0	0	0	0	
51	2	0		0		8		4		0		0		7		1		7		3		3		0		1	0	0	0	0	0	0	0	0	0	0	0	0	0		
58	5	0		0		0		8		7		1		8		1		0		1		2		0		1	0	0	0	0	0	0	0	0	0	0	0	0	0		
63	7	0		0		4		8		0		1		5		1		4		2		3		0		0	0	0	0	0	0	0	0	0	0	0	0	0	0	0	
58	3	0		0		0		7		8		1		7		2		2		2		2		2		2	0	0	0	0	0	0	0	0	0	0	0	0	0	0	
64	2	0		0		0		4		8		1		7		3		2		1		4		1		3	0	0	0	0	0	0	0	0	0	0	0	0	0	0	
51	5	0		0		4		7		2		2		16		3		2		2		1		4		1	0	0	0	0	0	0	0	0	0	0	0	0	0	0	
30	8	0		0		5		2		0		14		3		3		2		3		3		0		3	0	0	0	0	0	0	0	0	0	0	0	0	0	0	
48	10	0		0		5		4		0		8		2		0		4		4		8		0		3	0	0	0	0	0	0	0	0	0	0	0	0	0	0	
48	11	0		0		8		0		0		10		3		1		3		0		2		0		0	0	0	0	0	0	0	0	0	0	0	0	0	0	0	
51	15	0		0		7		3		0		8		2		3		2		2		5		0		2	0	0	0	0	0	0	0	0	0	0	0	0	0	0	
50	8	0		0		10		5		1		6		2		0		1		3		3		0		0	0	0	0	0	0	0	0	0	0	0	0	0	0	0	
52	3	0		0		10		8		1		7		2		1		2		1		2		0		5	0	0	0	0	0	0	0	0	0	0	0	0	0	0	
52	10	0		0		8		8		1		10		1		1		4		3		0		0		1	0	0	0	0	0	0	0	0	0	0	0	0	0	0	
47	5	0		0		1		10		5		1		10		3		2		3		3		0		1	0	0	0	0	0	0	0	0	0	0	0	0	0	0	
sum	1660.0	8.0	166.0	1.8	100.0	0.2	42.0	0.2	238.0	0.8	187.0	1.2	28.0	0.1	258.0	0.8	80.0	0.1	79.0	0.2	50.0	0.1	101.0	0.1	3.0	0.0	86.0	2.3	2.0	0.0	6.0	0.0	0.0	0.0	340.0	0.2	188.0	0.8	2.0	0.0	
average	47.6	0.8	54.0	0.5	0.3	0.2	1.2	0.2	8.8	0.3	4.8	0.4	0.7	0.1	7.4	0.6	1.7	0.1	2.3	0.2	1.4	0.1	7.9	0.1	0.1	0.0	1.9	0.6	0.1	0.0	0.2	0.0	0.2	0.0	99.0	0.2	5.3	0.8	0.1	0.0	
total sum	3508.0																																								
normalized	47.5		5.4		0.3		1.2		8.8		4.8		0.7		7.4		1.7		2.3		1.4		7.9		0.1		1.9		0.1		0.2		0.2		99.0		5.3		0.1		



r6287.7		2.5 mag		Calcite		Dolomite		Kaolinite		Clay		Pore/clay		Diss		Poroid/diss		Secondary porosity		Primary porosity		Oils over		Organics		Plugs		Carbonate		Siderite		Rock frag		Shale		Cgl		dolo		fossil						
Mono	size	Por	size	size	size	size	size	size	size	size	size	size	size	size	size	size	size	size	size	size	size	size	size	size	size	size	size	size	size	size	size	size	size	size	size	size	size	size								
42	1	20	2	0	0	0	0	0	0	0	0	0	0	0	0	0	0	0	0	0	0	0	0	0	0	0	0	0	0	0	0	0	0	0	0	0	0	0	0							
42	1.2	10	0.8	1	0.2	2	0.2	2	0.2	1	0.2	0	0	4	0.2	1	0.1	0	0.8	0	0	2	0.1	0	0	0	0	0	0	0	0	0	0	0	33	0.4	5	0.8	0							
34	1	30	1	0	0	0	0	0	0	0	0	0	0	5	0	2	0	0.2	1	0.2	1	0	0	0	0	0	0	0	0	0	0	0	0	0	0	0	0	0	0							
51	1.2	0	0	0	0	0	0	0	0	0	0	0	0	15	0	1	0	0.2	0	0	3	0	0	0	0	0	0	0	0	0	0	0	0	0	0	0	0	0	0							
50	0.8	10	0.8	0	0	0	0	1	4	0	0	1	0.1	0	0	0	0	0.2	0	0	2	0	0	0	0	0	0	0	0	0	0	0	0	0	0	0	0	0	0							
37	1	20	1.2	1	0	0	0	3	0	1	0	0	0	0	0	2	0	0	0	0	1	0	0	0	0	0	0	0	0	0	0	0	0	0	0	0	0	0	0	0						
36	0.8	25	1	0	0	0	0	0	0	0	0	0	0	1	0	1	0	0	0	0	0	0	0	0	0	0	0	0	0	0	0	0	0	0	0	0	0	0	0	0						
52	0	0	0	0	0	0	0	0	0	0	0	0	0	4	0	2	0	1	0	0	2	0	0	0	0	0	0	0	0	0	0	0	0	0	0	0	0	0	0	0						
45	10	0	0	2	0	0	0	2	1	0	0	0	0	12	0	3	0	0	0	0	3	0	0	0	0	0	0	0	0	0	0	0	0	0	0	0	0	0	0	0						
61	0	0	0	0	0	0	0	0	0	0	0	0	0	3	0	2	0	1	0	0	2	0	0	0	0	0	0	0	0	0	0	0	0	0	0	0	0	0	0	0	0					
42	20	1.2	0	0	0	0	0	0	1	0	0	0	0	7	0	1	0	0	0	0	3	0	0	0	0	0	0	0	0	0	0	0	0	0	0	0	0	0	0	0						
53	5	0	0	0	0	0	0	1	2	0	0	0	0	15	0	3	0	0	0	0	0	0	0	0	0	0	0	0	0	0	0	0	0	0	0	0	0	0	0	0	0					
49	10	0	0	0	0	0	0	0	0	0	0	0	0	4	0	1	0	0	0	0	1	0	0	0	0	0	0	0	0	0	0	0	0	0	0	0	0	0	0	0	0					
24	0	1	1	0	0	1	0	1	2	0	0	0	0	10	0	3	0	0	0	0	3	0	0	0	0	0	0	0	0	0	0	0	0	0	0	0	0	0	0	0	0					
32	0	2	0	0	0	0	0	0	0	0	0	0	0	0	0	0	0	0	0	0	0	0	0	0	0	0	0	0	0	0	0	0	0	0	0	0	0	0	0	0	0					
35	25	1	3	0	0	3	0	1	0	0	0	0	0	10	0	2	0	0	0	0	0	0	0	0	0	0	0	0	0	0	0	0	0	0	0	0	0	0	0	0	0					
63	0	0	2	0	0	2	0	1	0	0	0	0	0	8	0	2	0	2	0	0	3	0	0	0	0	0	0	0	0	0	0	0	0	0	0	0	0	0	0	0	0	0				
31	45	0	0	0	0	0	0	3	1	0	0	0	0	7	0	2	0	1	0	0	1	0	0	0	0	0	0	0	0	0	0	0	0	0	0	0	0	0	0	0	0	0				
36	15	0	0	0	0	0	0	1	2	0	0	0	0	8	0	1	0	0	0	0	1	0	0	0	0	0	0	0	0	0	0	0	0	0	0	0	0	0	0	0	0	0				
47	15	0	0	0	0	0	0	0	0	0	0	0	0	2	0	0	0	0	0	0	0	0	0	0	0	0	0	0	0	0	0	0	0	0	0	0	0	0	0	0	0	0				
5	3	3	3	0	0	3	0	1	4	0	0	0	0	3	0	1	0	0	0	0	0	0	0	0	0	0	0	0	0	0	0	0	0	0	0	0	0	0	0	0	0	0				
28	50	0	0	0	0	0	0	1	0	0	0	0	0	0	0	0	0	0	0	0	1	0	0	0	0	0	0	0	0	0	0	0	0	0	0	0	0	0	0	0	0	0				
66	6	0	0	0	0	0	0	0	1	0	0	0	0	1	0	0	0	0	0	0	1	0	0	0	0	0	0	0	0	0	0	0	0	0	0	0	0	0	0	0	0	0				
47	30	0	0	0	0	0	0	1	8	0	0	0	0	2	0	1	0	0	0	0	0	0	0	0	0	0	0	0	0	0	0	0	0	0	0	0	0	0	0	0	0	0				
85	5	0	0	0	0	0	0	7	9	0	0	0	0	4	0	1	0	0	0	0	0	0	0	0	0	0	0	0	0	0	0	0	0	0	0	0	0	0	0	0	0	0				
61	0	0	0	0	0	0	0	10	10	0	0	0	0	1	0	0	0	0	0	0	0	0	0	0	0	0	0	0	0	0	0	0	0	0	0	0	0	0	0	0	0	0	0			
sum																																														
1138.0	7.0	364.0	7.8	13.0	0.2	25.0	0.2	30.0	0.2	52.0	0.2	8.0	0.1	133.0	0.2	32.0	0.1	21.0	1.2	1.0	0.2	35.0	0.1	3.0	0.0	3.0	0.0	88.0	0.0	1.0	0.0	12.0	0.0	47.0	0.0	242.0	0.4	289.0	0.8	3.0	0.0	0.0				
average	43.8	1.0	14.0	1.1	0.5	0.2	1.0	0.2	1.2	0.2	2.0	0.2	0.2	0.1	5.1	0.2	1.2	0.1	0.8	0.3	0.0	0.2	1.3	0.1	0.1	0.0	0.1	0.0	3.8	0.0	0.0	0.0	0.5	0.0	1.8	3.0	2.3	0.4	11.1	0.8	0.1	0.0	0.0			
total sum																																														
2548.0																																														
normalized																																														
44.7		14.1		0.5		1.0		1.2		2.0		0.2		5.2		1.3		0.8		0.0		1.4		0.1		0.1		3.8		0.0		0.5		1.8		9.5		11.3		0.1		0.0		0.0		



mc11868		2.5 mag												Secondary		Primary														
Mono	size	Poly	size	Knofrite	size	Clay	size	Para/clay	size	Diss	size	Para-diss	size	porosity	size	porosity	size	Out over	size	organics	size	plag	size	shale	size	cal cement	size	do/cement	size	
54	0.8	10	0.6	1	0.2	5	0.1	1	0	4	0.2	1	0.1	2	0.2	2	0.1	4	0.1	0	0	0	0	0	0	8	0.1	8	0.1	
57	0.4	12	0.4	0		4		1	1	1		0		3		3		3		0	0	0	0	0	9		4	0.2		
60	0.4	15	0.4	0		3		0	2	0		0		2		3		6		0	0	0	0	0	5		4			
69	5	2	0.4	4		1		0	0	0		0		3		2		7		0	0	0	0	0	4		4			
74	3	0		3		1		0	0	0		0		2		3		4		0	0	0	0	0	6		2			
54	15	0		9		1		2	1	0		1		3		0		3		0	0	0	0	0	8		3			
62	15	0		4		1		1	1	0		0		3		1		3		0	0	0	0	0	7		4			
65	9	0		3		1		2	0	0		0		3		1		4		0	0	0	0	0	5		5			
61	12	0		4		1		4	0	0		0		1		0		8		0	0	0	0	0	5		8			
65	9	0		0		0		3	1	0		1		1		2		5		0	0	0	0	0	10		4			
53	9	0		3		1		3	1	0		3		3		2		1		0	1	0.1	0	0	10		6			
64	10	0		4		2		0	0	0		0		2		0		3		0	0	0	0	0	7		5			
64	12	0		3		1		2	1	0		1		2		0		5		0	0	0	0	0.4	4		2			
65	10	0		5		1		1	0	0		0		2		2		4		0	0	0	0	0	5		3			
72	3	0		7		0		2	0	0		0		2		1		5		1	0.2	0	0	0	4		2			
66	0	2		18		1		1	0	0		0		3		0		6		0	0	0	0	0	3		0			
61	10	0		13		1		2	0	0		0		2		0		7		0	0	0	0	0	4		1			
75	5	0		1		1		2	0	0		0		2		2		5		0	0	0	0	0	3		3			
66	9	0		2		1		3	1	0		1		1		1		3		0	0	0	0	0	6		4			
60	12	0		7		0		3	1	0		1		2		2		4		0	0	0	0	2	3		2			
62	5	0		7		1		2	0	0		0		2		0		3		0	0	0	0	5	6		2			
67	3	0		4		1		1	0	0		0		1		0		3		0	0	0	0	0	9		3			
75	5	0		2		1		1	0	0		0		0		0		2		0	0	0	0	0	8		4			
40	18	0		14		1		3	1	0		1		1		1		5		0	0	0	0	0	6		6			
65	9	0		5		1		1	0	0		0		2		0		2		0	0	0	0	0	7		4			
73	5	0		2		0		3	0	0		0		1		0		2		0	0	0	0	0	6		4			
69	12	0		4		0		1	0	0		0		1		0		4		0	0	0	0	0	2		5			
75	9	0		0		0		0	0	0		0		1		1		2		0	0	0	1	2		2		2		
sum																														
1790	0	1.4	255.0	1.4	5.0	0.6	140.0	0.1	22.0	0.0	50.0	0.2	8.0	0.1	53.0	0.2	29.0	0.1	111.0	0.1	1.6	0.2	1.0	0.1	11.0	0.4	161.0	0.1	104.0	0.3
average																														
64.1	0.5	9.1	0.5	0.2	0.5	5.0	0.4	0.8	0.0	1.8	0.2	0.3	0.1	1.9	0.2	1.0	0.1	4.0	0.1	0.0	0.2	0.0	0.1	0.4	0.4	5.8	0.1	3.7	0.2	
total sum																														
2747	0																													
normalized																														
65.4		9.3		0.2		5.1		0.8		1.8		0.3		1.9		1.1		4.0		0.0		0.0		0.4		5.9		3.6		

mc 13201		2.5 mg																																					
MoNo	size	Poly	size	Calcite	size	Dolomite	size	Kaolinite	size	Clay	size	Secondary	size	Qtz over	size	Heavy min	size	organics	size	muscovite	size	foram	size	crinoid	size	brach	size	chert	size	shale	size	zircon	size						
80	0.2	4	0.2	0	0	1	0.1	0	0	4	0	0	0	8	0	0	0	4	0	0	5	0.7	0	1	1	0.2	3	0.4	1	0.2									
79		1	0.2	0	0	1	0.3	4	0	7	0	0	0	7	0	0	0	5	0	0	3	0.8	5	0.3	1	0	0	0	0	0	0	0	0	0	0				
79		2	0.2	2	0.1	2	0.2	0	3	3	0	0	0	8	0	0	0	0	0	0	0	4	0.6	1	0	0	0	0	0	0	0	0	0	0	0				
80		3	1	0	0	0	0	3	0	8	0	0	0	8	1	0.2	0	0	0	0	3	0.8	2	0.5	3	1	0	0	0	0	0	0	0	0	0	0			
80		0	1	0	0	0	0	4	0	7	0	0	0	7	0	0	0	0	0	0	4	0	3	0	0	0	0	0	0	0	0	0	0	0	0	0			
81		0	0	2	0	0	0	2	0	7	0	0	0	7	0	0	0	0	0	0	2	1	1	0	2	2	0	0	0	0	0	0	0	0	0	0			
80		1	1	1	0	0	3	3	0	8	0	0	0	8	0	0	0	0	0	0	0	0	3	0	2	2	1	0	0	0	0	0	0	0	0	0	0		
79		1	2	0	0	0	5	5	0	8	0	0	0	8	0	0	0	0	0	1	1	1	0	2	2	0	0	0	0	0	0	0	0	0	0	0	0		
74		0	2	0	0	0	3	3	0	9	0	0	0	9	0	0	0	0	0	0	4	4	4	0	2	2	0	0	0	0	0	0	0	0	0	0	0	0	
72		0	3	1	0	0	3	3	0	9	0	0	0	9	0	0	0	0	0	0	2	2	2	0	3	1	0	0	0	0	0	0	0	0	0	0	0	0	
78		1	1	1	0	0	4	4	0	7	0	0	0	7	0	0	0	0	0	0	2	4	4	0	2	2	0	0	0	0	0	0	0	0	0	0	0	0	
73		2	0	1	0	0	2	2	0	14	0	0	0	14	0	0	0	0	0	1	2	3	0	1	1	0	0	0	0	0	0	0	0	0	0	0	0		
82		0	0	0	0	0	3	3	0	12	0	0	0	12	0	0	0	0	0	0	2	0	0	0	1	0	0	0	0	0	0	0	0	0	0	0	0	0	
sum																																							
1006.0	0.2	15.0	0.8	13.0	0.1	9.0	0.3	1.0	0.3	43.0	0.0	5.0	0.0	108.0	0.0	1.0	0.2	8.0	0.0	1.0	0.0	30.0	1.8	32.0	1.4	6.0	0.0	17.0	0.2	10.0	0.4	1.0	0.2						
average																																							
77.4	0.2	1.2	0.2	1.0	0.1	0.7	0.2	0.1	0.3	3.3	0.0	0.4	0.0	8.3	0.0	0.1	0.2	4.5	0.0	0.1	0.0	2.3	0.8	2.5	0.5	1.5	0.0	1.3	0.2	0.6	0.4	1.0	0.2						
total sum																																							
1307.0																																							
normalized																																							
77.0		1.1		1.0		0.7		0.1		3.3		0.4		8.3		0.1		0.7		0.1		2.3		2.4		0.5		1.3		0.6		0.1							

mc13302		2.5 meg																				
None	size	Calcite	size	Dolomite	size	Clay	size	Secondary	porosity	size	Qtz over	size	organics	size	siderite	size	foram	size	concho	size	chert	size
88	0.2	2	0.1	1	0.2	1		0		8	0.1	0		0		0		0		0		0
83		2		0		3		0		8		1	0.1	0		0		3	0.2	0		0
86		2		1		1		0		7		0		0		2		1		0		0
83		1		1		2		0		8		0		0		1		0		0		0
85		3		0		1		0		8		1		0		1		1		0		0
81		2		3		0		1		4		3		0		0		0		0		0
81		1		1		1		1		8		3		0		2		2		0		0
75		3		1		7		0		0		3		0		2		0		0		0
81		2		2		4		0		8		2		1		0		3		2		0
82		2		3		1		0		8		0		0		1		0		0		0
77		2		3		0		1		7		1		0		0		1		0		0
82		2		3		5		0		7		1		0		0		1		0		0
84		4		0		2		0		8		1		0		1		0		0		0
86		2		0		3		0		8		0		0		0		1		0		0
78		3		2		7		0		8		1		0		2		1		0		0
81		3		1		3				9		1				2		0		0		0
sum																						
1311	0.2	30.0	0.1	20.0	0.2	36.0	0.0	1.0	0.0	121.0	0.1	16.0	0.1	1.0	0.0	14.0	0.0	14.0	0.2	2.0	0.0	0.0
average																						
81.8	0.2	2.3	0.1	1.3	0.2	3.5	0.0	0.2	0.0	7.0	0.1	1.1	0.1	0.1	0.0	0.9	0.0	0.9	0.2	0.1	0.0	0.0
total sum																						
1500	0																					
normalized																						
82.1		2.3		1.3		3.5	0.0	0.2	0.0	7.0	0.0	1.1	0.0	0.1	0.0	0.9	0.0	0.9		0.1	0.0	0.0





b13629		2.5 mg																					
mono	size	Clay mix	size	Secondary porosity	size	galuconite	size	Heavy Mn	size	organics	size	plag	size	clay altered	size	muscovite	size	illite	size	char	size	shale	size
14	0.2	64		7	0.1	0		2	0.2	3	0.2	1	0.1		4	0.2	0	0		8	0.2	0	
8		73		8		0		0		4				4		0		0		5		0	
12		68		7		0		1		2				2		0		0		9		0	
11		81		8		1		0		4				4		0		0		5		0	
12		72		5		0		1		3				2		1		0		4		0	
13		67		8		1		0		4				2		1		0		3		0	
17		81		10		0		0		3				4		0		0		5		0	
13		72		7		1		0		2				3		0		0		8		0	
14		72		5		0		0		2				2		0		0		4		0	0.3
13		63		10		0		0		2				4		1		0		8		1	
10		77		3		0		0		3				4		0		0		3		0	
9		79		0		0		0		2				3		1		0		6		0	
11		77		1		1		0		1				3		0		0		8		0	
9		78		0		0		0		1				2		0		0		2		0	
10		88		8		0		0		1				1		1		1	0.4	8		0	
22		87		4		0		0		1				2		0		0		4		0	
20		86		5		0		0		3				1		0		0		3		0	
18		88		5		0		0		1				2		1		0		0		0	
14		73		8		0		0		2				2		0		1		2		0	
sum																							
260	0.2	1328	0.0	108	0.1	1	0.0	4	0.2	45	0.2	0.0	0.1	31	0.2	8	0.0	2	0.4	93	0.2	2	0.3
avg																							
137	0.2	899	0.0	57	0.1	0.2	0.0	0.2	0.2	74	0.2	0.0	0.1	27	0.2	0.3	0.0	0.1	0.4	49	0.2	0.1	0.3
total sum																							
1903	0																						
normalized																							
137	0.3	898	0.0	57	0.0	0.2	0.0	0.2	0.0	74	0.0	0.0	0.0	27		0.3	0.0	0.1	0.0	49	0.0	0.1	0.0



## APPENDIX 2

K 6256

This sample has a broad relaxation time distribution that ranges from 5 msec to over 1000 msec (figure 1). The dominant relaxation components are centered between 10-100 msec. The geometric mean, or average, of the  $T_2$  distribution is 53 msec. This value shifts towards 193 msec when the weighted  $T_2$  method is applied. The fast components (<10 msec) comprise only 14% of the total relaxation distribution.

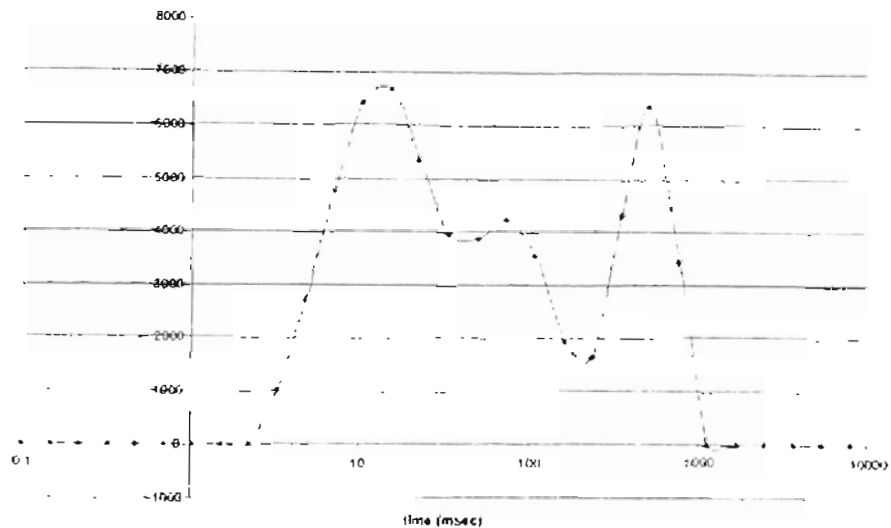


Figure 1. K 6256.6 relaxation distribution curve.

The petrographic data was determined from thin section analysis. This sample contains 59% quartz that has an average grain size of 700 microns. Chlorite composes 10% of the sample. The chlorite is found between quartz grains and in clusters within secondary porosity. Kaolinite makes up 7.6% of the thin section and is found in clusters filling the larger pore spaces. The only type of cement found in this thin section is quartz overgrowths. The quartz overgrowths comprise 2.5% of the thin section. The

sample contains less than 1% of calcite, dolomite, heavy minerals, organic matter, carbonate rock fragments, biotite and siderite.

The total optical porosity (TOP) is 11.5%, which is less than half of the original core porosity of 23.3%. In this study, the difference between core and visible porosity is referred to as optical microporosity. The optical microporosity for this sample is 11.8%. The dominant type of porosity as observed in thin section is a secondary porosity; it comprises 40% of the TOP. The average pore diameter for the secondary porosity is 200 microns. The secondary porosity is described as forming from dissolution of minerals. The secondary porosity contains large amounts of clay (both chlorite and kaolinite) and minerals in the process of being dissolved. The porosity associated with clay comprises 20% of the TOP. The largest pore size is 40 microns. The porosity associated with clay is described as the pores within the clay lattice. The large clusters of chlorite contain voids where soft mineral or fossils have dissolved. These voids can be up to 200 microns in diameter. The porosity associated with dissolution of quartz and feldspar comprises 19% of the total optical porosity. The average pore size associated with grain dissolution porosity is 120 microns. The porosity associated with dissolution is described as the voids that are produced when the mineral is being dissolved. These voids are the pore spaces within the circumference of the mineral being dissolved; the pore space surrounding the mineral is classified as secondary porosity. The primary porosity comprises 21% of the TOP. The pores associated with primary porosity are intergranular pore spaces, pathways between grains connecting other pore spaces. The primary pores are usually smaller and contain less clay than the secondary pores.

The total area under the relaxation distribution curve correlates with the total porosity. The porosity associated with the visible clay porosity is 20% of the TOP. This

correlates to the fast portion (5-10msec) of relaxation distribution curve, which is 14% of the total distribution. The percentage of TOP associated with dissolution of quartz and feldspar is 19%. This is in good agreement with the contribution from the 10 to 20 msec portion of the relaxation time distribution that is 21%. The percentage of primary porosity is 21% of the TOP. The portion of the relaxation curve associated with primary porosity ranges between 20 to 100 msec. For this sample the primary porosity is slightly less than the NMR distribution related to primary porosity. The percentage of the relaxation distribution curve that corresponds to primary porosity is 28%. The secondary porosity comprises 40% of the TOP. The distribution of the relaxation curve that corresponds to secondary porosity is between 100 to 1000 msec. For this sample 35% of the relaxation curve corresponds to secondary porosity.

K 6252

This sample has a broad relaxation time distribution that ranges from 1 msec to over 1000 msec (figure 2). The dominant relaxation components are centered between 10-100 msec. The geometric mean, or average T2 distribution is 53.6 msec. This is increased to 240 msec when the weighted T2 method is applied. The fast components (<10 msec) comprise only 18.5% of the total relaxation distribution.

The petrographic data was determined from thin sections. The sample contains 60% quartz that has an average grain size of 1530 microns. Chlorite composes 9.6% of the thin section. The chlorite is found filling the primary pore spaces between grains and in large clusters in the secondary porosity. The kaolinite comprises 2.3% of the thin section. The kaolinite is found in large clusters filling the secondary pore spaces. This sample contains just over 1% of dolomite. The sample contains less than 1% of calcite, muscovite and biotite.

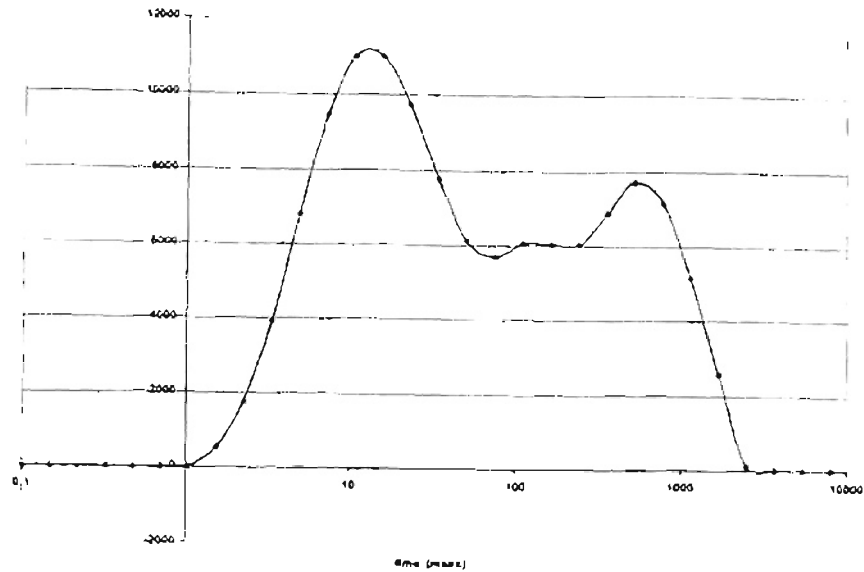


Figure 2. K 6252 Relaxation distribution curve.

The TOP is 8.8%, which is 38% of the core porosity of 22%. The difference between the core porosity and the optical porosity is referred to as optical microporosity. In this sample the optical microporosity is 13.9%. The dominant type of porosity observed in this sample is secondary porosity; it comprises 43% of the TOP. The average pore diameter is 530 microns. The secondary porosity contains large amounts of clay and dissolved minerals. The porosity associated with clay comprises 20% of the TOP. The largest diameter of the porosity associated with clay is 40 microns, these large pores are the result of soft minerals dissolving within the clusters of chlorite. The porosity associated with dissolution of quartz and feldspar comprises 17% of the TOP. The average diameter of these pores is 120 microns. The primary porosity comprises 19% of the TOP. The pore diameter of the primary pores is 200 microns.

The total area under the relaxation distribution curve correlates with the total porosity. The porosity associated with the visible clay porosity is 20% of the TOP. This correlates to the fast portion (1-10 msec) of the relaxation curve, which is 18.5% of the total distribution. The percentage of TOP associated with dissolution of quartz and feldspar is 17%. This agrees with the 10 to 20 msec portion of the relaxation time distribution that is 18%. The primary porosity comprises 19% of the TOP. The portion of the relaxation curve associated with the primary porosity ranges from 20 to 100 msec which is 24% of the total relaxation distribution. The percentage of the relaxation distribution curve related to primary porosity is 37% of the total curve. The secondary porosity makes up 39% of the TOP. The distribution of the relaxation curve that corresponds to secondary porosity is between 100 to 1000 msec. This time range comprises 38% of the relaxation curve.

K6259.8

This sample has a broad relaxation time distribution that ranges from 0.1 to 500 msec (figure 3). The dominant relaxation components are centered between 10-100 msec. The geometric mean, or average of the T2 distribution is 55.3 msec. This value shifts toward 264 msec when the weighted T2 method is applied. The fast components (<10 msec) comprise 13% of the total relaxation distribution.

The petrographic data was determined from thin sections. This sample contains 57% quartz that has an average grain size of 410 microns. The sample contains just over 1% calcite and 2% dolomite. Chlorite comprises 3% of the thin section. The chlorite is found between quartz, calcite and dolomite grains and as clusters within the secondary porosity. Kaolinite comprises 7% of the thin section. The kaolinite is found as clusters in the secondary porosity. This sample contains 3.6% quartz overgrowths as the main

type of cement. This sample contains less than 1% glauconite, heavy minerals, organics, carbonates, muscovite, siderite and rock fragments.

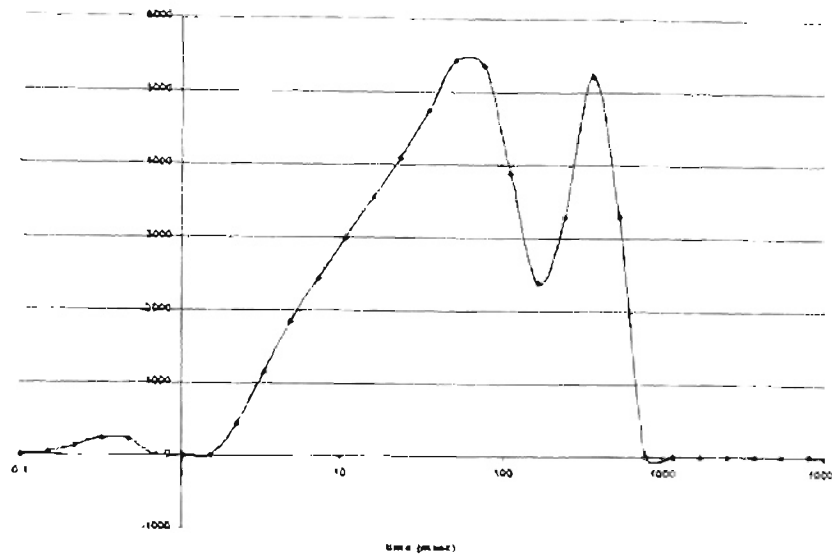


Figure 3. K 6259.8 relaxation distribution curve.

The TOP is 17.3%, which is close to the core porosity of 22.4%. The optical microporosity for this sample is 4.9%. The dominant type of porosity in this sample is secondary porosity; it comprises 49% of the TOP. The secondary pores have an average diameter of 500 microns. The secondary porosity contains abundant clay (both chlorite and kaolinite) and grains that are in the process of dissolving. The porosity associated with visible clay comprises 5% of the TOP. The small percentage of porosity associated with visible clay is apparent in the minor amount of optical microporosity. The pores associated with visible clay can be up to 40 microns in size due to the soft minerals or fossils being dissolved found in the cluster of clay. The percentage of porosity associated with dissolution of quartz and feldspar is 13%. The average diameter of the

pores associated with dissolution is 40 microns. Primary porosity comprises 33% of the TOP. The average pore diameter of primary pores is 120 microns. The primary pores are usually smaller than the secondary pores, they are found between grains and usually contain less clay than the secondary pores.

The total area under the relaxation distribution curve correlates with the total porosity. The porosity associated with the visible clay porosity is 5% of the TOP. This correlates to the fast portion (0.1-10 msec) of the relaxation distribution curve, with is 12%. The percentage of the TOP associated with dissolution of quartz and feldspar is 13%. The 10-20 msec range of the relaxation curve correlates to the porosity associated with dissolution. This percentage of the relaxation curve is 13%. The primary porosity comprises 33% of the TOP. This is in good correlation to the time range from 20-100 msec of the relaxation curve correlates to primary pore sizes. This time range makes up 38% of the relaxation distribution. The secondary porosity comprises 49% of the TOP. This correlates to the time range of 100-500 msec of the relaxation curve. This time range comprises 35% of the relaxation curve.

K 6264.1

This sample has a broad relaxation time distribution that ranges from 1-1000 msec (figure 4). The dominant relaxation components are centered between 10-100 msec. The geometric mean or average T<sub>2</sub> is 61.9 msec. This value shifts toward 222 msec when the weighted T<sub>2</sub> method is applied. The fast components (<10 msec) comprise 7.8% of the total relaxation distribution.

The petrographic data was determined from thin section work. The sample contains 62% quartz that has an average grain size of 1050 microns. This sample contains 2 % calcite and 4% dolomite. Chlorite comprises 6.5% of the thin section. The



chlorite is found between grains and as clusters within the secondary porosity. Kaolinite comprises 8.5% of the thin section. The kaolinite is mostly found filling the secondary pore spaces. The only type of cement found in the sample is quartz overgrowths. The quartz overgrowths comprise 3% of the thin section. The sample contains less than 1% of organic matter, plagioclase, carbonate rock fragments, and other rock fragments.

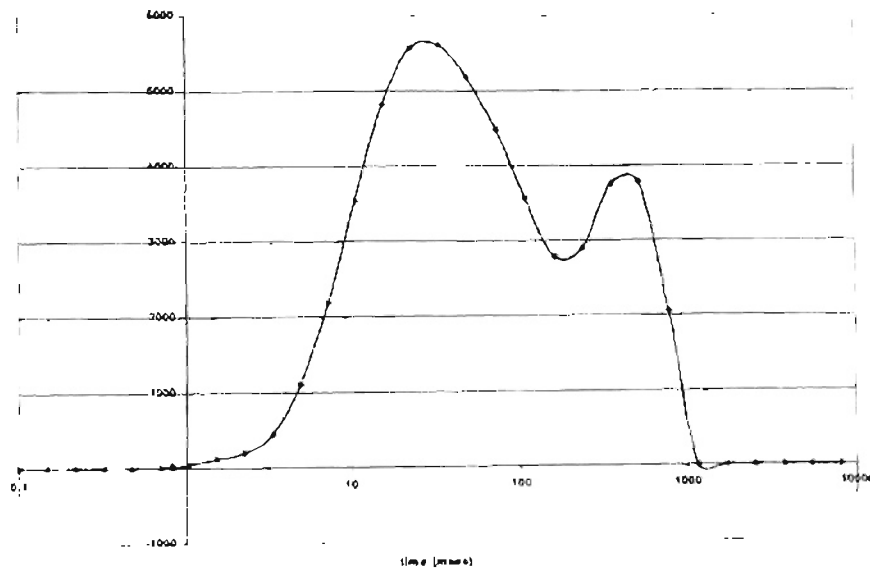


Figure 4. K 6264.1 relaxation distribution curve.

The TOP is 7.3%, this is less than half of the core porosity of 20.2%. The optical microporosity for this sample is 12.8%. The dominant types of porosity in this sample are secondary porosity and porosity associated with visible clay. Both types of porosity comprise 33% of the TOP. The average diameter of the secondary pores is 400 microns. The secondary pores contain abundant clay, organic matter and rock fragments. The pores associated with visible clay have a diameter less than 40 microns. The porosity

associated with the dissolution of quartz and feldspar comprises 12% of the TOP. The average diameter of these pores is 40 microns. Primary porosity comprises 22% of the TOP. The average diameter of the primary pores is 120 microns. The primary pores are the lines of connection of larger secondary pores between grains. The primary pores usually contain minor amounts of chlorite; the chlorite is usually surrounding the quartz grains.

The total area under the relaxation distribution curve correlates with the total porosity. The porosity associated with the visible clay is 33% of the TOP. The pores associated with visible clay correlates to the time range of 1-10 msec. This time range comprises only 8% of the total relaxation time distribution. The porosity associated with dissolution of quartz and feldspar comprises 12% of the TOP. This correlates well to the time range of 10-20 msec. This time distribution comprises 16% of the relaxation curve. The primary porosity comprises 22% of the TOP. The primary pores correlate to a time range of 20-100 msec. The percentage of the relaxation distribution curve that corresponds to this time range is 40%. The secondary porosity comprises 33% of the TOP. The secondary pores correlate to a time range of 100-1000 msec. The percentage of the relaxation curve that corresponds to this time range is 36%.

K 6257.1

This sample has a broad relaxation time distribution that ranges from 1-1000 msec (figure 5). The dominant relaxation components are centered between 10- 100 msec. The geometric mean or average T2 distribution is 48 msec. This value increases to 243 msec when the weighted T2 method is applied. The fast components (<10 msec) comprise 14% of the total relaxation distribution.

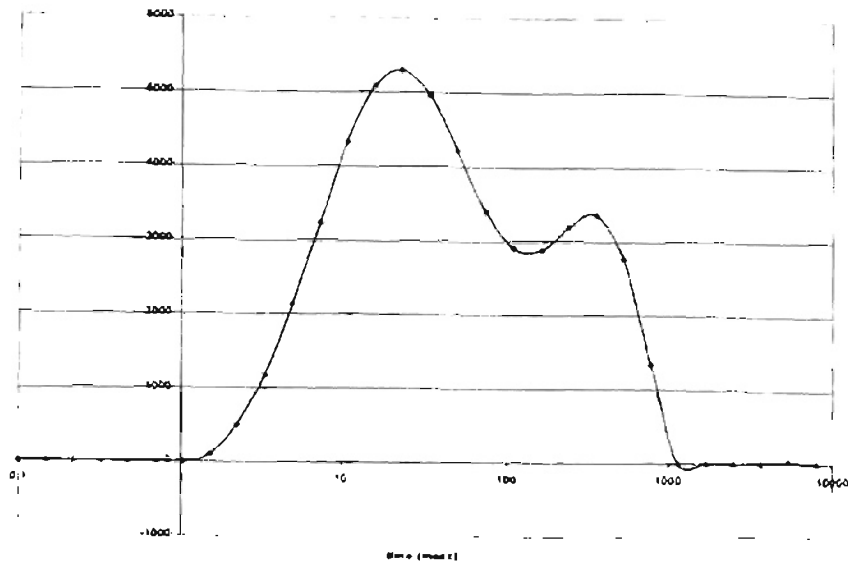


Figure 5. K 6257.1 relaxation distribution curve.

The petrographic data was determined from thin sections. This sample contains 67% quartz, which has an average grain size of 930 microns. The chlorite comprises 4.4% of the thin section. The chlorite is found between quartz grains and filling the secondary porosity. Kaolinite makes up 8% of the sample. The kaolinite is found as clusters filling the secondary porosity. The only cement found in the sample is quartz overgrowths. The make up just over 1% of the sample. The sample contains less than 1% of calcite, dolomite, glauconite, heavy minerals, organic matter, plagioclase, carbonate rock fragments, biotite and siderite.

The TOP for this sample is 7.2, which is less than half of the core porosity of 18.6%. The optical microporosity for this sample is 11.4%. The dominant type of porosity as observed in thin section is secondary porosity; it comprises 37% of the TOP. The average pore diameter of the secondary porosity is 550 microns. The secondary

porosity contains the glauconite, heavy minerals and organic matter. Large amounts of clay (both chlorite and kaolinite) are found in the secondary porosity. The porosity associated with visible clay comprises 15% of the TOP. The largest diameter of the pores associated with visible clay is 40 microns. The porosity associated with dissolution of quartz and feldspar is 35% of the TOP. The average diameter of the pores associated with dissolution is 120 microns. Primary porosity comprises 13% of the TOP. The primary pores are usually smaller than the secondary pores and contain less clay. The average diameter of the primary pores is 120 microns.

The total area under the relaxation distribution curve correlates with the total porosity. The porosity associated with the visible clay porosity is 15% of the TOP. This correlates to the fast portion (1-10 msec) of the relaxation curve, which is 14%. The percentage of the TOP associated with dissolution of quartz and feldspar is 35%. The time range of 10-20 msec correlates to porosity associated with dissolution, this comprises 18% of the total relaxation distribution. The primary porosity comprises 13% of the TOP. The portion of the relaxation distribution that correlates to the primary porosity is between 20-100 msec. This time range is 35% of the total relaxation distribution. The secondary porosity comprises 37% of the TOP. This is good agreement with the slowest portion (100-1000 msec) of the relaxation curve; which is 32%.

K 6263

This sample has a broad relaxation time distribution that ranges from 0.5 to 800 msec (figure 6). The dominant relaxation components are centered between 10-100 msec. The geometric mean or the average T2 distribution is 32 msec. This value

increases to 182 msec when the weighted T2 method is applied. The fast components (<10 msec) comprise 17% of the relaxation curve.

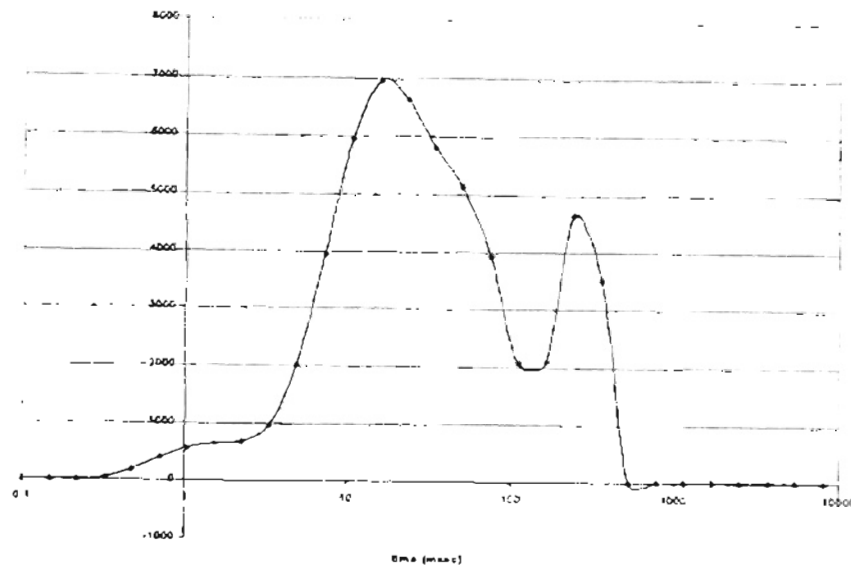


Figure 6. K 6263 relaxation distribution curve

The petrographic data was determined from thin section. This sample contains 63% quartz that has an average diameter of 400 microns. The sample contains just fewer than 2% of calcite and dolomite. Chlorite makes up 5.5% of the thin section. The chlorite is found between quartz, calcite and dolomite grains. Clusters of chlorite are found filling the secondary porosity. Kaolinite makes up 11.5% of the sample. The kaolinite is found filling the secondary pore spaces. The only type of cement found in the sample is quartz overgrowths. They comprise 2% of the thin section. Organic matter comprises just over 1% of the sample and is found in the secondary porosity. The sample contains less than 1% glauconite, plagioclase, carbonate rock fragments, muscovite, biotite, and other rock fragments.

The TOP is 5.4%, this is less than half of the core porosity of 18.1%. The optical microporosity for this sample is 12.5%. The dominant type of porosity as observed in thin section is secondary porosity; it comprises 41% of the TOP. The average diameter of the secondary pores is 200 microns. The secondary pores contain abundant clay and rock fragments. The porosity associated with visible clay comprises 10% of the TOP. The largest diameter of these pores is 40 microns. The porosity associated with dissolution of quartz and feldspar makes up 26% of the TOP. The average diameter of the pores associated with dissolution is 120 microns. Primary porosity comprises 24% of the TOP. The average primary pore size is 120 microns. The majority of the primary pores is conduits between grains for larger pores and therefore is smaller than secondary pores. The primary pores contain minor amounts of clay, mainly chlorite found coating the grains.

The total area under the relaxation distribution curve correlates with the total porosity. The porosity associated with visible clay is 10% of the TOP. This correlates to the fast portion (0.1-10 msec) of the relaxation distribution curve, which is 17%. The porosity associated with dissolution of quartz and feldspar comprises 26% of the TOP. This correlates to the time range of 10-20 msec of the relaxation distribution curve, which is 23% of the curve. Primary porosity comprises 24% of the TOP. The portion of the relaxation curve associated with primary porosity ranges from 20-100 msec, which is 38% of the curve. The secondary porosity comprises 41% of the TOP. This is in good correlation with the slowest portion of the relaxation distribution curve (100-1000 msec), which is 21% of the curve.

K 6250.8

This sample has a broad relaxation time distribution that ranges from 1 to 1000 msec (figure 7). The dominant relaxation components are centered between 10 to 100 msec. The geometric mean or average T2 distribution is 41 msec. This shifts towards 225 msec after the weighted T2 method is applied. The fast components (<10 msec) comprise 23% of the total relaxation distribution.

The petrographic data was determined from thin sections. This sample contains 69% quartz that has an average grain size of 1400 microns. This sample contains just over 1% calcite and just over 2% dolomite. Chlorite comprises 9% of the thin section. The chlorite is found around quartz grains and as clusters filling the secondary porosity. The kaolinite comprises 2.4% of the sample. The kaolinite is found mainly filling the secondary porosity. The sample contains 1% or less of heavy minerals, quartz overgrowths, plagioclase, carbonate rock fragments, and muscovite.

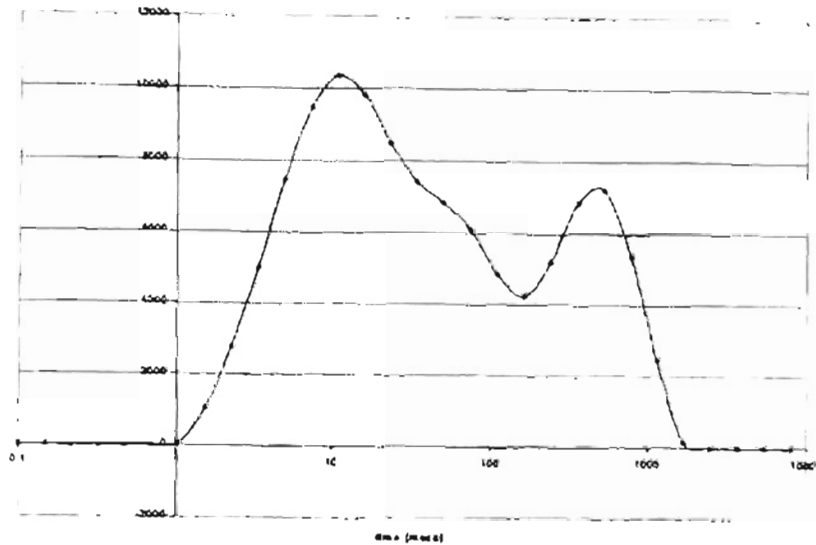


Figure 7. K 6250.8 relaxation distribution curve.

The TOP for this sample is 6.7%, this is less than half of the core porosity of 17.8%. The optical microporosity for this sample is 10.4%. The dominant type of porosity as observed in thin section is secondary porosity; it comprises 48% of the TOP. The average diameter of the secondary pores is 200 microns. Chlorite and kaolinite are found as cluster in the secondary pores along with the different types of rock fragments. The porosity associated with visible clay comprises 15% of the TOP. The largest diameter of these pores is 40 microns. The porosity associated with dissolved quartz and feldspar comprises 18% of the TOP. The average diameter of these pores is 120 microns. Primary porosity comprises 19% of the sample. The average diameter of the primary pores is 120 microns. The primary pores are usually smaller than the secondary pores and contain less clay.



The total area under the relaxation distribution curve correlates with the total porosity. The porosity associated with the visible clay porosity is 15% of the TOP. This correlates to the fast portion (1-10 msec) of the relaxation distribution curve, which is 23% of the curve. The percentage of the porosity associated with dissolution of quartz and feldspar is 18% of the TOP. This is in excellent agreement with the portion of the relaxation curve associated with dissolution is between 10-20 msec, which is 18% of the curve. The percentage of primary porosity is 19% of the TOP. Primary porosity correlates to the time range of 20-100 msec of the relaxation curve, this is 26% of the total curve. The secondary porosity comprises 48% of the TOP. The secondary porosity correlates to the relaxation distribution time range 100-1000 msec, this is 33% of the total curve.

K 6246

This sample has a broad relaxation time distribution that ranges from 1 to 1000 msec (figure 8). The dominant relaxation components are centered between 10 to 100 msec. The geometric mean, or average, of the T2 distribution is 0.71 msec. This is increased to 193 msec when the weighted T2 method is applied. The fast components (<10 msec) comprise 28% of the total relaxation curve.

The petrographic data was determined from thin section. This sample contains 60% quartz. The average grain size is 940 microns. Chlorite comprises 8.5% of the thin section. The chlorite is found filling secondary pores and as a thin layer around the quartz grains. Kaolinite comprises 1% of the thin section. The kaolinite is found filling the secondary pores. This sample contains 6.7% calcite and 7.3% dolomite. Less than 1% of plagioclase, organic matter and quartz overgrowths are present in the thin section.

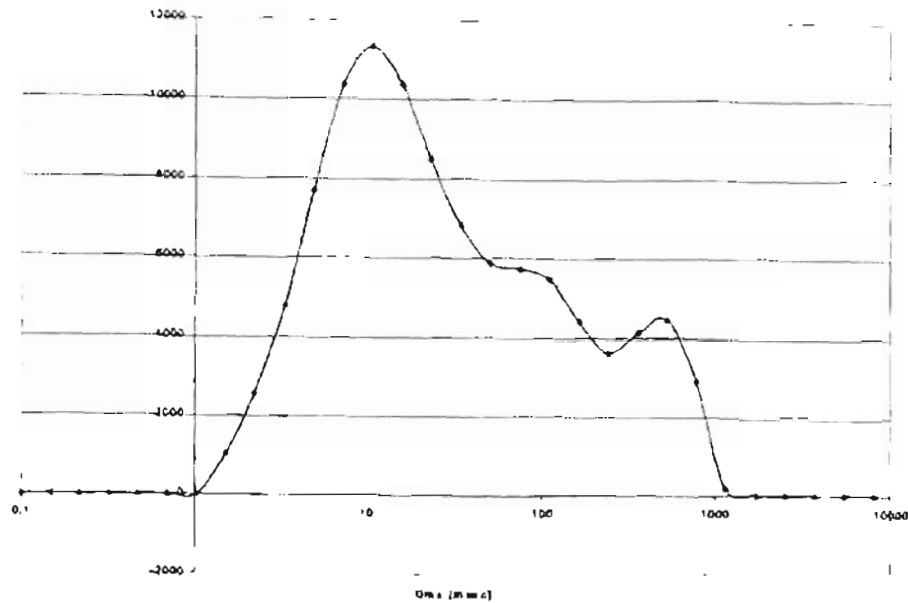


Figure 8. K 6246 relaxation distribution curve.

This sample has a TOP of 9.8%. This is just over half of the core porosity of 17.2%. The microporosity for this sample is 7.4%. The dominant type of porosity is secondary porosity; it comprises 41% of the TOP. The average diameter of the secondary pores is 200 microns. The secondary pores contain abundant clay and organic matter. The porosity associated with visible clay is 33% of the TOP. The largest diameter of the pores associated with visible clay is 40 microns. The porosity associated with dissolution of quartz and feldspar is 14% of the TOP. The average pore size of the pores associated with dissolution is 120 microns. Primary porosity composes 12% of the TOP. The average diameter of the primary pores is 120 microns. The primary pores are usually smaller than the secondary pores and contain less clay.

The total area under the relaxation distribution curve correlates with the total porosity. The porosity associated with the visible clay is 33% of the TOP. This

correlates to the fast portion (1-10 msec) of the relaxation distribution, which is 28% of the total curve. The percentage of TOP associated with dissolution of quartz and feldspar is 14%. This correlates to the relaxation distribution between 10-20 msec, which is 23% of the total curve. Primary porosity comprises 12% of the TOP. This correlates to the relaxation distribution between 20-100 msec, which is 20% of the total curve. The secondary porosity comprises 41% of the TOP. This correlates to the time range of 100-1000 msec of the relaxation distribution. This time range is 27% of the total curve.

K 6266

This sample has a broad relaxation time distribution that ranges from 5 to 500 msec (Figure 9). The dominant relaxation components are centered between 10 to 100 msec. The geometric mean, or average, T2 distribution is 32 msec. This value increases to 184 msec when the weighted T2 method is applied.

The petrographic data was determined from thin sections. This sample contains 65% quartz that has an average grain size of 780 microns. This sample contains 2.3% calcite and 4.5% dolomite. Chlorite comprises 5% of the sample. The chlorite is found coating some quartz, calcite and dolomite grains. It is also found as clusters filling the secondary porosity. Kaolinite comprises 7% of the thin section. The kaolinite is found filling secondary pores. The only type of cement in the sample is quartz overgrowths, it comprises about 3% of the thin section. The sample contains less than 1% of organic matter, plagioclase, carbonate rock fragments, muscovite and other rock fragments.

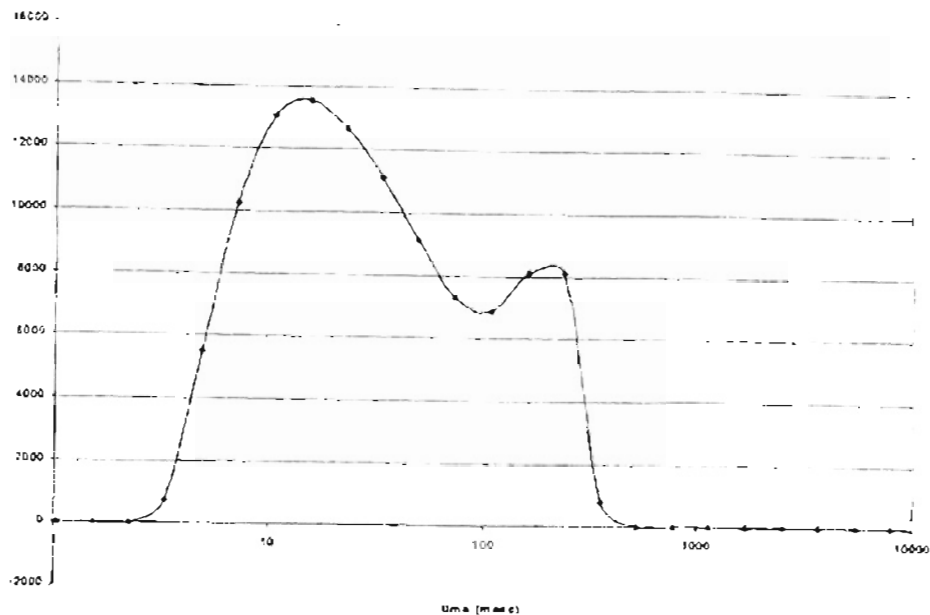


Figure 9. K 6266 relaxation distribution curve.

The TOP for this sample is 4.5%. This is less than half of the core porosity of 17.1%. The optical microporosity for this sample is 12.6%. The dominant type of porosity for this sample is secondary porosity; it comprises 41% of the TOP. The average diameter of the secondary pores is 260 microns. The secondary porosity contains large amounts of clay and rock fragments. The porosity associated with visible clay comprises 14% of the TOP. The largest diameter of the pores associated with visible clay is 40 microns. The porosity associated with dissolution of quartz and feldspar comprises 24% of the TOP. The pores associated with dissolution have an average diameter of 120 microns. Primary porosity comprises 21% of the TOP. The average diameter of the primary pores is 200 microns. The primary pores tend to be smaller than the secondary pores, and they usually contain less clusters of clay.

The total area under the relaxation distribution curve correlates with the total porosity. The porosity associated with the visible clay is 14% of the TOP. The correlates to the fast portion (5-10 msec) of the relaxation distribution curve, which is 15% of the total curve. The percentage of TOP associated with dissolution of quartz and feldspar is 24%. This is in good agreement with the contribution from the 10 to 20 msec portion of the relaxation time distribution that is 25%. The percentage of primary porosity is 21% of the TOP. The portion of the relaxation curve associated with primary porosity ranges between 20 to 100 msec. For this sample the primary porosity is slightly less than the NMR distribution related to primary porosity. The percentage of the relaxation distribution curve that corresponds to primary porosity is 37%. The secondary porosity comprises 41% of the TOP. The distribution of the relaxation curve that corresponds to secondary porosity is between 100-1000 msec. For this sample 22% of the relaxation curve corresponds to secondary porosity.

K 6249B

This sample has a broad relaxation time distribution that ranges from 1 to 900 msec (figure 10). The dominant relaxation components are centered between 10 to 100 msec. The geometric, or average, T2 distribution is 28 msec. This value shifts toward 182 msec when the weighted T2 method is applied. The fast components (<10 msec) comprise 30% of the total relaxation distribution.

The petrographic data was determined from thin sections. This sample contains 70% quartz that has an average grain size of 1400 microns. This sample contains less than 2% of calcite and dolomite. Chlorite composes 10% of the thin section. The chlorite is found surrounding quartz, calcite and dolomite grains. It is also found as clusters filling the secondary pores. Kaolinite composes 4% of the thin section. The

kaolinite is mainly found filling the secondary pores. This sample contains less than 1% of quartz overgrowths, glauconite, plagioclase, carbonate rock fragments, chert and fossils.

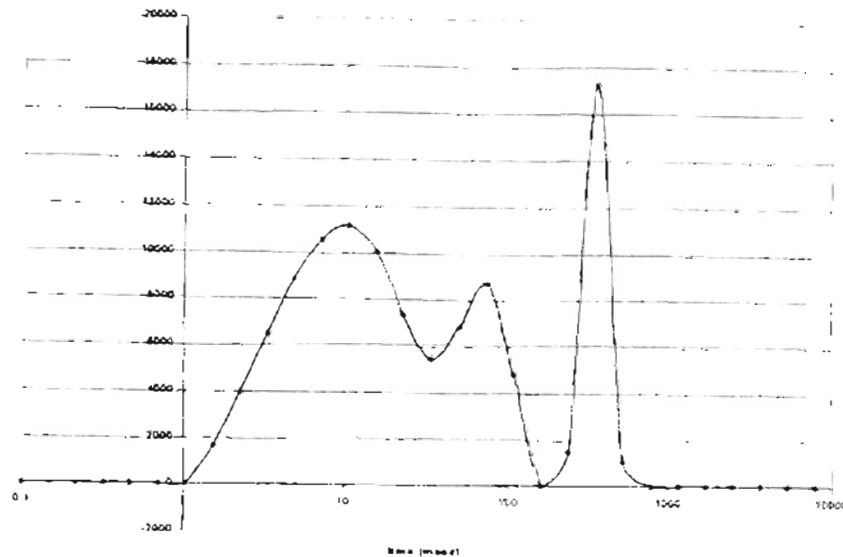


Figure 10. K 6249B relaxation distribution curve.

The TOP for this sample is 6.7%, this is less than half of the core porosity of 17.1%. The optical microporosity for this sample is 10.3%. The dominant type of porosity as observed in thin section is porosity associated with visible clay; which is 37% of the TOP. The largest diameter associated with the visible clay pores is 40 microns. The majority of the porosity associated with visible clay is found as clusters filling the secondary pores. Minor amounts of clay are found surrounding the quartz, calcite and dolomite. The porosity associated with dissolution of quartz and feldspar comprises 18% of the TOP. The average diameter of the pores associated with dissolution is 120 microns. Primary porosity comprises 13% of the TOP. The average

diameter of the primary pores is 160 microns. Secondary porosity comprises 31% of the TOP. The average diameter of the secondary pores is 300 microns. The secondary pores tend to be larger than the primary pores and contain more clay. The primary pores serve as conduits between quartz, calcite, and dolomite grains to larger pores.

The total area under the relaxation distribution curve correlates with the total porosity. The porosity associated with the visible clay porosity is 37% of the TOP. This correlates to the fast portion (1-10 msec) of the relaxation distribution curve, which is 30% of the total distribution. The percentage of the TOP associated with dissolution of quartz and feldspar is 18%. This is in good agreement with the contribution from the 10 to 20 msec portion of the relaxation time distribution that is 20%. The percentage of primary porosity is 13% of the TOP. The portion of the relaxation curve associated with primary porosity ranges from 20 to 100 msec. For this sample the primary porosity is less than the NMR distribution related to primary porosity. The percentage of the relaxation distribution curve that corresponds to primary porosity is 27%. The secondary porosity comprises 31% of the TOP. The distribution of the relaxation curve that corresponds to secondary porosity is between 100-1000 msec. For this sample the NMR distribution of 23% is less than the TOP percentage of secondary porosity.

K 6261

This sample has a broad relaxation time distribution that ranges from 0.1 to 1000 msec (figure 11). The dominant relaxation components are centered between 10 to 100 msec. The geometric mean, or average, T<sub>2</sub> distribution is 44 msec. This value increases to 246 msec when the weighted T<sub>2</sub> method is applied.

The petrographic data was determined from thin section. This sample contains 59% quartz that has an average grain size of 780 microns. This sample contains 2.7%

calcite and just over 2% dolomite. Chlorite comprises 5.7% of the thin section. The chlorite is found between the quartz, calcite and dolomite grains and as clusters filling the secondary porosity. Kaolinite composes 8% of the thin section. The kaolinite is mainly found filling the secondary porosity. Quartz overgrowths are the only type of cement found in this sample; it comprises 2.7% of the thin section. The sample contains less than or just over 1% of organic matter, heavy minerals, plagioclase, biotite, carbonate and other rock fragments.

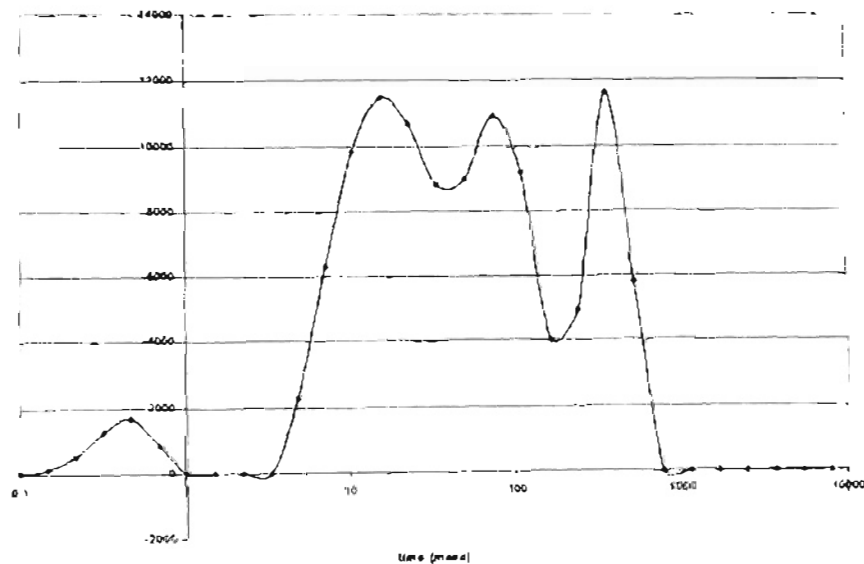


Figure 11. K 6261 relaxation distribution curve.

The TOP for this sample is 7.6% this is less than half of the core porosity of 17.1%. The optical microporosity for this sample is 9.3%. The dominant type of porosity is secondary porosity; it comprises 38% of the TOP. The average diameter of the secondary pores 200 microns. The secondary porosity contains abundant clay, organic matter, heavy minerals and rock fragments. The porosity associated with visible



clay is 20% of the TOP. The largest diameter of the pores associated with visible clay is 40 microns. The majority of the clay is found in cluster filling the secondary porosity. The porosity associated with dissolution of quartz and feldspar is 26% of the TOP. The average diameter of the pores associated with dissolution is 120 microns. Primary porosity comprises 16% of the TOP. The primary pores tend to be smaller than the secondary pores. The average pore diameter is 120 microns. The primary pores usually contain less clay than the secondary pores.

The total area under the relaxation distribution curve correlates with the total porosity. The porosity associated with the visible clay porosity is 20% of the TOP. This correlates to the fast portion (0.1-10 msec) of the relaxation distribution curves, which is 12% of the total distribution. The percentage of the TOP associated with dissolution of quartz and feldspar is 26%. This correlates to the 10 to 20 msec portion of the relaxation time distribution that is 19% of the total curve. The percentage of the primary porosity is 16% of the TOP. The portion of the relaxation curve associated with primary porosity ranges from 20 to 100 msec. For this sample the primary porosity is slightly less than the NMR distribution related to primary porosity. The percentage of the relaxation distribution curve that corresponds to primary porosity is 36%. The secondary porosity comprises 38% of the TOP. This is in good agreement with the portion of the relaxation distribution that corresponds to secondary porosity. The distribution of the relaxation curve that corresponds to secondary porosity is between 100 to 1000 msec. For this sample 32% of the relaxation curve corresponds to secondary porosity.

K 6245.1

This sample has a broad relaxation time distribution that ranges from 0.5 to 1000 msec (figure 12). The dominant relaxation components are centered between 10 to 100

msec. The geometric mean, or average, T2 distribution is 20 msec. This shifts towards 171 msec when the weighted T2 method is applied. The fast components (<10 msec) comprise 37% of the relaxation distribution.

The petrographic data was determined from thin sections. This sample contains 65% quartz that has an average grain size of 930 microns. The sample contains 5% calcite and 3% dolomite. Chlorite composes 9 % of the sample. The chlorite is found between the quartz, calcite and dolomite grains. The chlorite is also found as cluster filling the secondary porosity. The sample contains less than 1% of heavy minerals, plagioclase, glauconite, muscovite and quartz overgrowths.

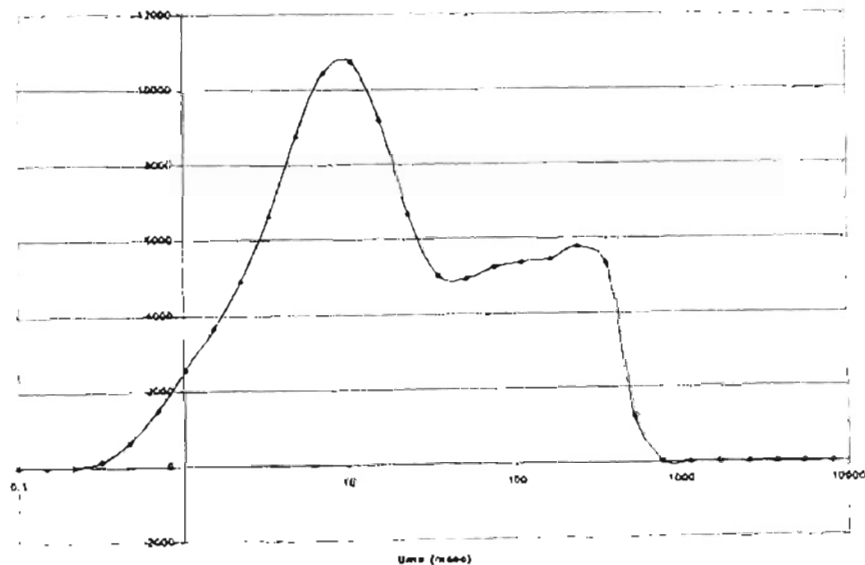


Figure 12. K 6245.1 relaxation distribution curve.

The TOP for this sample is 12%, this is slightly lower than the core porosity of 16%. The optical microporosity for this sample is 4%. The dominant type of porosity as

observed in thin section is secondary porosity; it comprises 46% of the TOP. The average diameter of the secondary porosity is 200 microns. The secondary porosity contains abundant clay and heavy minerals. The porosity associated with visible clay composes 24% of the TOP. The largest diameter of the pores associated with visible clay is 40 microns. The majority of the clay porosity is found in the cluster of clay contained in the secondary porosity. The porosity associated with dissolution of quartz and feldspar is 14% of the TOP. The average diameter of the pores associated with dissolution is 40 microns. Primary porosity composes 19% of the TOP. The average diameter of the primary pores is 120 microns. The primary pores usually contain less clay than the secondary pores and do not contain the fragments that are found in the secondary porosity.

The total area under the relaxation distribution curve correlates with the total porosity. The porosity associated with the visible clay porosity is 24% of the TOP. This correlates to the fast portion (0.5-10 msec) of relaxation distribution curve, which is 37% of the total distribution. The percentage of TOP associated with dissolution of quartz and feldspar is 14%. This is close to the contribution from the 10 to 20 msec portion of the relaxation time distribution that is 19%. The percentage of primary porosity is 19% of the TOP. The portion of the relaxation curve associated with primary porosity ranges from 20 to 100 msec. For this sample the primary porosity is slightly less than the NMR distribution related to primary porosity. The percentage of the relaxation distribution curve that corresponds to primary porosity is 21%. The secondary porosity comprises 46% of the TOP. The distribution of the relaxation curve that corresponds to secondary porosity is between 100-1000 msec. For this sample 22% of the relaxation curve corresponds to secondary porosity.

K 6249A

This sample has a broad relaxation time distribution that ranges from 1 to 1000 msec (figure 13). The dominant relaxation components are centered between 10 to 100 msec. The geometric mean, or average, of the T2 distribution is 33 msec. This value shifts towards 205 msec when the weighted T2 method is applied.

The petrographic data was determined from thin sections. This sample contains 55% quartz, which has an average grain size of 940 microns. Chlorite composes 9.7% of the sample. The chlorite is found between quartz, calcite, and dolomite. The chlorite is also found as cluster that is filling the secondary porosity. Kaolinite composes 2.2% of the thin section. The kaolinite is found mainly filling the secondary porosity. The sample contains 8.9% carbonate rock fragments. The thin section contains less than 1% of calcite, dolomite, quartz overgrowths, heavy minerals, and plagioclase.

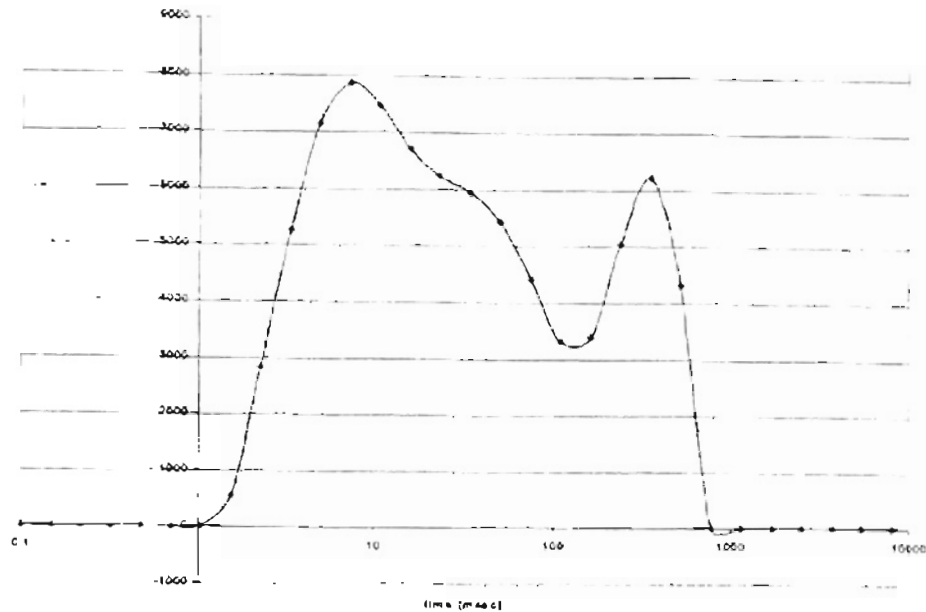


Figure 13. K 6249A relaxation distribution curve.

The total optical porosity is 9.4%. The TOP is slightly less than the core porosity of 14.5%. The optical microporosity for this sample is 5%. The dominant types of porosity are primary and secondary porosity; each comprises 32% of the TOP. The average diameter of the primary pores is 200 microns. The primary pores contain little clay. The average secondary pores are 400 microns. The secondary pores contain abundant clay, the heavy minerals and rock fragments. The porosity associated with visible clay comprises 22% of the TOP. The largest pore diameter associated with visible clay 40 microns. The porosity associated with dissolution of quartz and feldspar is 14% of the TOP. The average pore diameter of the pores associated with dissolution is 300 microns.

The total area under the relaxation distribution curve correlates with the total porosity. The porosity associated with the visible clay porosity is 22% of the TOP. This correlates to the fast portion (1-10 msec) of relaxation distribution curve, which is 28% of the total distribution. The percentage of TOP associated with the dissolution of quartz and feldspar is 14%. This is in good agreement with the contribution from the 10 to 20 msec portion of the relaxation time distribution that is 17%. The percentage of primary porosity is 32% of the TOP. The portion of the relaxation curve associated with primary porosity ranges between 20 to 100 msec. For this sample the primary porosity is slightly less than the NMR distribution related to primary porosity. The percentage of the relaxation distribution curve that corresponds to primary porosity is 26%. The secondary porosity comprises 32% of the TOP. The distribution of the relaxation curve that corresponds to secondary porosity is between 100 to 1000 msec. For this sample 27% of the relaxation curve corresponds to secondary porosity.

K 6266.4

This sample has a broad relaxation time distribution that ranges from 0.5 to 1000 msec (figure 14). The dominant relaxation components are centered between 10 to 100 msec. The geometric mean, or average, T2 distribution is 41 msec. This shifts towards 222 msec when the weighted T2 method is applied. The fast components (<10 msec) comprise only 13% of the relaxation distribution.

The petrographic data was determined from thin section. This sample contains 52% quartz that has an average grain size of 800 microns. Calcite comprises almost 10% of the thin section. Dolomite comprises 5.3% of the thin section. This sample contains just over 1% of quartz that is being replaced by dolomite. Chlorite composes 4.7% of the thin section. The chlorite is found mainly as clusters filling the secondary

porosity. Minor amounts of chlorite are found between the quartz grains. Kaolinite comprises 6.7% of the thin section. The kaolinite is found mainly as clusters filling the secondary porosity. The only type of cement found in this sample is quartz overgrowths; it comprises almost 3% of the sample. The sample contains fewer than 3% of carbonate rock fragments. The sample contains less than 1% of quartz being replaced by calcite, organic matter, biotite, fossils, and rock fragments.

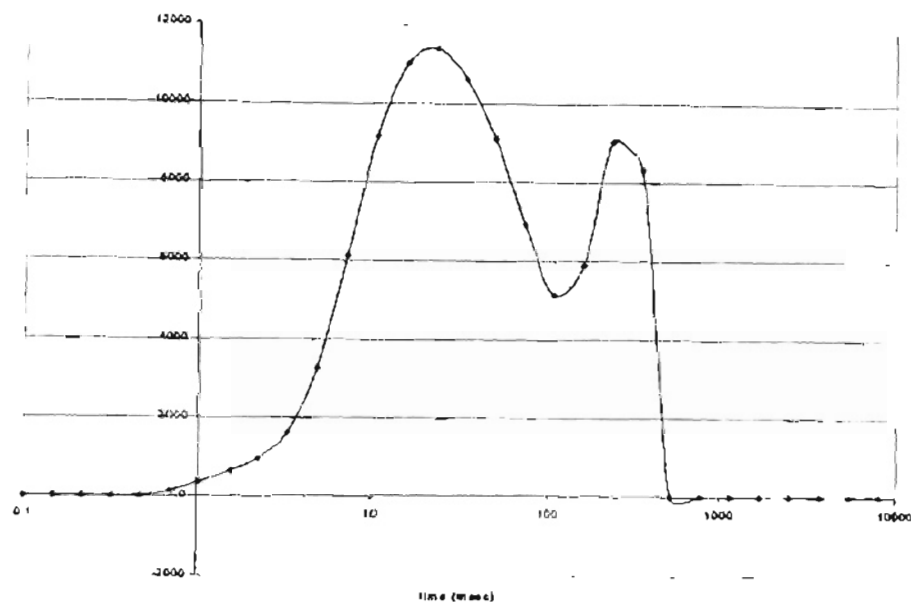


Figure 14. K 6266.4 relaxation distribution curve.

The TOP for this sample is 6.1%. The TOP is just less than half of the core porosity, of 14%. For this sample the optical microporosity is 7.9%. The dominant type of porosity is secondary porosity; it comprises 37% of the TOP. The average pore diameter of the secondary porosity is 200 microns. The secondary porosity contains abundant clay and rock fragments. The porosity associated with visible clay comprises 12% of the TOP. The largest diameter of the porosity associated with visible clay is 40

microns. The majority of the porosity associated with the clay is found within the clay clusters found within the secondary porosity. The porosity associated with dissolution of quartz and feldspar is 28% of the TOP. The average diameter of the porosity associated with dissolution is 120 microns. Primary porosity composes 23% of the TOP. The average diameter of the primary pores is 120 microns. The primary pores contain less clay than the secondary pores. The primary pores act as conduits between quartz grains to connect larger pores.

The total area under the relaxation distribution curve correlates with the total porosity. The porosity associated with visible clay porosity is 12% of the TOP. This agrees with the fast portion (5-10 msec) of relaxation distribution curve, which is 13% of the total distribution. The percentage of the TOP associated with the dissolution of quartz and feldspar is 28%. This correlates to the contribution from the 10 to 20 msec portion of the relaxation time distribution that is 20%. The percentage of primary porosity is 23% of the TOP. The portion of the relaxation curve associated with primary porosity ranges between 20 to 100 msec. For this sample the primary porosity is less than the NMR distribution related to primary porosity. The percentage of the relaxation distribution curve that corresponds to primary porosity is 38%. The secondary porosity comprises 37% of the TOP. The distribution of the relaxation curve that corresponds to secondary porosity is between 100 to 1000 msec. For this sample 28% of the relaxation curve corresponds to secondary porosity.

K 6243.1

This sample has a broad relaxation time distribution that ranges from 0.1 to 1000 msec (figure 15). The dominant relaxation components are centered between 10 to 100 msec. The geometric mean, or average, T2 distribution is 18 msec. This shifts towards



109 msec when the weighted T2 method is applied. The fast components (<10 msec) comprise only 39% of the relaxation distribution.

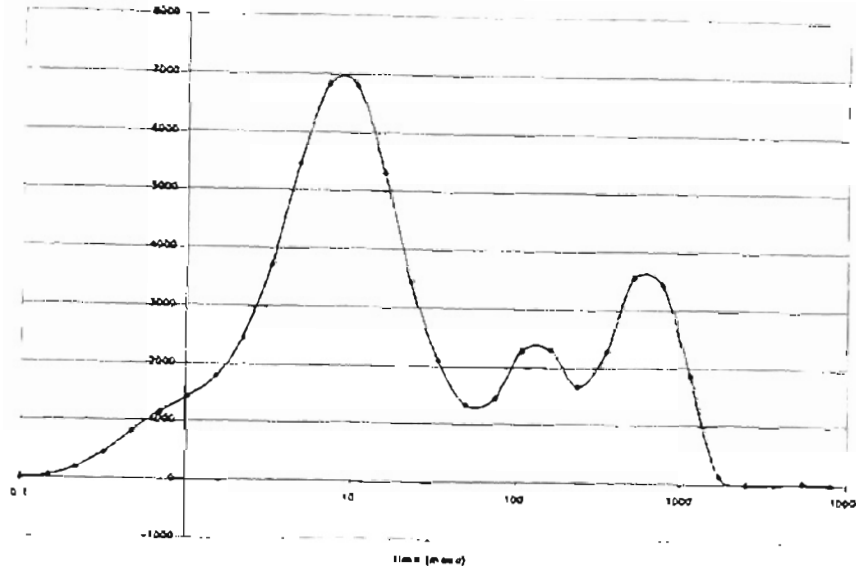


Figure 15. K 6243.1 relaxation distribution curve.

The petrographic data was determined from thin section. This sample contains 68% quartz that has an average grain size of 1250 microns. Calcite comprises 2.7% of the sample. Dolomite composes 4.3% of the thin section. Chlorite composes 9.5% of the sample. The chlorite is found as clusters filling the secondary porosity and as a thin layer surrounding the quartz, calcite and dolomite grains. The sample contains less than 1% of heavy minerals, kaolinite and rock fragments.

The TOP for this sample is 8.6% this is slightly less than the core porosity of 10.8%. The optical microporosity for this sample is 2.2%. The dominant type of porosity is secondary porosity; it comprises 44% of the TOP. The average diameter of the secondary porosity is 330 microns. The secondary porosity contains abundant clay

and heavy minerals. The porosity associated with visible clay is 36% of the TOP. The largest pores associated with visible clay are 40 microns. The clusters of clay filling the secondary pores contain large voids (120 microns) when soft minerals or fossils have dissolved. The porosity associated with dissolution of quartz and feldspar comprises 12% of the TOP. Primary porosity composes 8% of the TOP. The average diameter of the primary pores is 200 microns. The primary pores contain less clay than the secondary pores and are usually smaller than the secondary pores.

The total area under the relaxation distribution curve correlates with the total porosity. The porosity associated with the visible clay porosity is 36% of the TOP. This agrees with the fast portion (5-10 msec) of the relaxation distribution curve, which is 39% of the total distribution. The percentage of TOP associated with dissolution of quartz and feldspar is 12%. This corresponds to the 10 to 20 msec portion of the relaxation distribution that is 19%. The percentage of primary porosity is 8% of the TOP. The portion of the relaxation curve associated with primary porosity ranges between 20 to 100 msec. For this sample the primary porosity is slightly less than the NMR distribution related to primary porosity. The percentage of the relaxation distribution curve that corresponds to primary porosity is 13%. The secondary porosity comprises 44% of the TOP. The distribution of the relaxation curve that corresponds to secondary porosity is between 100 to 1000 msec. For this sample 28% of the relaxation curve corresponds to secondary porosity.

K 6267

This sample has a broad relaxation time distribution that ranges from 0.8 to 200 msec (figure 16). The dominant relaxation components are centered between 10 to 100 msec. The geometric mean, or average, T2 distribution is 18 msec. This shifts towards

109 msec when the weighted T2 method is applied. The fast components (<10 msec) comprise only 24% of the relaxation distribution.

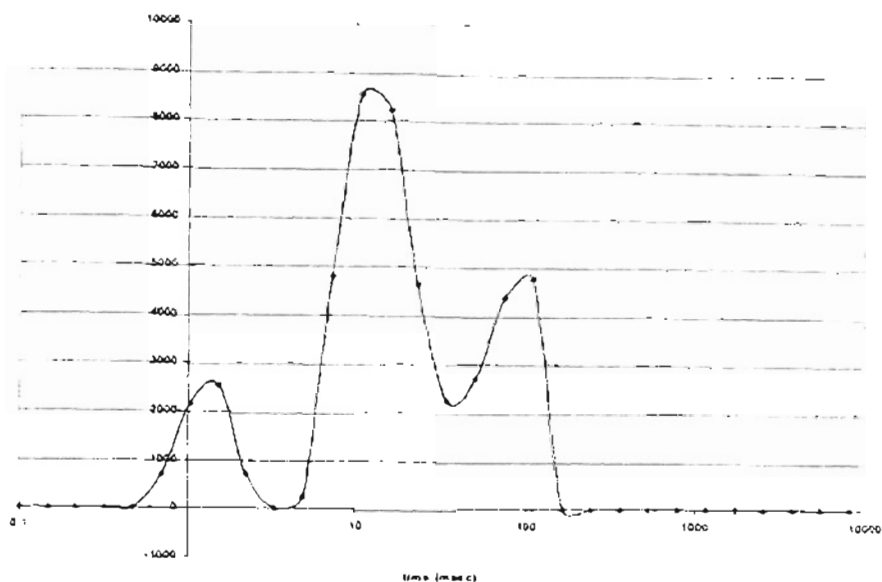


Figure 16. K 6267.7 relaxation distribution curve.

The petrographic data was determined from thin section. This sample contains 58% quartz that has an average grain size of 400 microns. Chlorite composes only 2% of the sample. The majority of the chlorite is found surrounding the quartz grains. The percentage of kaolinite in the thin section is just over 1%. The kaolinite is found filling the secondary pores. The sample contains 9.4% calcite cement. Dolomite cement comprises 11.3% of the thin section. The calcite and the dolomite cement are replacing the secondary porosity. The decrease in the weighted T2 value is due to the increase in cement. The sample contains 3.1% carbonate rock fragments and 1.8% shale rock fragments. The rock fragments are found within the calcite and dolomite cements. The

sample contains less than 1% of calcite grains, dolomite grains, organic matter, plagioclase, siderite, fossils and other rock fragments.

The TOP for this sample is 2.3%, this is less than half of the core porosity of 9.6%. For this sample the optical microporosity is 7.2%. The dominant type of porosity in this sample is the porosity associated with dissolution; it comprises 54% of the TOP. The average diameter of the pores associated with dissolution is 120 microns. The porosity associated with visible clay comprises 10% of the TOP. The largest pore diameter associated with visible clay is 40 microns. Primary porosity comprises 1.3% of the TOP. The average primary porosity diameter is 200 microns. The secondary porosity comprises 35% of the TOP. The average diameter of the secondary porosity is 300 microns. The primary and secondary porosity is decreased due to the increase in cement.

The total area under the relaxation distribution curve correlates with the total porosity. The porosity associated with the visible clay porosity is 10% of the TOP. This correlates to the fast portion (0.7-10 msec) of the relaxation curve, which is 24% of the total distribution. The percentage of the TOP associated with dissolution of quartz and feldspar is 54%. The porosity associated with dissolution corresponds to the 10 to 20 msec portion of the relaxation curve. For this sample the percentage of the relaxation distribution that corresponds to porosity associated with dissolution is 36% of the total relaxation curve. Primary porosity comprises only 1.3% of the TOP. The portion of the relaxation curve associated with primary porosity ranges from 20 to 100 msec. For this sample the primary porosity is significantly less than the NMR distribution related to primary porosity. The percentage of the relaxation distribution curve that corresponds to primary porosity is 30%. The secondary porosity comprises 35% of the TOP. The

distribution of the relaxation curve that corresponds to secondary porosity is between 100 to 200 msec. For this sample 10% of the relaxation curve corresponds to secondary porosity.

B 13629

This sample has a broad relaxation time distribution that ranges from 0.1 to 400 msec (figure 17). The dominant relaxation components are centered between 1 to 10 msec. The geometric mean, or average, T2 distribution is 9.7 msec. This shifts towards 178 msec when the weighted T2 method is applied. The fast components (<10 msec) comprise only 51% of the relaxation distribution.

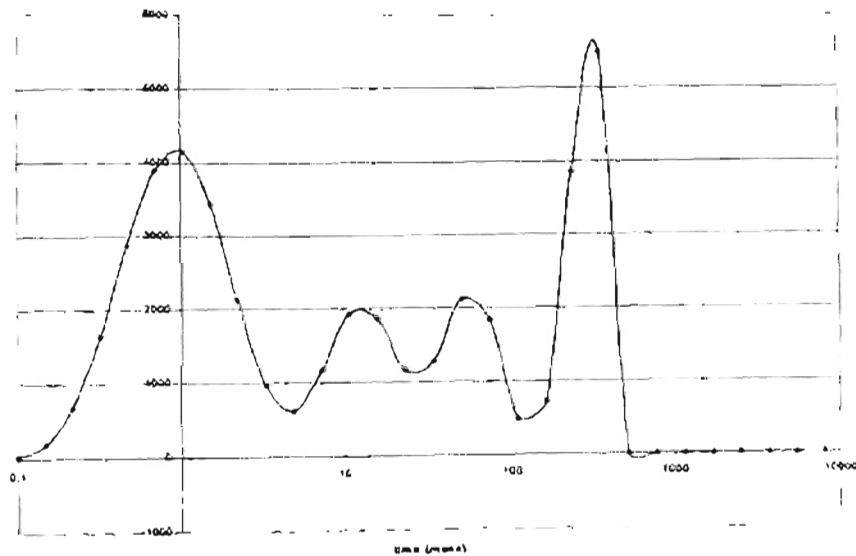


Figure 17. B 13629 relaxation distribution curve.

The petrographic data was determined from thin section. This sample contains 13% quartz. The majority of the thin section is composed of clay matrix, which is chloritic in nature. The clay matrix composes 69% of the thin section. Within the clay

matrix chert fragments are present. The chert fragments comprise 2% of the thin section. Less than 1% of glauconite, heavy minerals, plagioclase, muscovite, siderite, and shale rock fragments are present.

The TOP for this sample is 5.6%, which is slightly less than the core porosity of 9%.

The optical microporosity for this sample is 3.3%. The only type of porosity measured through thin section is porosity associated with visible clay. It comprises 100% of the TOP. The porosity associated with visible clay is formed from voids in the clay matrix where the clay has dissolved soft minerals or fossils.

The total area under the relaxation distribution curve correlates with the total porosity. The portion of the NMR relaxation distribution associated with porosity from visible clay corresponds to the fast portion (0.1-10 msec) of the relaxation curve. This portion of the relaxation distribution comprises 51% of the total curve. The portion of the relaxation distribution that corresponds to porosity associated with dissolution is between 10 to 20 msec. This portion of the relaxation distribution comprises 9% of the total distribution. Primary porosity corresponds to the portion of the relaxation curve between 20 to 100 msec. The portion of the NMR relaxation curve that corresponds to primary porosity is 15% of the total distribution. Secondary porosity corresponds to the slow portion (100-400 msec) of the relaxation curve, which is 24% of the total distribution.

M 11888

This sample has a broad relaxation time distribution that ranges from 1 to 400 msec (figure 18). The dominant relaxation components are less than 100 msec. The geometric mean, or average, T2 distribution is 81 msec. This shifts towards 281 msec

when the weighted T2 method is applied. The fast components (<10 msec) comprise only 17% of the relaxation distribution.

The petrographic data was determined from thin section. This sample contains 74% quartz that has an average grain size of 400 microns. Chlorite composes 5% of the thin section. The chlorite is found as a thin layer between quartz grains. The sample contains three types of cement. The quartz overgrowths comprise 4% of the thin section. The quartz overgrowths formed in the primary pores. Calcite cement comprises almost 6% of the thin section. The calcite cement filled in the secondary pores. Besides calcite cement filling the secondary porosity, dolomite cement also formed; it comprises just less than 4% of the thin section. The sample contains less than 1% of organic matter, plagioclase, kaolinite and shale rock fragments.

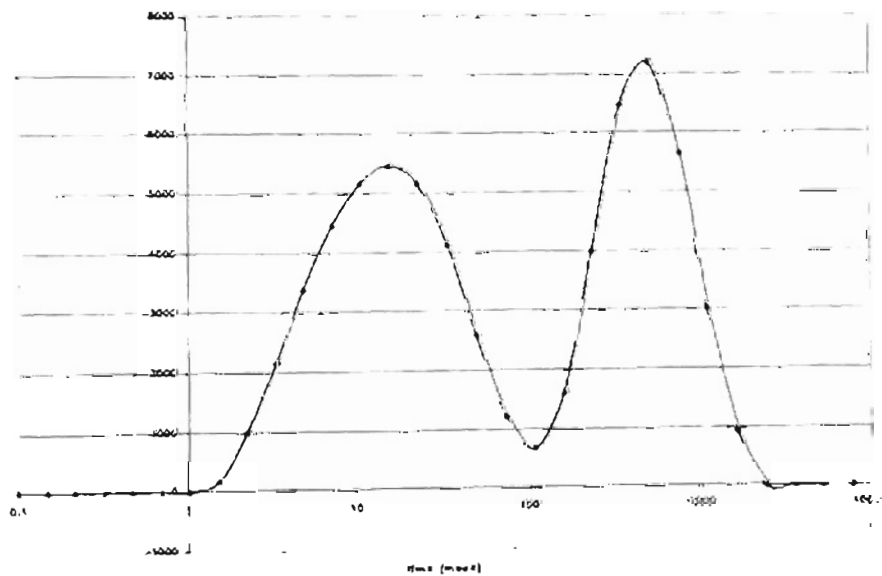


Figure 18. M 11888 relaxation distribution curve.

The TOP for this sample is 4%, which is less than the core porosity of 7.9%. The optical microporosity for this sample is 3.9%. The dominant type of porosity is secondary porosity; it comprises 47.5% of the TOP. The average secondary pore diameter is 200 microns. The small pores are due to the cement that has filled the large voids. The porosity associated with visible clay comprises 20% of the TOP. The largest pore diameter associated with visible clay is 10 microns. The porosity associated with dissolution of quartz and feldspar is 7.5% of the TOP. The average pore diameter associated with dissolution is 100 microns. Primary porosity comprises 25% of the TOP. The average pore diameter is 120 microns.

The total area under the relaxation distribution curve correlates with the total porosity. The porosity associated with visible clay composes 20% of the TOP. This correlates to the fast portion (1-10 msec) of the relaxation distribution curve, which is 17% of the total curve. The percentage of the TOP that is associated with dissolution of quartz and feldspar is 7.5%. This correlates to the 10 to 20 msec portion of the relaxation time distribution that is 16%. The percentage of primary porosity is 25% of the TOP. The portion of the relaxation curve associated with primary porosity ranges between 20 to 100 msec. For this sample the NMR distribution related to primary porosity is 20% of the total distribution. The secondary porosity comprises 47.5% of the TOP. This closely agrees with the distribution of the relaxation curve between 100 to 400 msec. For this sample 46% of the relaxation curve corresponds to secondary porosity.

K 6240.6

This sample has a broad relaxation time distribution that ranges from 0.1 to 500 msec (figure 19). The dominant relaxation components are centered between 1-10 msec.



The geometric mean, or average, T2 distribution is 3.5 msec. This shifts towards 72 msec when the weighted T2 method is applied. The fast components (<10 msec) comprise 79% of the relaxation distribution.

The petrographic data was obtained from thin section analysis. This sample contains 26% quartz that has an average grain size of 70 microns. The sample contains 67% clay matrix. Within the clay matrix minor amounts of muscovite, plagioclase, heavy minerals, siderite, zeolites, carbonate rock fragments and glauconite are present in the thin section. The sample contains 1% of calcite grains.

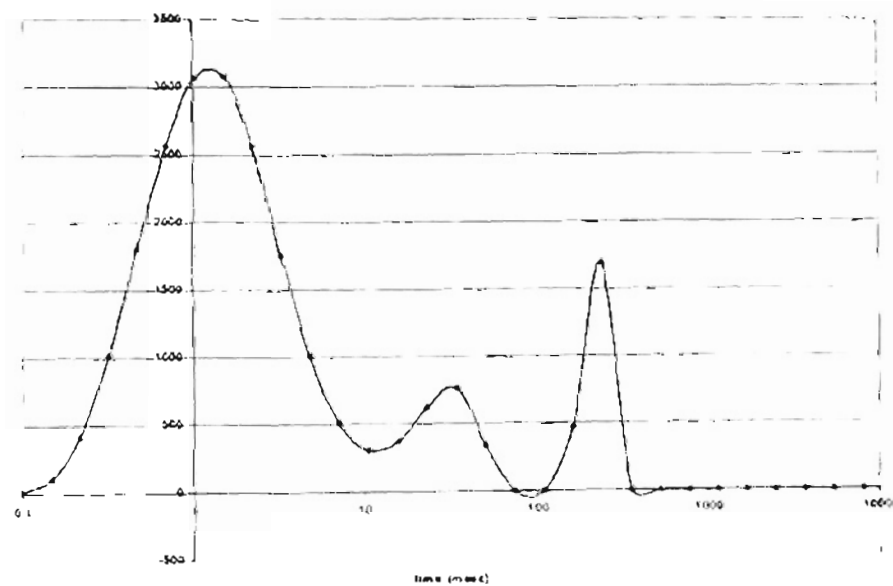


Figure 19. K 6240.6 relaxation distribution curve.

The TOP for this sample is 2.3%, which is half of the core porosity of 7.2%. The optical microporosity for this sample is 4.9%. The dominant type of porosity is porosity associated with visible clay. The porosity associated with visible clay comprises 100% of the TOP. The largest pore diameter of the visible clay porosity is 40 microns. The

porosity associated with dissolution of quartz and feldspar, primary porosity and secondary porosity are greatly reduced because of the increase clay content.

The total area under the relaxation distribution curve correlates with the total porosity. The porosity associated with visible clay comprises 100% of the TOP. The portion of the relaxation curve that corresponds to visible clay porosity is the fast portion (0.1 –10 msec) of the relaxation distribution. This time range contributes to 80% of the NMR relaxation distribution. The portion of the relaxation curve that corresponds to porosity associated with dissolution of quartz and feldspar is between 10 to 20 msec, which is 3% of the total relaxation distribution. Primary porosity corresponds to the 20 to 100 msec portion of the relaxation distribution. This time range corresponds to 7% of the total relaxation distribution. Secondary porosity correlates to the time range of 100 to 500 msec of the relaxation distribution, which is 9% of the total relaxation curve.

M 13288

This sample has a broad relaxation time distribution that ranges from 0.1 to 800 msec (figure 20). The dominant relaxation components are centered between 1-10 msec. The geometric mean, or average, T2 distribution is 8 msec. This shifts towards 23 msec when the weighted T2 method is applied. The fast components (<10 msec) comprise 68% of the relaxation distribution.

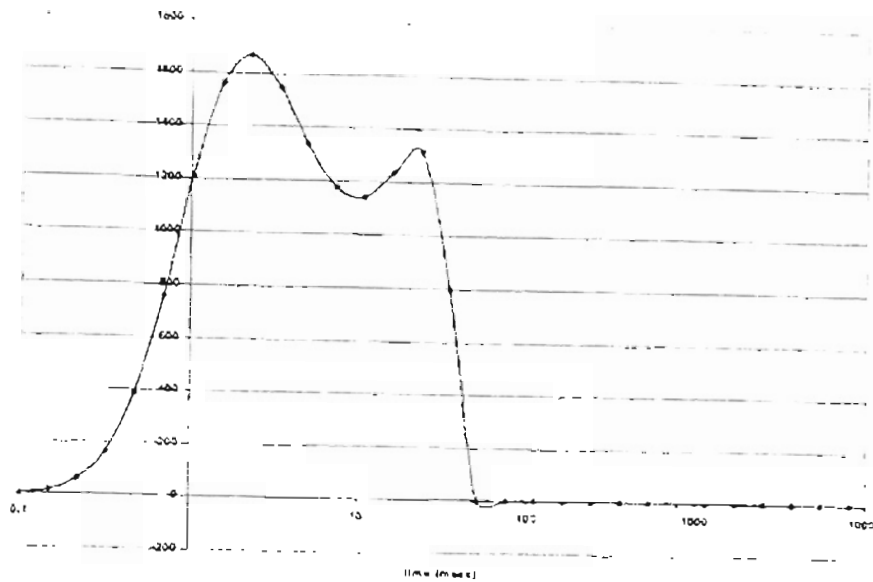


Figure 20. M 13288 relaxation distribution curve.

The petrographic data was determined from thin section analysis. This sample contains 78% quartz that has an average grain size of 780 microns. The sample contains 2.3% chlorite clay. The chlorite is found mainly as dust rims around quartz grains. Quartz overgrowths are the main type of cement found in the thin section, it comprises 6.2% of the thin section. Dolomite cement comprises 2.6% of the thin section. The quartz overgrowths fills the primary porosity while the dolomite cement is filling the secondary porosity. The sample contains 7.5% of shale rock fragments, with an average grain size of 900 microns. The sample contains 1.2% fossils that are replaced by clay. The sample contains less than 1% of calcite cement and zircon.

There is less than 1% of TOP. The core porosity for this sample is 4.5%. The optical microporosity for this sample is 4%. The only type of porosity observed in the

thin section is secondary porosity. This porosity occurs because of a stylolite in the thin section. The average pore diameter of the secondary porosity is less than 40 microns.

The total area under the relaxation distribution curve correlates with the total porosity. The portion of the relaxation distribution that corresponds to visible clay porosity ranges between 0.1 to 10 msec. This fast portion of the relaxation distribution is 68% of the total distribution. The portion of the relaxation distribution that corresponds to porosity associated with dissolution is between 10 to 20 msec; which is 16% of the total distribution. Primary porosity corresponds to the 20 to 100 msec portion of the relaxation distribution; which is 14% of the total distribution. Secondary porosity composes 100% of the TOP. Secondary porosity corresponds to the slow portion of the relaxation distribution from 100 to 800 msec. For this sample 0% of the NMR relaxation corresponds to secondary porosity.

M 11886

This sample has a broad relaxation time distribution that ranges from 3 to 1000 msec (figure 21). The dominant relaxation components are centered between 10-10 msec. The geometric mean, or average, T2 distribution is 45 msec. This shifts towards 231 msec when the weighted T2 method is applied. The fast components (<10 msec) comprise 26% of the relaxation distribution.

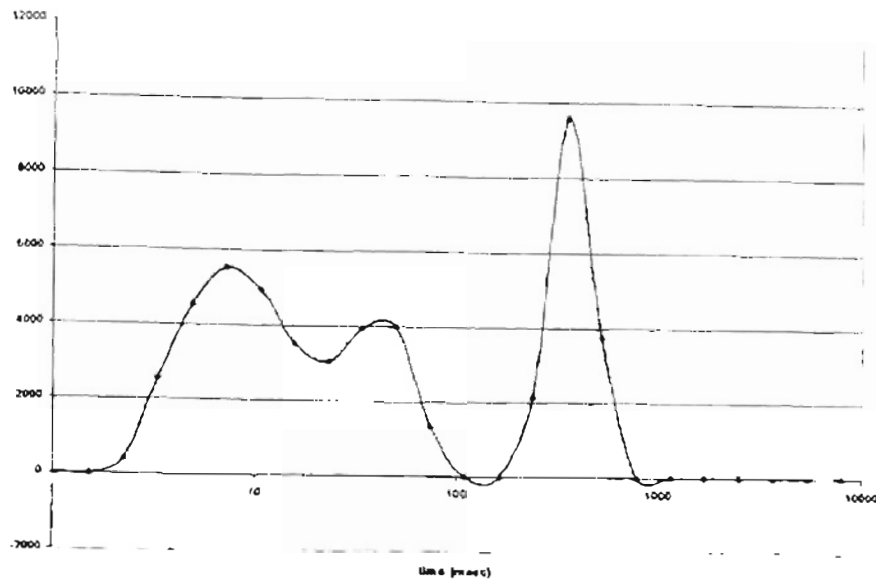


Figure 21. M 11886 relaxation distribution curve.

The petrographic data was determined from thin section analysis. The sample contains 78% quartz that has an average grain size of 400 microns. Chlorite composes 7.1% of the thin section. The chlorite is found surrounding quartz grains and as clusters in the secondary pore space. The sample contains three types of cement. Quartz overgrowths comprise 2.6% of the thin section. Dolomite cement comprises 2.2% of the sample and calcite cement composes only 1% of the thin section. The sample contains less than 1% of kaolinite, organic matter, plagioclase, carbonates rock fragments, siderite, and other rock fragments.

For this sample the TOP is 3.7%, which is slightly less than the core porosity of 4.4%. The optical microporosity for this sample is 0.7%. The dominant type of porosity as observed in thin section is secondary porosity; it comprises 50% of the TOP. The average diameter of the secondary porosity is 200 microns. The secondary pores contain



clusters of clay and calcite and dolomite cement. The different types of rock fragments are also present in the secondary porosity. The porosity associated with visible clay is 31% of the TOP. The largest pore diameter of the porosity associated with visible clay is 40 microns. The porosity associated with dissolution of quartz and feldspar is 19% of the TOP. The average pore diameter of the porosity associated with dissolution is 120 microns. There is no primary porosity observed in the thin section.

The total area under the relaxation distribution curve correlates with the total porosity. The porosity associated with the visible clay is 31% of the TOP. This correlates to the fast portion (3-10 msec) of the relaxation distribution curve, which is 26% of the total distribution. The percentage of the TOP associated with dissolution of quartz and feldspar is 19%. This is in good agreement with the contribution from the 10 to 20 msec portion of the relaxation time distribution that is 17%. There was no primary porosity observed in the thin section. The portion of the relaxation curve corresponding with primary porosity ranges from 20 to 100 msec. For this sample the percentage of the NMR relaxation distribution related to primary porosity is 25%. Secondary porosity comprises 50% of the TOP. The distribution of the relaxation curve that corresponds to secondary porosity is between 100 to 1000 msec. For this sample 31% of the relaxation curve corresponds to secondary porosity.

M 13302

This sample has a broad relaxation time distribution that ranges from 0.1 to 1000 msec (figure 22). The dominant relaxation components are centered between 1-10 msec. The geometric mean, or average, T<sub>2</sub> distribution is 12msec. This shifts towards 20 msec when the weighted T<sub>2</sub> method is applied. The fast components (<10 msec) comprise 73% of the relaxation distribution.

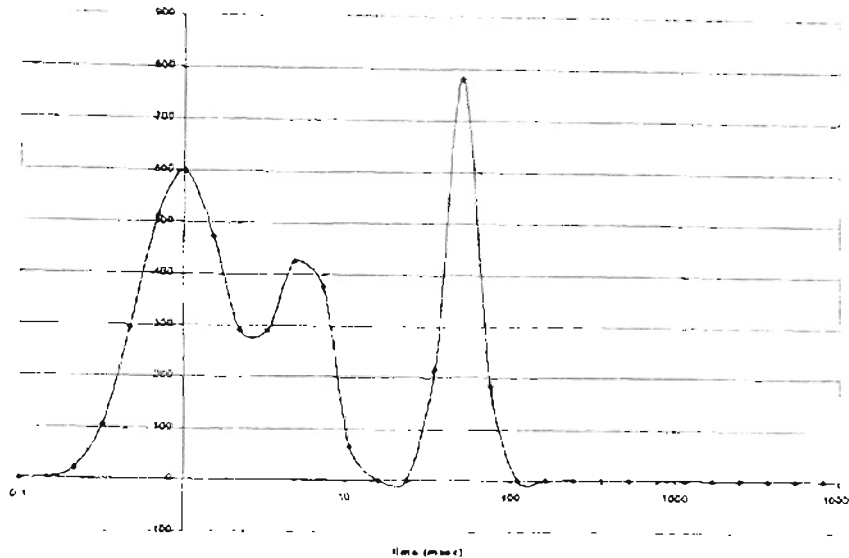


Figure 22. M 13302 relaxation distribution curve.

The petrographic data was obtained from thin section analysis. The sample contains 82% quartz that has an average grain size of 200 microns. Quartz overgrowths are the only type of cement present in the sample. They comprise 7.5% of the sample. Calcite comprises 2.2% of the sample and dolomite comprises just over 1% of the sample. Chlorite comprises 3.5% of the sample. The chlorite is in the form of dust rims, surrounding the quartz grains. The sample contains 1% or less of organic matter, siderite, chert fragments, and fossils – crinoids and forams. The fossils contained within the cement.

The TOP for this sample is 0.1%, which is less than half of the core porosity of 2.2%. The optical microporosity for this sample is 2%. The dominant type of porosity observed from this section is secondary porosity; it comprises 99% of the TOP. The average secondary pore diameter is less than 40 microns. The secondary porosity

contains chlorite, organic matter, siderite and chert fragments. The smaller pore size is due to the increase in quartz overgrowths. Porosity associated with visible clay comprises 1% of the TOP. This is the only other type of porosity observed from thin section. The average diameter of the visible clay porosity is less than 40 microns.

The total area under the relaxation distribution curve correlates with the total porosity. The porosity associated with visible clay is 1% of the TOP. This correlates to the fast portion (0.1-10 msec) of the relaxation distribution curve, which is 73% of the total distribution. The portion of the relaxation distribution that correlates to porosity associated with dissolution of quartz and feldspar is between 10 to 20 msec, which is 1% of the total distribution. Primary porosity corresponds to the 20 to 100 msec range of the relaxation distribution. For this sample, 25% of the total relaxation distribution correlates to primary porosity. The secondary porosity comprises 99% of the TOP. The distribution of the relaxation curve that corresponds to secondary porosity is between 100 to 1000 msec. For this sample the relaxation distribution is not present.

B 12807

This sample has a broad relaxation time distribution that ranges from 0.1 to 200 msec (figure 23). The dominant relaxation components are centered between 1-10 msec. The geometric mean, or average, T<sub>2</sub> distribution is 12 msec. This shifts towards 76 msec when the weighted T<sub>2</sub> method is applied. The fast components (<10 msec) comprise 64% of the relaxation distribution.

The petrographic data was determined from thin section analysis. The sample contains only 26% quartz that has an average grain size of 330 microns. The sample contains 48% quartz overgrowths. The quartz overgrowths are replacing the visible porosity in the sample. The sample contains 12% calcite. Chert fragments are present in



the thin section, but only in minor amounts. The chert fragments comprise just over 2% of the thin section. The sample contains 1.5% of rock fragments. Less than 1% of organic matter, plagioclase, biotite, siderite, dolomite, forams, and shale rock fragments are present in the thin section.

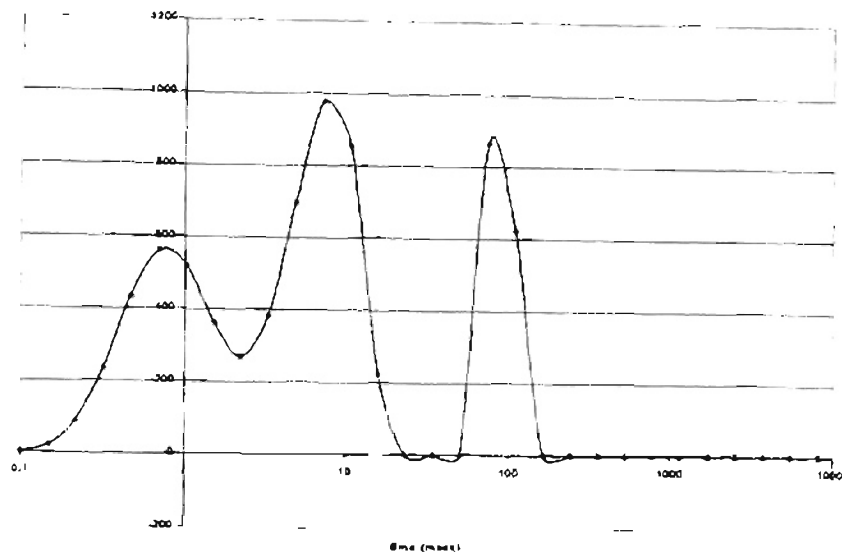


Figure 23. B 12807 relaxation distribution curve.

There is not visible porosity in the sample. The core porosity is 0.51%, therefore the core porosity is also the optical microporosity. The percentages of the NMR relaxation distributions are shown in Table T. The portion of the relaxation distribution that corresponds to visible clay porosity ranges from 0.1 to 10 msec, which is 64% of the total distribution. Porosity associated with dissolution of quartz and feldspar corresponds to the 10 to 20 msec time range of the relaxation distribution. This portion of the relaxation distribution comprises 15% of the total distribution. Primary porosity corresponds to the 20 to 100 msec portion of the relaxation distribution, which is 12% of

the total distribution. Secondary porosity corresponds to the 100 to 200 msec portion of the relaxation distribution, which is 9% of the total distribution.

B 13624

This sample has a broad relaxation time distribution that ranges from 0.1 to 15 msec (figure 24). The dominant relaxation components are centered between 1-10 msec. The geometric mean, or average, T2 distribution is 21 msec. This shifts towards 8 msec when the weighted T2 method is applied. The fast components (<10 msec) comprise 92% of the relaxation distribution.

The petrographic data was determined from this section analysis. This sample contains 38% quartz that has an average grain size of 200 microns. The sample contains 45% clay matrix. Chert fragments, which comprise 6% of the sample. Shale fragments compose 3% of the sample. The chert and shale fragments are both found in the clay matrix. The sample contains 1% or less of organic matter, glauconite, plagioclase, muscovite, biotite, forams, and other rock fragments.

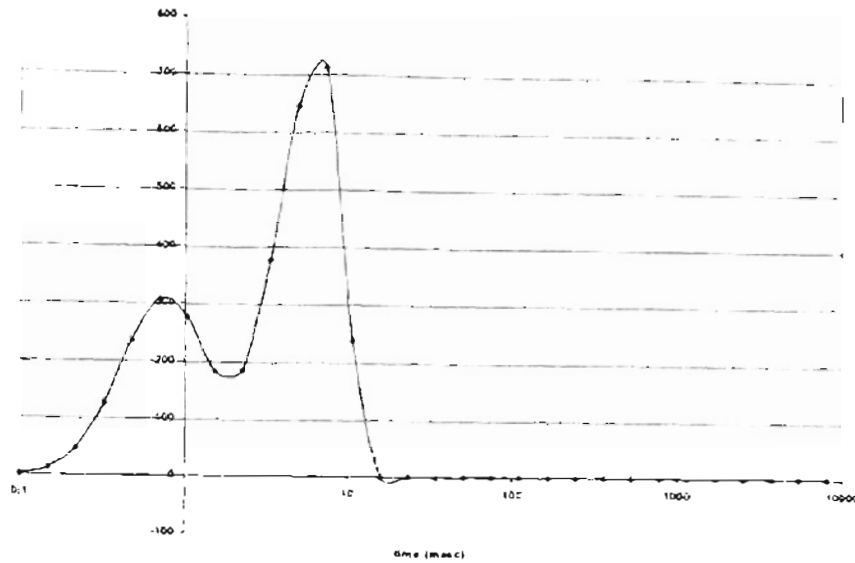


Figure 24. B 13624 relaxation distribution curve.

Both the TOP and the core porosity for this sample is 0.4%. Therefore there is not optical microporosity. Porosity associated with visible clay is the only type of porosity observed in the thin section.

The total area under the relaxation distribution curve correlates with the total porosity. The porosity associated with visible clay porosity is 100% of the TOP. This corresponds to the fast portion (0.1-10 msec) of the relaxation distribution, which is 92% of the total distribution. The portion of the relaxation curve that correlates to the porosity associated with dissolution of quartz and feldspar is between 10 to 20 msec. This portion of the relaxation curve comprises 7% of the total distribution.

M 13291

This sample has a broad relaxation time distribution that ranges from 0.1 to 500 msec (figure 25). The dominant relaxation components are centered between 1-10 msec.

The geometric mean, or average, T2 distribution is 9 msec. This shifts towards 150 msec when the weighted T2 method is applied. The fast components (<10 msec) comprise 58% of the relaxation distribution.

The petrographic data was obtained from thin section analysis. This sample contains 77% quartz that has an average grain size of 200 microns. The sample contains 8.2% quartz overgrowths. The abundance of quartz overgrowths significantly decreases the porosity. The sample contains just over 2% of forams and crinoids. These fossils are found in the quartz overgrowths. The sample contains 3.7% chlorite clay. The clay is found as dust rims between the quartz grains and the quartz overgrowths. The sample contains 1% or less of chert fragments, calcite, dolomite, heavy mineral, organic matter, muscovite, brachiopods, shale fragments and zircon.

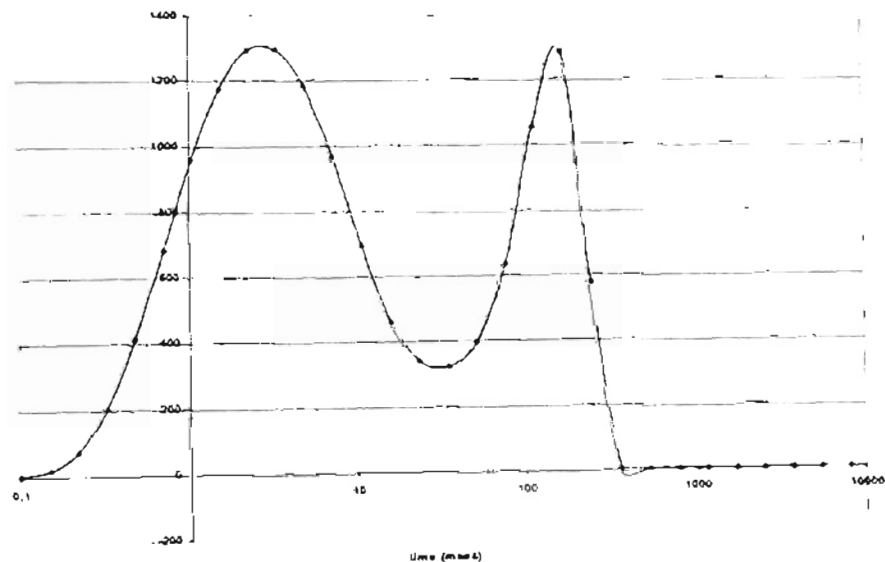


Figure 25. M 13291 relaxation distribution curve.

The geometric mean, or average, T2 distribution is 9 msec. This shifts towards 150 msec when the weighted T2 method is applied. The fast components (<10 msec) comprise 58% of the relaxation distribution.

The petrographic data was obtained from thin section analysis. This sample contains 77% quartz that has an average grain size of 200 microns. The sample contains 8.2% quartz overgrowths. The abundance of quartz overgrowths significantly decreases the porosity. The sample contains just over 2% of forams and crinoids. These fossils are found in the quartz overgrowths. The sample contains 3.7% chlorite clay. The clay is found as dust rims between the quartz grains and the quartz overgrowths. The sample contains 1% or less of chert fragments, calcite, dolomite, heavy mineral, organic matter, muscovite, brachiopods, shale fragments and zircon.

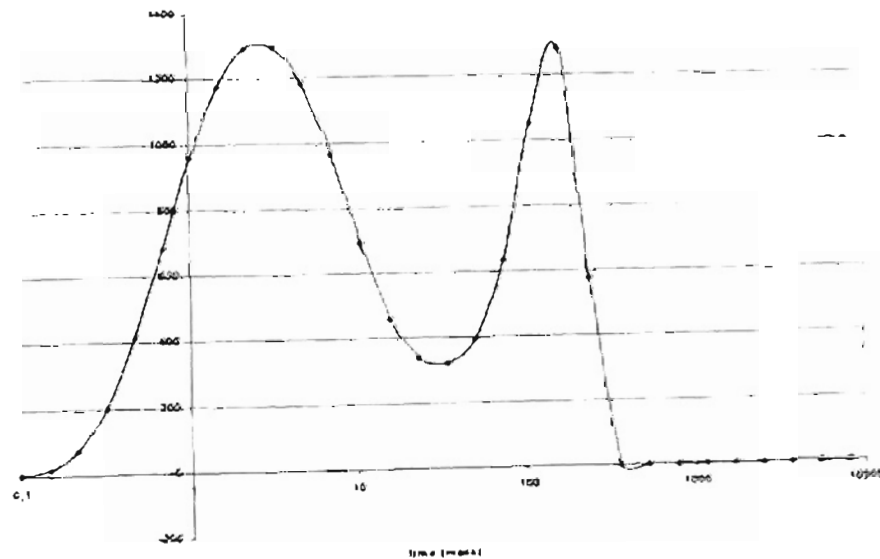


Figure 25. M 13291 relaxation distribution curve.

The TOP for this sample is 0.38%. The core porosity did not give an accurate value for this sample. The only type of porosity observed in the thin section is secondary porosity. The average pore diameter for the secondary porosity is 10 microns. The secondary porosity is found between the quartz overgrowths.

The total area under the relaxation distribution curve correlates with the total porosity. The porosity associated with visible clay corresponds to the fast portion (0.1-10 msec) of the relaxation curve, which is 59% of the total relaxation. The porosity associated with dissolution of quartz and feldspar corresponds to the 10 to 20 msec portion of the relaxation distribution. This portion of the relaxation distribution comprises 8% of the total distribution. Primary porosity corresponds to the 20 to 100 msec portion of the relaxation distribution, which is 12% of the total distribution. Secondary porosity comprises 100% of the TOP. This correlates to the slow portion (100-500 msec) of the relaxation distribution, which is 20% of the total distribution.

Reference:

- Andrews, Richard D. "Morrow Gas Play in Western Oklahoma". Oklahoma Geological Society Special Publication, 99-4, 1999.
- Coates, George R.; Xiao, Lizhi; Prammer, Manfred G. *NMR Logging Principles and Applications*. Halliburton Energy Services 1999.
- Dullien, F.A.L. *Porous Media Fluid Transport and Pore Structure*. Academic Press Inc, 1992.
- Halliburton Energy Services. Personal Communication, 2000.
- Johnson, K.S. "Geologic Evolution of the Anadarko Basin". Oklahoma Geological Survey Circular #90, 1989.
- Kenyon, W.E. "Petrophysical Principles of Application of NMR Logging". *The Log Analyst* v. 38, no. 1, 1997.
- Puckette, Jim; Abdalla, Azhari; Rice, Arron; Al-Shaieb, Zuhair. "The Upper Morrow Reservoirs: Complex Fluvio-Deltaic Depositional System". Oklahoma Geological Survey Circular #98. 1996.
- Vavra, Charles L.; Kaldi, John G.; Sneider, Robert M. "Geological Applications of Capillary Pressure: A Review". *AAPG* v. 76, no. 6, 1992.

VITA

Rachael Aivano

Candidate for the Degree of

Master of Science

Thesis: NMR RELAXATION TIMES AND RELATED PORE GEOMETRY IN THE MORROW GROUP (PENNSYLVANIAN), HEMPHILL COUNTY, TEXAS AND TEXAS COUNTY, OKLAHOMA

Major Field: Geology

Biographical:

Personal: Born in Houston, Texas on October 28, 1976, the daughter of John and Pat Aivano.

Education:

Graduated from Alief Elsik High School in May 1995; received Bachelor of Science Degree in Geophysics from Texas Tech University in May 1999; complete requirements for the Master of Science degree at Oklahoma State University in December 2001.

Professional Experience:

Summer Geophysics Intern, Phillip Petroleum Company; Member of Sigma Gamma Epsilon; President of AAPG Student Chapter at Oklahoma State University.



